CFD Modeling of Two-Stage Parallel Plate Sedimentation Centrifuge for Microalgae Dewatering

Bowen Yu

(this page is intentionally left blank)

CFD Modeling of Two-Stage Parallel Plate Sedimentation Centrifuge for Microalgae Dewatering

Bowen Yu

A Master thesis submitted to Department of Sustainable Process and Energy Faculty of Mechanical, Maritime and Materials Engineering in Delft University of Technology. The research presented in this thesis has been carried out in Sustainable Process and Energy Department from September 2010 to April 2012.

Author: Bowen Yu
Report number: 2507
Student number: 1190814
Email: yubowen@gmail.com

This thesis has been reviewed and approved by the following committee members:

Dr. Zuopeng Qu
Dr. ir. Martijn van der Kraan
Dr. ir. M.J.B.M. Pourquie
Prof. Dr. G. J. Witkamp

Process and Energy Department
Faculty of Mechanical, Maritime and Materials Engineering
Delft University of Technology

ABSTRACT

As one of the most fast growing species on earth, microalgae provides great potential to satisfy the ever increasing demand in food, energy and material in a sustainable way. Besides microalgae's well-known use as food or biodiesel, valuable components of pharma, nutrient, pigment, cosmetic, basic chemicals etc. could be extracted from microalgae. In order to obtain breakthrough of microalgae utilization mainly two bottle necks need to be dealt with: firstly how to efficiently and economically grow the desired algae species and secondly how to harvest microalgae from a very diluted source and process to get the valuable products.

The focus for this thesis work is on one of the most important bottle neck of microalgae harvest process: microalgae dewatering, by 3D CFD modeling of the flow and sedimentation separation in Evodos SPT centrifuge. Various microalgae dewatering technologies have been reviewed and evaluated. Compare to traditional conical disk centrifuge Evodos SPT centrifuge provides 10% to 20% energy consumption, removing up to 95% extra-cellular water and other benefits i.e. mechanical simplicity and process flexibility etc.

Although the Evodos SPT centrifuge has been developed since the mid-1990s for water-oil separation on offshore platforms very few research was done on Computational Fluid Dynamics (CFD) modeling of the flow inside this type of centrifuges. With the recent development of computing power in PC processors and the inherent difficulties to observe and measure the flow field and sedimentation phenomena inside the parallel plate centrifuge, CFD studies will provide an efficient, economical, and timesaving tool to investigate flow field, separation and optimize mechanical design.

In this research a complete 3D CFD model of the Evodos centrifuge consisting of five sub components have been built. In the model, the fluid dynamic behaviors of multiphase flow has been considered. The conservation equations of mass, momentum, are applied to solve the numerical problem by using the finite control volume method in each computational domain. The particle behavior for the centrifugation separation is based on DPM (Discrete Phase Model) in Fluent.

The result of the 3D CFD model gives a clear overview of the pathline, flow pattern and pressure profile inside the centrifuge. It also indicates the most unsteady whirl region of the flow field. The pressure profile analysis has indicate a relative recirculation inside a typical flow channel. A result separation efficiency on different particle sizes has been acquired and compared with the test result. The model has been validated through visual result from algae separation test runs, theoretical equations and starch test run measurements.

A test and sample taking with starch solution instead of real microalgae culture has also been carried out on Evodos site in Breda. Particle size distribution measurement and photo spectrometry measurement have been done for inlet and outlet samples from the starch test. The result of the measurement support the separation cut-off rate of 2-3 μm of SPT centrifuge claimed by Evodos. The CFD simulation results are also support the test results.

This thesis work laid a good foundation for future studies in the CFD modeling of Evodos SPT centrifuge and similar machineries. The future focus should be on optimizing the geometry of the parallel plates, impeller chamber for separation efficiency; understanding the effects and impacts of operation conditions and further develop the multiphase model considering the air core.

KEY WORDS: sustainable, microalgae, dewatering, CFD, sedimentation, Evodos, SPT, centrifuge, parallel plate, flow field, flow pattern, discrete particle model, etc.

ACKNOWLEDGMENTS

I would like to express my deepest gratitude to my supervisors: Prof. Dr. Geert Jan Witkamp, Dr. Zuopeng Qu from P&E TU Delft, Dr. Ir. Martijn van der Kraan, Mr. Adreas Weber from Feyecon and Mr. Hen Boele from Evodos. Thank you for the opportunity, guidance, inspiration and kind support during the span of my master thesis project. Thanks for Dr. ir. M.J.B.M. Pourquie from P&E TU Delft take part in my exam committee.

Thanks for all the cooperation, help and good discussions given by my colleagues: Alex Argilaga, Andreas Metlen, Angela Gayosom, Cristina lopez, Raquel Ernemann, Nieves Gonzalez-Ramon, Thijs Nell from Feyecon and Marco Brocken, Jan-Kees Boele, Remko van Dam from Evodos during this project.

I sincerely thank all my teachers from TU Delft: Ir. Nico Woudstra, Ir. Theo Woudstra, Professor dr. ir. Ad H.M. Verkooijen, Prof. Dr. Ing. Hartmut Spliethoff, Dr. ir. Carlos A. Infante Ferreira, Dr. ir. M.J.B.M. Pourquie, Dr. ir. Piero Colonna, Dr. ir. Wiebren de Jong, Prof. dr. ir. Dolf H.C. van Paassen, Prof. ir. Jos P. van Buijtenen, Prof. ir. Rob W. J. Kouffeld, Prof. dr. ir. P.J. Jansens and Ir. A.E.M. Huesman. Thank your all for not only technical knowledge, the way to do research but also beyond. I am grateful to secretaries of the department Leslie, Eveline and Judith for all the help and support.

I am grateful to my friends and colleagues around and beyond TU Delft: Eva Promes, Dwi Hartono, Yanfei Wang, Koko H. Wei, Ming Liu, Liyuan Fan, Jie Lu, Yuan Wang, Xiaoqian Liu, Xiaohua Tang, Xiangmei Meng, Xin Zhao, Xin Liu, Ningjie Fu, Vikrant Venkataraman, Jürgen Fernengel, Yovita Adisresti etc. Thanks for your inspiring casual discussion and encouragement during this project.

Thanks to all the friends and colleagues for the wonderful time we had together studying and having fun in TU Delft and in the Netherlands. No matter where are you right now, no matter whether your name have been put down here or not please accept my sincere gratitude.

Finally I am especially grateful to my mother and all my family members. Without their support, understanding, trust and love it is not possible for me to finish my study. This thesis and my master degree are my best gifts to them.

Bowen Yu

March 24th, 2012 in Delft

(this page is intentionally left blank)

CONTENT

LIST OF FIGURES

LIST OF TABLES

Nomenclature

$\hat{a}$	unit direction vector [-]
A	cross-sectional area [m^2]
b_k	Coefficients of dynamic viscosity [-]
c_k	Coefficients of thermal conductivity[-]
C_p	Specific heat [*J/mol-K*]
d	Plate thickness of parallel plates [m*m*]
D	Circular pipe diameter [*m*]
D_i	Inner diameter of parallel plates [*mm*]
D_o	Outer diameter of parallel plates [*mm*]
D_H	Hydralic diameter [*m*]
E	Internal energy [*kJ/kg*]
E_r	Relative internal energy [*kJ/kg*]
$\vec{F}$	Model dependent momentum source term [kg/m^2-s^2]
$\vec{g}$	Gravitational acceleration [m/s^2]
h	Length between inner wall to hinge of parallel plates [*mm*]
H	Total enthalpy [*kJ/kg*]
H_r	Relative total enthalpy [*kJ/kg*]
k	Heat transfer coefficient [*kJ/kg-K*]
M_w	Molecular weight [*g/mol*]
$M_{w,i}$	Molecular weight of species *i* [*g/mol*]
micron	Micro meter
n	Number of parallel plates [-]
nm	Nano meter
N	Avogadro's number [*1/mol*]
p	Pressure [*bar*]
P	Static pressure [*bar*]
Q_{ex}	Exchange heat [*J*]
R	Universal gas constant [*J/mol-K*]

R_P	Radius of parallel plates curvature [*mm*]
Re	Reynolds number [-]
S_e	Energy source term [W/m^3]
S_m	Mass source term [kg/m^3-*s*]
$S_{m,i}$	Mass source of species *i* [kg/m^3-*s*]
$\vec{S}_m$	Momentum source term [N-*s*/m^3]
S_ϕ	Source term of a scalar [*NA*]
T	Temperature [*K*]
T_0	Standard temperature [*K*]
$\vec{u}_r$	Whirl velocity vector (rotating reference frame) [*m/s*]
v_c	Settling velocity centrifuge [*m/s*]
v_g	Settling velocity gravity [*m/s*]
$\vec{v}$	(absolute) Velocity vector [*m/s*]
$\vec{v}_r$	Relative velocity vector [*m/s*]

Greek symbols

α	Sector angle [°]
β	Channel angle of parallel plates [°]
ϕ	A scalar quantity [*NA*]
μ	Dynamic liquid viscosity [*cP*] [*mPa-S*]
ν	Kinetic liquid viscosity [m^2/s]
ρ	Density (of the suspension) [kg/m^3]
ρ_{air}	Air density [kg/m^3]
ρ_p	Particle density [kg/m^3]
τ_s	Viscous shear stress tensor [N/m^2]
ω	Rotational speed [N/m^2]
$\vec{\omega}$	Rotation vector [N/m^2]
Γ_ϕ	diffusion coefficient for scalar ϕ [-]

Abbreviations:

CIP	Clean in Place
CFD	Computational Fluid Dynamics
DPM	Discrete Phase Model

Evodos SPT	Evodos Spiral Plate Technology
FVM	Finite Volume Method
GM	Genetically Modified
LES	Large-Eddy Simulation
LHS	Left Hand Side
MOM	Minutes of Meeting
NIR	Near Infra-red
PBR	Photobioreactor
PISO	The Pressure-Implicit with Splitting of Operators (pressure-velocity coupling scheme)
PSA	Partical Size Analyzer
QUICK	One of the spatial discretization methods in Fluent i.e. First Order Upwind, Second Order Upwind etc.
RANS	Reynolds averaged Navier–Stokes equations
RHS	Right Hand Side
RNG	Renormalization Group
RSM	Reynolds Stress Model
SDC	Sample Delivery Controller
SST	Shear Stress Transport
TSS	Total Suspended Solids
UDF	User Defined Functions in Fluent
UDM	User Defined Memories in Fluent
URANS	Unsteady Reynolds averaged Navier–Stokes equations
UV	Ultraviolet
VIS	Visible
VOF	Volume of Fluid

CHAPTER 1: INTRODUCTION

1.1 Background: The big picture

As we set our foot step into the 2nd ten years of the 21st century the outlook is not so bright as we had expected. Economic crisis, climate change, depleted resources, we are facing the biggest problem of maintain the balance of nature and society: how can we sustainably increase the welfare of all mankind without push the limit even further of our fragile environment?

In the 1990s a German chemist Michael Braungart[1] and a U.S. architect William McDonough come up with an revolutionary idea on how should we design, produce and consume things which will answer the big question above. In their inspiring 2002 book "Cradle to Cradle: Remaking the Way We Make Things" they have stated the 3 most important principles of their idea[1]:

- Waste equals Food
- Use current solar income
- Celebrate diversity

If those three above mentioned criteria should be used as a guideline to identify direction of finding sustainable solutions to solve the biggest problem of our time, microalgae and microalgae based products could be chosen as an excellent example.

Microphytes or microalgae are unicellular (from few µm to few hundred µm) plankton species which capable of performing photosynthesis. Microalgae could be grown in fresh water and/or marine systems. The nutrient they needed to grow is water, sun shine, CO_2 and minerals. The growing of algae improves the overall atmospheric CO_2 balance due to their activity as CO_2 sink (1 kg algae dry weight can subsequent approx. 1.8kg CO_2) potentially replacing intensive use of fossil fuels. Minerals (Nitrate and phosphate) that is essential for microalgae growth often could be found in industrial or municipal waste streams.

From the energy point of view microalgae uses current solar income quite well. All renewable energy (except tidal and geothermal power), and even the energy in fossil fuels, ultimately comes from the sun. The sun radiates 174,423,000,000,000 kilowatt hours (kWh) of energy to the earth every hour. In other words, the earth receives 3 yottajoule (10^{24} J) from the sun annually[2]. This energy supplied by the sun comes to the earth and has been divided as hydropower at 90 exajoule (10^{18} J), 630 exajoule as wind and 1250 exajoule via bio-photosynthesis. It is to say about 0.02 to 0.04 percent of the energy coming from the sun is converted into biomass by all plants on earth mostly algal biomass. It is enormous compare to est. 550 exajoule for annual primary energy consumption for the year 2010 in which over 80% from fossil fuels[2].

Last but not least it has been estimated that about 200,000-800,000 microalgae species exist of which about 35,000 species has been described[3]. The bio-diversity of microalgae species is so huge that the potential of growing, extracting and utilizing various microalgae and its valuable components is limitless not to mention the possibilities of genetically modified super microalgae strains with higher productivity, more valuable products and adaptiveness in various environment. As an example, the present productivity of penicillin synthesis by fungi is 5000 times as high as it was 50 years ago[4] due to natural and GM (Genetically Modified) selection.

[1] : Michael Braungart is now a professor in the Faculty of Social Sciences of Erasmus university Rotterdam.

1.2 The advantage and bottle necks of microalgae utilization

The cultivation of microalgae has long history. It is estimated total world commercial microalgae biomass production at about 10,000 ton per year with 98% is produced in open ponds rather than closed photobioreactors (PBRs). The most cultivated microalgae species are Spirulina, Chlorella, Dunaliella and Haematococcus for nutritional products rather than transport fuel products[5, 6].

Beside the characteristic mentioned in previous section microalgae has shown unique advantages in many aspects. Microalgae can be cultivated where land is not suitable for conventional crops, production is largely dependent of the seasons, and harvesting is all year round. Microalgae can serve as a superior alternative and sustainable source of energy in the forms of biodiesel, bioethanol and biogas than other biomass as they are oil-rich (up to 50% dry weight lipids content) and grow many times faster than plants. Showed in Table 1-1 microalgae has the most rapid growth rate and highest photosynthesis efficiency among some typical biomass[7].

	Food Corp	Mischanthus	Sugarcane	Highest C3 plants	Highest C4 plants	Bamboo	Micro algae
Growth Rate dry weight [kg/m^2·year]	1	3.7	n.a.	n.a.	n.a.	15	3-7, up to 12
Photosynthesis Efficiency[1] [-]	0.28%	<1%	1%	2.4%	3.7%	3.8%	4.2%

Table 1-1: Growth rate and photosynthesis efficiency of different biomass

Due to the higher lipids content of microalgae, microalgae derived biodiesel is an very attractive alternative for petroleum transport fuels. The majority triglycerides from the lipids could be converted to biodiesel by trans-esterification reactions. Unfortunately the large scale production and application of microalgae is still not economically feasible. The challenge lies on cheap and efficient cultivation and harvesting microalgae species.

In order to develop a more sustainable and economically feasible process, all biomass components (e.g. proteins, lipids, carbohydrates) should be used and therefore biorefining of microalgae is very important for the selective separation and use of the functional biomass components.[8] Valuable components of pharma, nutrient, pigment, cosmetic, basic chemicals etc. can be extracted from algae providing economic viability of the process. Please refer to Figure 1-1 for a list of valuable components from microalgae[9].

In order to obtain breakthrough of microalgae utilization several bottle necks need to be dealt with. On the cultivation side (upstream) a multidisciplinary approach in which systems biology, metabolic modeling, strain development, photobioreactor design should be developed.[8] On the other hand (downstream) because of the dilute and low energy density nature of microalgae culture, the harvesting, processing/drying should be focused on together with biorefinery process operation and system integration. In this research work the attention is on one of the most important bottle neck of microalgae utilization : microalgae dewatering processes.

[1] : The global incident solar energy average is 164 W/m^2. 200 W/m^2 is presumed.

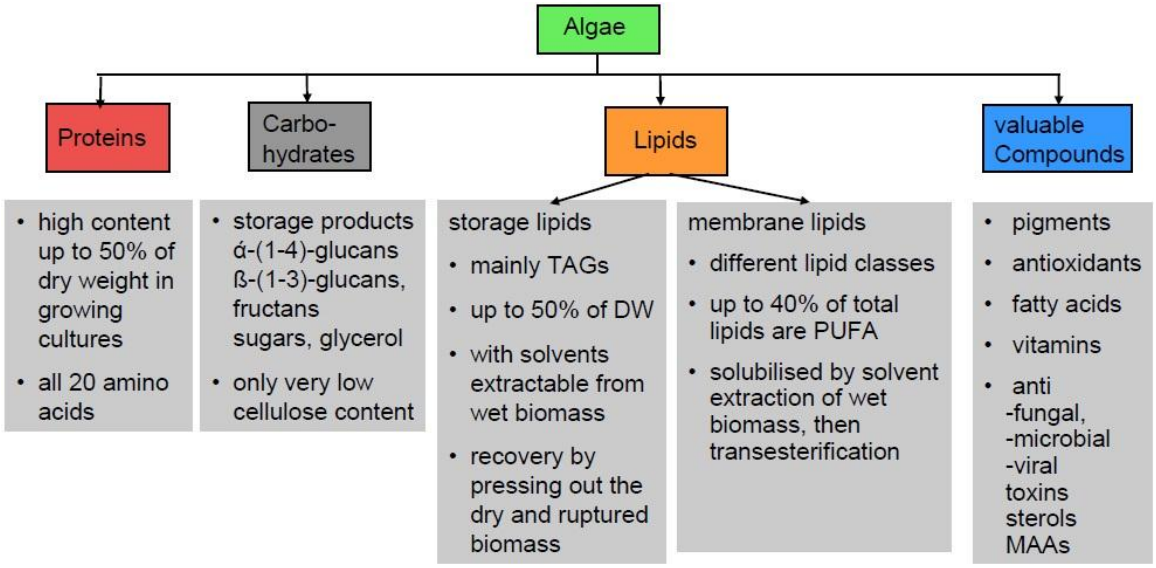

Figure 1-1: Main components of microalgae

1.3 Introduction to microalgae dewatering technologies

In microalgae harvesting, the first step is dewatering/harvesting or combined single step concentration as shown in microalgae processing flow diagram Figure 1-2. The degree of concentration of dewatering step is dependent on algae species and following extraction step based on desired product.

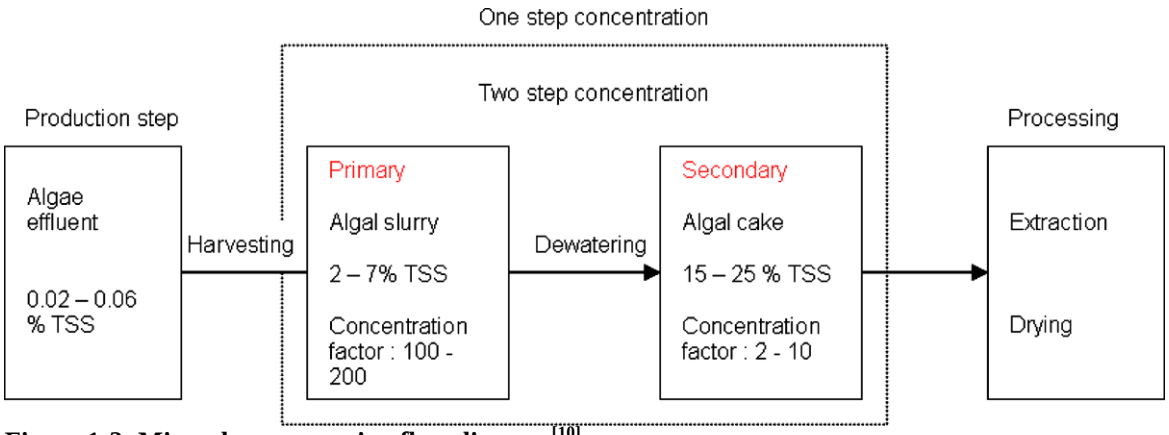

Figure 1-2: Microalgae processing flow diagram[10]

Dewatering/harvesting consists of biomass recovery from the culture medium[11]. Due to the size of microalgae and dilute nature of the typical microalgae culture without pre-concentration (< 3g/L) the dewatering is the most costly and energy intensive step and regarded as the bottle neck for industrial scale microalgae utilization.

Ideally the dewatering could be achieved using flocculation followed by sedimentation as primary concentration step and centrifugation or filtration as secondary concentration step. This will substantially reduce harvesting costs and energy requirements.

Several techniques for the dewatering of microalgae cultures have been developed. These techniques rely on properties that simplify the harvesting and recovery process. The properties

include large cell size, high specific gravity compared to the medium, and reliable auto-flocculation or induced flocculation.[12] The current microalgae dewatering and harvesting techniques include flocculation, centrifugation, filtration and screening, gravity sedimentation, flotation, and electrophoresis techniques. These are reviewed in Uduman's [13] article . A revised table summarize the performances of different harvesting and dewatering techniques including Evodos SPT centrifuge has been reproduced from the reference.[13]

Dewatering techniques	Type of concen-tration could be used[1]	Highest possible yield [%]	Highest possible concentration factor [-]	Energy usage [kWh/m^3]	Reliability	Limitations Micro algae
Flocculation	I, II	>95% removal of microalgae [12]	200–800, efficiencies of ≥80%[14]	Low, varies largely	Very good	Expensive at high dose, contamination issues
Centrifugation	II	Up to 22% TSS[15], 80%–90% clarification [16]	120, >95% cell harvest efficiency[17]	Very high, 8 kWh/m^3 [18]	Very good	High energy input, high shear stress
Evodos SPT (Spiral Plate Technology) centrifuge	II	95% TSS Solid discharge[19]	200, >95% cell harvest efficiency[19]	Medium, 0.95-1.1 kWh/m^3 [19]	Very good	Medium energy input, low shear stress, flexibility over feed and product
Gravity sedimentation	I	0.5%-1.5% TSS[15]	Lamella separator, 16[20]	Very low, 0.1 kWh/m^3 [20]	Poor	Take weeks or longer process time Not applicable for certain species
Filtration and screening (natural filtration)	I	1%–6% TSS[20]	15-60[20]	Low, vibrating screen filter, 0.4 kWh/m^3 [20]	Good	Filters and screens need to be replaced periodically
Filtration and screening (pressure filtration)	I, II	5%–27% TSS[20]	50-245[20]	Medium, chamber filter press,0.9 kWh/m^3 [20]	Very good	Filters and screens need to be replaced periodically
Tangential flow filtration	I	70%–89% microalgae recovery[21]	5-40[21]	High, 2.06 kWh/m^3 [18]	Good to very good	High energy input; filters need to be replaced periodically

[1] : Type I for primary concentration step and II for secondary concentration step

Cont.	Type of concen-tration could be used[1]	Highest possible yield [%]	Highest possible concentration factor [-]	Energy usage [kWh/m^3]	Reliability	Limitations Micro algae
Flocculation-flotation	I	Dissolved air flotation, 1%–6% TSS[15], dispersed air flotation, 90% microalgae removal[22]	NA	High, dissolved air flotation, 10–20 kWh/m^3 [23]	Good to very good	Electrodes need to be replaced periodically
Electro-coagulation	I	95% microalgae removal[18], 99.5 TSS	NA	Medium-high, 0.8-1.5 kWh/m^3 [24]	Very good	Electrodes need to be replaced periodically
Electro-flotation	I	3%-5% TSS[15]	300-600[25]	Very high, NA	Very good	Electrodes need to be replaced periodically
Electrolytic flocculation	I	>90% microalgae removal[26]	NA	Low-medium, 0.33 kWh/m^3 [18]	Very good	Electrodes need to be replaced periodically

Table 1-2: Summary of the performances of different harvesting and dewatering techniques

Flocculation

Flocculation is the process where a solute particle in a solution forms an aggregate called a floc. [13] Microalgae could be considered as particles with slightly electro-negative charged surface. Flocculation occurs when the solute particles collide and adhere to each other by a combination of charge neutralization and particle bridging.[13] Organic polymer or inorganic chemical called flocculants are added to the microalgae culture to induce flocculation.

Sedimentation of microalgae flocs may not be sufficient for certain species with very small particle size and density difference. The disadvantage also includes higher operation expanses of flocculants and recovery/contamination of the flocculants for downstream microalgae extraction processes. For flocculation of marine microalgae species the required flocculants dose is 5 to 10 times higher compared to fresh water species.[22]

Filtration and Screening

Filtration and screening involves passing the suspension through a screen/filter with a specific pore size with or without pressure. The permeable medium retains microalgae particles and the liquid pass through.

Filtration methods that operate under pressure or vacuum are suitable for recovering microalgae species with large cell size but inadequate to recover microalgae species with sizes approaching

[1] : Type I for primary concentration step and II for secondary concentration step

micron and sub-micron level bacterial dimensions.[14] Another major problem is that filters tend to bind and therefore require regular backwashes. This results in a decrease in the amount of microalgae concentrate.

Tangential flow filtration has great potentials on large scale microalgae harvesting over traditional filtration technologies. But it has higher energy consumption and is under development.

Gravity sedimentation
Gravity sedimentation is the most traditional way of separate microalgae species in to a slurry from clear water. But it works poorly or does not work for microalgae species with small size and density.

Flotation
Flotation can be described as a physiochemical type of gravity separation in which air or gas is bubbled through a solid-liquid suspension and the gaseous molecules are attached to the solid particles carried to the surface, accumulated as float and get removed.[13]

Flotation works well for small and light particles. It often combined with flocculation and can be considered more advantageous and effective than sedimentation.

Electrophoresis techniques
Microalgae particles have a slightly negative surface charge and can be separated from water by moving in an electric field. The above mentioned three electrophoresis techniques use metal electrodes combined with flocculation and/or flotation methods to separate microalgae.

Besides the relative lower energy consumption, electrophoresis techniques has similar disadvantage related with flocculation and flotation. The metal electrodes also need to be replaced constantly leading to higher operation costs.

Centrifugation
Centrifugation is a separation process uses centrifugal force (artificial gravity) to separate liquid/liquid, solids/liquid or solid/liquid/liquid. Because of the size and difficult-flocculation nature of some microalgae cells, centrifugation is often used as most preferred and efficient harvesting method.

The sedimentation rate of solid particles or droplets in the gravity field is a function of the particle (or droplet) size, the density difference, and the viscosity of the suspension (or emulsion). Particles smaller than 2 μm in diameter are, in general, poorly separated by gravity sedimentation, but maybe adequately processed in a sedimenting centrifuge[27]. The diffusional forces on very small particles are much less relevant in a centrifuge, hence sedimenting centrifuges can be used to capture particles which would never settle in gravity sedimentation basins.

Due to the low microalgae concentration (< 3g/L) currently available separation technologies are simply too expensive, economically (Capex and Opex) and energy balance-wise. To pursue low value products, such as liquid fuel energy a break-even point has to be reached which means the energy used in the harvesting process has to be less than the energy content with in the harvested microalgae.

The discharge of solid sludge has some drawbacks in conventional conical disk centrifuge. To make automatic discharge of solids possible shooting or nozzle separators has been developed. These machines need a liquid to support the discharge of the collected material. This results in a

limited dry solid content of the discharged sludge. Sticky materials (sludges) or abrasives limit the field of application of shooting separators or nozzle separators.[28] Those disadvantages of the traditional conical disk centrifuges have been solved with the newly developed Evodos SPT centrifuge.

Evodos SPT (Spiral Plate Technology) centrifuge
A novel separation technology developed by Evodos could make this process economically viable and relatively easy to scale up. The new type of centrifuge which uses, instead of a conventional conical disk stack, spiralized vertical plates. The plates (vanes) inside the centrifuge, which are almost perpendicular to the centrifugal force, are able to separate very small particles (1.9-4 μm with a density almost equal to water). This creates a special laminar flow pattern, heavier material moves outwards and the lighter fraction moves inwards (in the shape of a 'Y'). Thanks to the spiral plates inside the drum, there is no cross flow, which not only reduces the energy consumption, but more importantly, makes the use of chemicals such as flocculants and polymers obsolete.

The main advantage of Evodos SPT centrifuge lies in the minimum energy consumption of the microalgae dewatering (10% to 20% compare to normal conical disk centrifuge). This will bring the energy balance of dewatering microalgae positive which is unique in the industry. [19] Also find in the following Figure 1-3 the energy consumption and particle size to compare with other technologies. It has unique character for microalgae dewatering.

The Evodos SPT centrifuge could be used in liquid/liquid, solid/liquid and solid/liquid/liquid three phase separation which greatly increased flexibility of the centrifuge i.e. the microalgae could be harvested before break their cell wall or after break their cell wall (cell debris/oil/water separation). The semi batch Evodos SPT centrifuge could be used stand along or parallel in modules. The machine is made of stainless steel (capable to handle both fresh and marine microalgae cultures), can be operated full automatically, easy to disassemble for inspection and capable of CIP (Clean in Place).

Compare to a conventional conical disk stack centrifuge, Evodos SPT centrifuge use spiral vertical plates. Long retain times in the plate stack and avoiding cross or counter current flow of the liquids leads to high separation efficiency. This solution allows a free interface level making SPT machines self-adapting to changes in process parameters.

A detailed Evodos SPT centrifuge proposed design and description of working principle will be presented in section 3.1.1 Evodos SPT centrifuge design.

Summary of dewatering technologies
Currently there is no superior method of dewatering microalgae. The choice of which harvesting technique to apply depends on the microalgae species (size, shape, etc.) and final product desired. The Evodos SPT centrifuge has shown great potential in dewatering microalgae for its superiority in energy consumption, feed and process flexibility and other attributes.

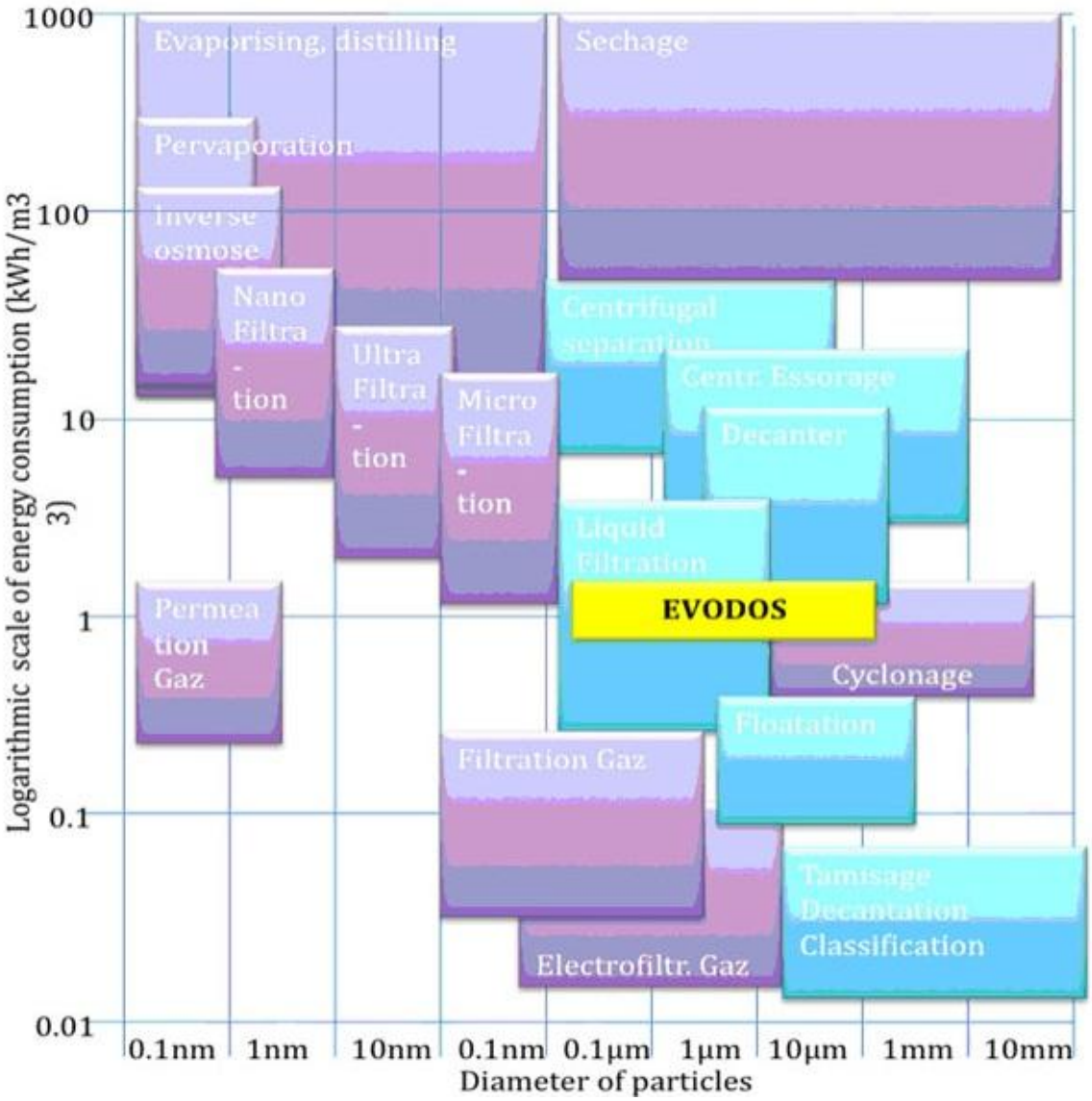

Figure 1-3: Relation between the particle size and energy consumption needed to separate these particles. ADEME (agence de l'environnnement et de la maîtrise de l'Energie)[19]

1.4 Status of 3D CFD modeling for centrifuges

Computational fluid dynamics (CFD) is a branch of fluid mechanics that uses numerical methods and algorithms to solve and analyze problems that involve fluid flows. Computers are used to perform the calculations required to simulate the interaction of liquids and gases with surfaces defined by boundary conditions.[29] With the recent development of computing power in PC processors, CFD provides an efficient, economical, and timesaving tool to investigate flow pattern, particle separation and therefore enables optimization of centrifuge performance, operating conditions and mechanical design.

Although CFD has been used to develop models of flow in some industrial devices. But only recently research works have being done on the field of CFD modeling of 3D multiphase flow in centrifuges[30-32], gas/hydro cyclones[33-36], and other equipments utilize centrifugal force [37]

due to the complexity of the problem and enormous computer power it needs. It is also quite time-consuming and constrained by available measuring techniques to do experimental works to study and understand the flow pattern and other detailed behavior inside the centrifuge. CFD simulation is becoming an effective tool to assist design, optimization and simulation for centrifuges. Many of them are done with commercial CFD package Fluent [30-38].

Due to the rarity of the research literature on 3D CFD modeling of centrifuges using algae or other cell sized bio-particles, a wide range literature has been studied. The type of problem, turbulence/numerical/multiphase methods and simulation results of those typical studies of 3D CFD modeling of centrifugal flow in process equiptments has been summarized in Table 1-3. The detailed discussion on turbulence model, numerical method and multiphase model will be discussed in CHAPTER 2:.

Looking at the recent CFD modeling studies, the difference lies in the type of applications (sludge removal, uranium enrichment, cell material collection etc.); type of fluid being studied (liquid or gas); type of configuration (conical disk, solid bowl, tubular or cyclones); geometry of the CFD model (2D or 3D) and last but not least type of approach (single/multi-phase, steady state/transient etc.).

Many parameters associated with the operation of the centrifuge (g-force, residence time, discharge frequency) and the associated material being separated (e.g., cell density, viability at harvest) has great impact on the effective efficiency of the centrifuge. The relation of the parameters is also being mentioned in some experimental studies as well as CFD simulation ones.

In the work of Fernandez [30] a 3D model of an industrial solid bowl centrifuge for removal of particles from industrial process stream has been developed. A gas-liquid 2-phase volume of fluid (VOF) has been used to track the interface between air and water. The velocity and pressure profile in the flow have shown agreeable results. The discrete phase model has been used to track the particle movement.

There are also some relevant CFD work which give interesting aspects such as the work of Xia [32] on the fluid velocity profile, liquid circulation flow, shear stress, and circulation time distribution of centrifugal impeller bioreactor for shear sensitive biological systems.

Herman [31] discussed the benefits and effectiveness of modeling for novel engine lube centrifuge design and optimization. The separation efficiency and particle cut-off size could be predicted from the model for a vertical spiral vane design

Nowakowski [33] and Cullivan[34] did quite in-depth research on 3D CFD modeling of hydro-cyclones. Although without any moving parts hydro-cyclone share many similarities with centrifuge. They both use centrifugal force to separate multiphase fluid. Nowakowski [33] outlined some developments and challenges for 2D and 3D CFD model of hydro-cyclones. Some important factors, namely proper representation of geometry, imposition of boundary conditions and the choice of turbulence model, are discussed. Cullivan[34] focused on flow field, air core development and particle separation mechanism.

Azadi [35] studied the size and its effect on gas cyclones performance parameters. The velocity and pressure field, separation efficiency and cut-off size with experimental validation is presented. On the other hand Cortes [36] gives a review on the recent algebraic and CFD modeling of gas cyclones. Cortes found the double-vortex structure that makes up the basic flow is essentially unstable, and develops a phenomenon of quasi-periodic oscillations known as a ‘‘processing

vortex core'' [36]. This quasi-periodic oscillation could also be found in the Evodos SPT centrifuge. Cortes also pointed out the complexity involved in the unsteady flow inside the cyclone for CFD modeling and the difficulties of a turbulence model for high swirl, high radial shear and adverse pressure gradients plus recirculation flow field. Therefore Cortes believe the second order Reynolds Stress Model (RSM) is much suitable compare to the first order turbulence closure, including two-equation models (i.e., the k-ε model and its variations) at capturing the real flow. [36]

Wardle[37] obtained qualitatively accurate results from a 3D CFD modeling of an annular centrifugal contactor with simplified assumptions and widely used turbulence/numerical models. The assumptions including steady-state, full liquid (no air core) and single liquid phase. Particle track has been achieved using DPM method. . Interestingly a grid resolution study has been carried out and the results showed great favor of a quadrilateral structured mesh over a tetrahedral unstructured mesh.

Most studies use DPM to study the behavior of particles in the multiphase flow system, Eularian-Eularian methods are relatively rarely used. Many literatures show that multiphase flow simulation of centrifuges is certainly still in development and demands several improvements. VOF simulation of the air core and air-liquid interface is often neglected from simulation.

On the one hand, factors like inter-particle behavior and conditions at the wall have not been addressed in the literatures. Most importantly, modern multiphase flow simulations have turned out to be too costly, due to the necessity of reproducing unsteadiness of the liquid flow and combine it with the simulation of a particulate system.

There are always limitations of the CFD numerical solution to exactly simulate the physical reality of the studies natural phenomena in the centrifuge. The numerical method in the model could introduce certain small amount of errors and inaccuracies. It needed to bear in mind for numerical simulation assumptions and approximations are being made. The assumptions, level of approximations and the model made should suit the propose, objective of the real problem. Nonetheless, the simulation results should be carefully validated by comparing with experiment data and real life data.

Summary of 3D CFD modeling for centrifuges

The experiments and measurements to study flow field inside the centrifuge is costly, time consuming and with many technological constrains. With the help of faster computers and modeling algorithms, 3D CFD modeling for centrifuges shows great potential for the understanding the phenomena and physics inside the centrifuge.

Although CFD in centrifuge has been studies from different aspects, CFD studies of cell sized (microalgae) particles in centrifuge is rarely studied. The unique character of the shape, size and density difference of the microalgae particles posed great challenge to the understanding of their flow behavior and performance of the centrifuge. It is also challenging to simulate the flow in a complicated geometry such as the Evodos SPT centrifuge with divided curved vertical flow channels, middle disk and complex inlet/outlet geometry.

Despite the current bottle necks and ongoing developments, CFD modeling of sedimentation centrifuge with turbulence/multiphase models by Fluent gives acceptable accuracy and can give great insights into the proposed design. The predictions of the flow field, particle trajectory, particle distribution and separation efficiency could be also achieved via CFD modeling.

Authors	Type of problem	Turbulence model	Numerical method	Multi-phase model	Simulation results	Remarks
X. Romaní Fernández [30]	3D CFD modeling of solid bowl centrifuge for industial sludge revomal, transient	k-ε RNG, RSM	PISO	VOF+ DPM	Liquid-gas interface, velocity field, pressure field, grade efficiency, theoretical validation and particle tracks	Air, liquid, solid three phase model, long computing time due to VOF
P. Herman [31]	3D CFD modeling of centrifuges including spiral vane centrifuge for lube oil cleaning	NA	NA	NA	Velocity field, pressure field, separation efficiency, cut-off size etc.	Overview on several centrifuges models
A. F. Nowakowski [33]	3D CFD modeling of hydro cyclones, review	k-ε RNG, RSM, LES	NA	Eulerian-Eulerian, DPM	Velocity field, pressure field, particle distributions, separation efficiency effect of geometry	Review of recent development in modeling hydro cyclones
J. C. Cullivan [34]	3D CFD modeling of hydro cyclone for china clay fines from grinding mill	RSM	SIMPLEC, QUICK, PRESTO	DPM	Velocity field, pressure field, particle distributions, separation efficiency	Water only simulation, VOF not used due to numerical divergence
M Azadi [35]	3D CFD modeling of Gas-solid cyclone	k-ε RNG, RSM	SIMPLEC	DPM	Velocity and pressure field, separation efficiency, cut-off size exp. validation and effect of geometry particle size and inlet velocity.	Gas-solid seperation instead of liquid-solid seperation
C. Cortes [36]	3D CFD modeling of Gas-solid particle flow in cyclone separator, transient, review	k-ε RNG, RSM, LES	SIMPLEC	DPM	Velocity field, pressure field, separation efficiency, cut-off rate exp. validation and effect of geometry particle size and inlet velocity.	Gas-solid seperation instead of liquid-solid seperation
K. E. Wardle [37]	3D CFD modeling of an annular centrifugal contactor for nuclear spent fuel solution extraction, steady state	k-ε RNG	PISO	DPM	Liquid-gas interface, velocity field, pressure field and particle tracks	Single liguid only simulation, VOF not used. Structured mesh

Table 1-3: Summery of reference studies of 3D CFD modeling of centrifugal flow in process equiptment

1.5 Objective and scope

1.5.1 Objective

This project is part of an effort between FeyeCon BV, Evodos BV, CleanAlgae BV and TU Delft under the EU INNOWATER program within water technologies. By 3D CFD modeling of the curved flow channels of the Evodos SPT centrifuge a better understanding of the flow fields and separation behavior of the centrifuge could be achieved. Based on the result of the CFD simulation the centrifuge designs could be optimized.

The purpose of this thesis work is to develop CFD models to study the fluid flow field and sedimentation of microalgae and similar diameter (several micron i.e. starch) particles in a Evodos SPT centrifuge. The project has the challenge in both modeling the flow in a complex 3D geometry and modeling of the separation of microalgae particle.

By understanding flow field and sedimentation in the Evodos SPT centrifuge the geometry parameter, mechanical configuration and separation efficiency could be optimized. The model will also be validated using the currently available proto type centrifuge experiments data from starch tests.

1.5.2 Scope

To achieve this purpose the following eleven tasks have been fulfilled during the thesis work.

1. Literature research on the prospect, development, utilization and dewatering technologies of microalgae.
2. Literature research on the CFD simulation of flow and sedimentation in centrifuges (for microalgae).
3. Study modeling method, related theory and working with CFD simulation using commercial CFD software Fluent.
4. Build up three-dimensional models of a single flow channel between parallel plates to study the flow field and sedimentation for 32 and 96 plates configuration.
5. Build up three-dimensional models of a complete parallel plate centrifuge, including impeller chamber, 1st stage parallel plate stack, intermediate disk, 2nd stage parallel plate stack, outlet chamber, excluding shaft, two pairing wheels and discharges.
6. Investigate the flow field of the complete centrifuge 3D model, such as velocity and pressure profile at different locations.
7. Investigate the solid particle distribution and separation efficiency with different sized by DPM methods
8. Sampling of feed and effluent stream from Evodos SPT centrifuge starch test run.
9. Measurement of particle size distribution and spectrophotometry of samples.
10. Validate the 3D CFD model with measurement data from the centrifuge starch test runs.
11. Based on results and analysis give recommendations and suggestions to optimize design of the centrifuge.

The original project proposal could be seen in APPENDIX C:.

1.6 Outline of the thesis

This thesis has six chapters and several appendices.

Chapter 1 section 1.1 and 1.2 gives introduction and background of microalgae utilization, section 1.3 describes microalgae dewatering technologies and the literature research overview of the current CFD modeling of the flow in centrifuge is presented in section 1.4. The motivation, objective, scope of this thesis and project work is presented in section 1.5. Finally the outline of the thesis is given in section 1.6.

Chapter 2 deals with the theory and numerical method used in 3D CFD modeling of the centrifuge. A basic theory of centrifugal sedimentation has been shown in section 2.1. The principles for calculate the mass, momentum and energy balance used in the CFD simulation is presented in section 2.2. The turbulence model, numerical solution methods and discrete phase model will be described in section 2.3, 2.4, 2.5 respectively.

The design of the Evodos SPT centrifuge, proposed 3D model design and general approach of CFD modeling is introduced in section 3.1. In order to investigate the flow and pressure field, flow parameters and particle distribution in the Evodos SPT centrifuge, a complete model consists of impeller chamber, 1st stage plate stack, middle disk, 2nd stage plate stack to the inner outlet and outer outlet has been developed. The rest of chapter 3 elaborates on the geometry, dimensions, meshing information, operation conditions, boundary conditions, mesh interface and model specifications of the model.

In chapter 4, the simulation results for the complete model will be presented. Firstly, the result of flow pattern, pressure profile, velocity profiles is shown followed by the result of separation efficiency by different particle sizes.

The description and report of sampling of feed and effluent stream from starch test run at Evodos site is presented in chapter 5. The introduction and experiment setup, measurement of particle distribution with laser particle size analyzer and measurement of starch granule concentration in suspension by spectrophotometry is given in section 5.1, 5.2 and 5.3 respectively.

The last chapter, chapter 6 conclude the thesis based on the simulation results and experiment data. Conclusions is made regarding the flow pattern, pressure profile, particle track and particle count for single flow channel and for complete centrifuge model. Recommendation is made for future development of the CFD model for Evodus SPT centrifuge and mechanical design of the centrifuge.

A number of meetings has been scheduled and conducted during the execution of the project. MOMs are included in APPENDIX A: Innowater project minutes of meeting followed by APPENDIX B: Fluent computing environment and APPENDIX C: Original Project Proposal.

(this page is intentionally left blank)

CHAPTER 2: THEORY AND MODELING METHODS

In this chapter the theory and modeling method of the three-dimensional CFD model of the centrifuge will be elaborated. Firstly in section 2.1 the basic knowledge of centrifugal sedimentation will be presented and the idea of settling velocity, settling time and settling distance will be discussed. The principles for calculate the mass, momentum and energy balance used in the CFD simulation is presented in section 2.2. The information about the selection of turbulence model, numerical solution methods and discrete phase model will be described in section 2.3, 2.4, 2.5 respectively. Some of the unique problems faced in this 3D CFD modeling sedimentation centrifuge will also be discussed, i.e. the rotating reference frame for calculation, viscous models in transition flow region, multiphase model to simulate the separation process, etc.

For all flows, ANSYS FLUENT solves conservation equations for mass and momentum. For flows involving heat transfer or compressibility, an additional equation for energy conservation is solved. For flows involving species mixing or reactions, a species conservation equation is solved. Additional transport equations are also solved when the flow is turbulent. Most of the detailed theory and explanations of Fluent options could be found in the Fluent theory guide and Fluent user's guide. [39, 40]

As mentioned in section 3.1.2 due to the complexity of the geometry of the centrifuge the complete 3D CFD model consists of the five components (sub volumes) from bottom to up includes: impeller chamber, 1st stage plate stack, middle disk, 2nd stage plate stack and outlet chamber. In the model, the fluid dynamic behaviors of flows and multiphase flow has been considered. The conservation equations of mass, momentum, are applied to solve the numerical problem by using the finite control volume method in each computational domain. These partial differential equations are solved using the finite volume method integrated in the software Fluent. Considering the centrifugation process is under normal temperature and pressure without heat or cold source the energy equation is not considered. The particle behavior for the centrifugation separation is based on DPM (Discrete Phase Model) in Fluent.

2.1 Basic theory of centrifugal sedimentation

Sedimentation centrifuges could be used for liquid-liquid, liquid-solid or liquid-liquid-solid (so called three phase) separation.[41] By rotating the process feed fluid in the centrifuge the sedimentation efficiency could be increased by thousands of times. According to Stokes law the settling velocity under gravity could be written as:

$$v_g = \frac{(\rho_P - \rho) d_P^2}{18\mu} g$$

Equation 2-1

It is very clear to see from Equation 2-1 that the settling velocity of the particles under gravity is a fundamental property of a suspension. It is much more easier for the particle to settle quickly if the particle has bigger density difference from the liquid or has bigger size or the liquid has lower viscosity. Easily derived the settling velocity under centrifugal force could be written as:

$$v_c = \frac{(\rho_P - \rho) d_P^2}{18\mu} r \bullet \omega^2$$

Equation 2-2

If the acceleration factor (g number) $G = \frac{r \bullet \omega^2}{g}$ is introduced in the Equation 2-2 become $v_c = \frac{(\rho_P - \rho) d_P^2}{18\mu} G$. It is much easier for centrifuges to separate particle with smaller size and similar density i.e. microalgae which normally wouldn't settle under gravity conditions. The G number for a centrifuge is 500 to 30000 and sometimes to 900000[41]. The Evodos SPT centrifuge G is 3000.

Besides the intrinsic property of settling velocity of gravity and the acceleration factor G of the centrifuge, the settling efficiency also depends on the settling distance and residence time. The small gravitational settling velocity of microalgae demands longer settling time (spinning time), higher g number or shorter settling distance.

As shown in Figure 2-1, for conventional conical disk (bowl disk) centrifuge, the feed suspension flows downward near the shaft and enters the space with several conically arranged disks through the weir near the bottom of the bowl. The light component goes upward and heavy component goes downward between conical disks. Instead of the short settling distance shown in the red straight line the particle follows the spiral shaped green line in 3D rotating around the axis and approaching the upper disk simultaneously. So the actual settling distance is much longer than the desired settling distance.

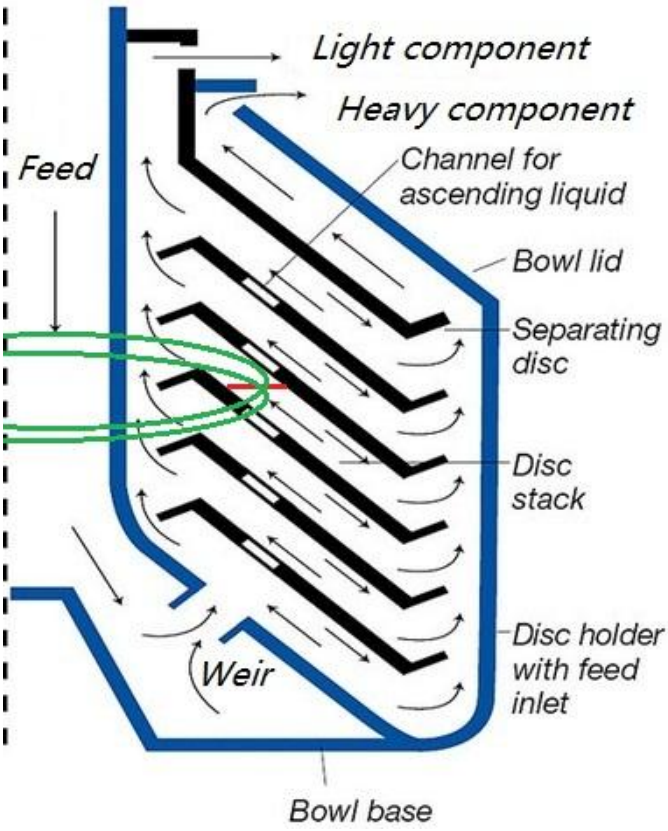

Figure 2-1: Schematic settling distance in conical disk centrifuge (side view)

On the contrary for the ingenious Evodos design shown in Figure 2-2 the settling distance is more or less follow the exactly the distance shown in green color between two vertically arranged parallel plates as indicated in the schematic settling distance in Evodos SPT centrifuge. In later CFD modeling results the visualized particle trajectory clearly shown the similar 3D settling distance which is significantly shorter compare to the conical disk centrifuge. The particle trajectory also conforms well with the desired design. Therefore the 3000G Evodos design can provide the same sedimentation efficiency compare to conventional conical disk centrifuge with 20000G.

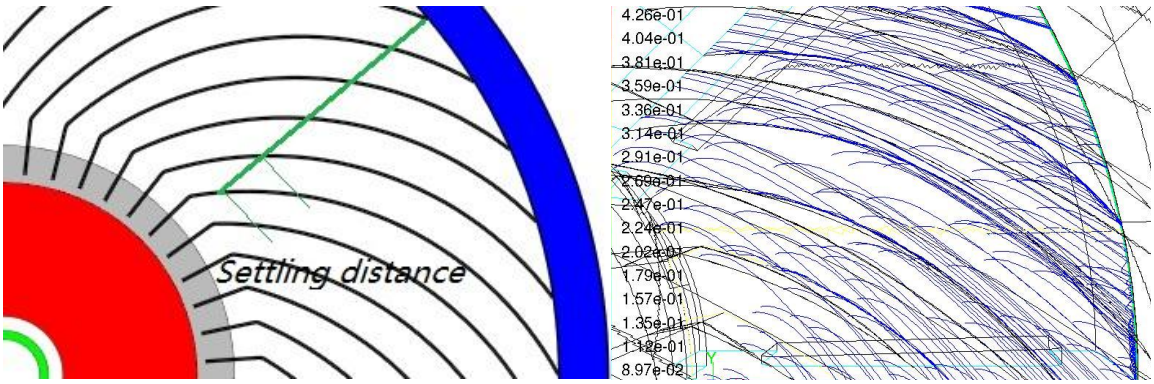

Figure 2-2: Schematic settling distance in Evodos SPT centrifuge (left, top view) and particle trajectory visualization result CFD modeling (right, top view)

2.2 Conservation equations for simulation

2.2.1 Mass conservation equation

For fluid dynamic mass conservation equation or continuity equation for fluid could be generally written as:

$$\frac{\partial(\rho)}{\partial t} + \nabla\bullet(\rho\,\vec{v}) = s_m$$

Equation 2-3

Where,

ρ is the density of the liquid [kg/m³]

t is time in a non-steady state way [s]

$\vec{v}$ is the liquid velocity vector [m/s]

∇ denotes the divergence operator of vector. The divergence is defined as:

$$\nabla\bullet\vec{v} = \frac{\partial v_1}{\partial x} + \frac{\partial v_2}{\partial y} + \frac{\partial v_3}{\partial z}$$

s_m is source term for mass source or sink [kg/m³-s]

The liquid flow rates in the flow channel does not change along the flow path through the entire centrifuge. The liquid flow is incompressible, and the source term is 0 for this simulation (i.e. no evaporation of droplet etc.) the mass conservation equation for the non-steady state (transient) liquid can be expressed as:

$$\frac{\partial(\rho)}{\partial t} + \nabla \cdot (\rho \vec{v}) = 0$$

Equation 2-4

Then, the term on the left-hand side represents the time dependent total mass flow through the surface of control volume divided by the volume. The right hand side present additional mass sources which is zero in this model.

2.2.2 Momentum conservation equation

Conservation of momentum in an inertial (non-accelerating) reference frame could be generally described as:

$$\frac{\partial(\rho\vec{v})}{\partial t} + \nabla\bullet\left(\rho\vec{v}\vec{v}\right) = -\nabla P + \nabla\bullet\tau_s + \rho\vec{g} + \vec{F}$$

Equation 2-5

In this equation, the term at left-hand side represents the momentum accumulation and net flux momentum through the surface of control volume. ρ represents the density of the liquid, P is the static pressure, τ_s is the stress tensor, $\vec{g}$ is the gravitational acceleration and $\vec{F}$ is the external body force or model dependent momentum source term could be defined in UDF. In this simulation the external body force is the centrifugal force caused by the rotation of the centrifuge without additional model based momentum sources.

In the Equation 2-5, the third term on the right-hand side is the gravitational body force effect. While, the first term on the right-hand side express the gradient of pressure which represents the effect of pressure in the control volume. $\nabla\bullet\tau_s$ expresses the viscosity effect of momentum in the control volume, which is:

$$\tau_s = \mu\left(\nabla\vec{v} + \nabla\vec{v}^T\right) - \frac{2\mu}{3}\nabla\bullet\vec{v}$$

Equation 2-6

Where, μ is the viscosity of the liquid, the first term on the right-hand side represents the tensor due to velocity and the second term is the effect of volume dilation.

2.2.3 Energy conservation equation

The energy conservation equation could be generally written as:

$$\frac{\partial(\rho E)}{\partial t} + \nabla\bullet\left(\rho\vec{v}E\right) + \nabla\bullet\left(p\vec{v}\right) = \nabla(k\nabla T) + \nabla\bullet(\tau_s\bullet\vec{v}) + S_e$$

Equation 2-7

In this equation above, the term at left-hand side represents the energy accumulation and net flux energy with mass flow through the surface of control volume. The third term on the LHS represent the flow work. The second and third term could be combined and rewritten as the enthalpy flux with flow $\nabla\bullet\left(\rho\vec{v}H\right)$. On the RHS the first term is the heat transfer through heat transfer coefficient *k* and temperature T ingredient. The second term on the RHS is the dissipation energy by viscosity. ρ represents the density of the liquid, p is the pressure, τ_s is the stress tensor

and S_e is the energy source term which is zero in inert particle separation in this model.

The temperature change and heat transfer of fluid in the centrifuge has no significant impact on the flow field and not studied for the separation process. Therefore the energy conservation equations will not be considered during this entire simulation.

2.2.4 Rotating reference frame and 3D rotating flows

Due to the nature of the constant rotating centrifuge (and the fluid rotates together with the centrifuge) a single moving reference frame is used instead of a stationary (inertial) frame. It is possible to transform the equations for fluid motion steadily rotating frame (the rotational speed is constant) into the rotating frame. Changing rotating frame could also be modeled using UDF in Fluent.

ANSYS FLUENT permits the activation of a moving reference frame with a steady rotational speed which is the case in this model. If the rotational speed is not constant, the transformed equations will contain additional terms which are not included in ANSYS FLUENT's formulation (although they can be added as source terms using user-defined functions). The details about the moving reference frame capabilities in ANSYS FLUENT could be found in the chapter 10 Fluent User's Guide.[40]

The fluid velocities can be transformed from the stationary frame to the rotating frame using the following relation:

$$\vec{v} = \vec{v}_r - \vec{u}_r$$

Equation 2-8

With, $\vec{v}$ is the absolute velocity (the velocity viewed from the stationary frame), $\vec{v}_r$ is the relative velocity (the velocity viewed from the rotating frame), $\vec{u}_r$ is the "whirl" velocity (the velocity due to the moving frame $\vec{u}_r = \vec{\omega} \times \vec{r}$) and $\vec{\omega}$ is the axis of rotation vector defined by rotational speed ω times a unit direction vector $\hat{a}$, $\vec{\omega} = \omega \hat{a}$.

Than the above mentioned mass conservation equation and momentum conservation equation could be formulate and calculate in absolute and relative velocities. The relative velocity formulation are shown as the following equations:

Mass conservations equation:

$$\nabla \bullet (\rho \vec{v}_r) = 0$$

Equation 2-9

Momentum conservations equation:

$$\frac{\partial (\rho \vec{v}_r)}{\partial t} + \nabla \bullet \left(\rho \vec{v}_r \vec{v}_r \right) + \rho (2\vec{\omega} \times \vec{v}_r + \vec{\omega} \times \vec{\omega} \times \vec{r}) = -\nabla P + \nabla \bullet \tau_s + \vec{F}$$

Equation 2-10

The two additional acceleration terms are the Coriolis acceleration $2\vec{\omega} \times \vec{v}_r$ and the centrifugal (centripetal) acceleration $\vec{\omega} \times \vec{\omega} \times \vec{r}$.

Energy conservations equation:

$$\frac{\partial(\rho E_r)}{\partial t} + \nabla\bullet\left(\rho\vec{v}_r H_r\right) = \nabla(k\nabla T) + \nabla\bullet(\tau_s\bullet\vec{v}_r) + S_e$$

Equation 2-11

E_r is the relative internal energy and H_r is the relative total enthalpy.

$$H_r = E_r + \frac{p}{\rho} = h + \frac{1}{2}(\vec{v}_r^2 - \vec{u}_r^2)$$

Equation 2-12

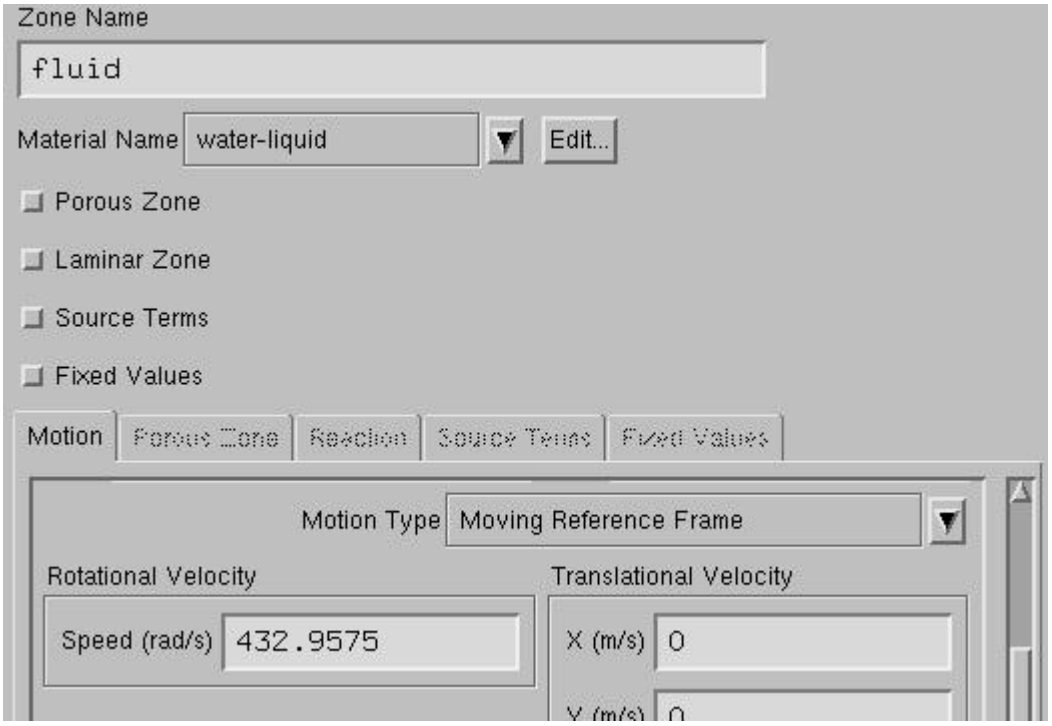

Figure 2-3: Moving reference frame options in Fluent

The above Figure 2-3 shows the moving reference frame options for fluid zone in Fluent. A steady rotational velocity of 432.9575 rad/s, representing 4500rpm, must be given for the simulation. It is worth to mention that for a quicker and better simulation solution it is advised to run the model first in a smaller rotational velocity and increase it to the desired rotational velocity step by step.

2.3 Turbulence model

Microalgae culture is a liquid with a concentration of approximately 3g/L concentration of microalgae and water. It could be treated as an incompressible Newtonian viscous liquid. And for viscous liquid the flow regime could be laminar or turbulent depending the dimensionless Reynolds number Re. The Reynolds number Re gives an indication of the ratio between inertial forces and viscous forces and consequently quantifies the relative importance of these two types of forces for given flow conditions.

Overall Reynolds number estimation:

For flow in a pipe of diameter D, experimental observations show that for "fully developed" flow, laminar flow occurs when $Re_D < 2300$ and turbulent flow occurs when $Re_D > 4000$. In the interval between 2300 and 4000, laminar and turbulent flows are possible ('transition' flows), depending on other factors, such as pipe roughness and flow uniformity). The result could be generalized to non-circular channels using the hydraulic diameter, allowing a transition Reynolds number to be calculated for other shapes of channel.[42]

For the Evodos STP centrifuge the Re number of flow between the flow channels inside the parallel plate flow path could be estimated by the calculation of the hydraulic diameter.

For flow in a pipe or tube, the Reynolds number is generally defined as:

$$\mathrm{Re} = \frac{\rho v D_H}{\mu} = \frac{v D_H}{\nu} = \frac{Q D_H}{\nu A}$$

Equation 2-13

where:

D_H is the hydraulic diameter of the pipe; its characteristic length $D_H = D_o - D_i$, [m]

Q is the volumetric flow rate [m³/s]

A is the centrifuge cross-sectional area [m²]

v is the mean velocity, , of the object relative to the fluid [m/s]

μ is the dynamic viscosity of the fluid [Pa·s or N·s/m² or kg/(m·s)]

ν is the kinematic viscosity ($\nu = \mu / \rho$) [m²/s]

ρ is the density of the fluid [kg/m³]

By using the relevant values from for the centrifuge D_H is 0.184 m, Q is 0.083 m³/s, A is 0.256 m² and water as working fluid with a dynamic viscosity μ of 1 cP the Re of Evodos centrifuge could be estimated below 2000.

The Re number could also be observed during the complete simulation. The flow regime is regarded as laminar in between parallel plates and transitional in the middle disk and outlet chamber. Stronger turbulent at certain locations inside the impeller chamber has been observed from the simulation results. Therefore to select a suitable turbulence model instead of laminar simulation is necessary for the CFD model. It is also supported by literature study that turbulent model is used in similar CFD simulations.

Turbulence model selection:

The turbulent flow is a flow regime characterized by recirculation, eddies, and randomness or chaotic behavior. This includes low momentum diffusion, high momentum convection, and rapid variation of pressure and velocity in space and time.[39] To simulate turbulence in the Fluent 3D CFD model turbulence model need to be used instead of the computationally expansive instantaneous (exact) governing equation. Various turbulence model has been developed using time or ensemble averaged equations to make the model less demanding. Figure 2-4 shows a list of viscous model options available in the Fluent software and their relevant parameters from inviscid flow to large eddy simulation.

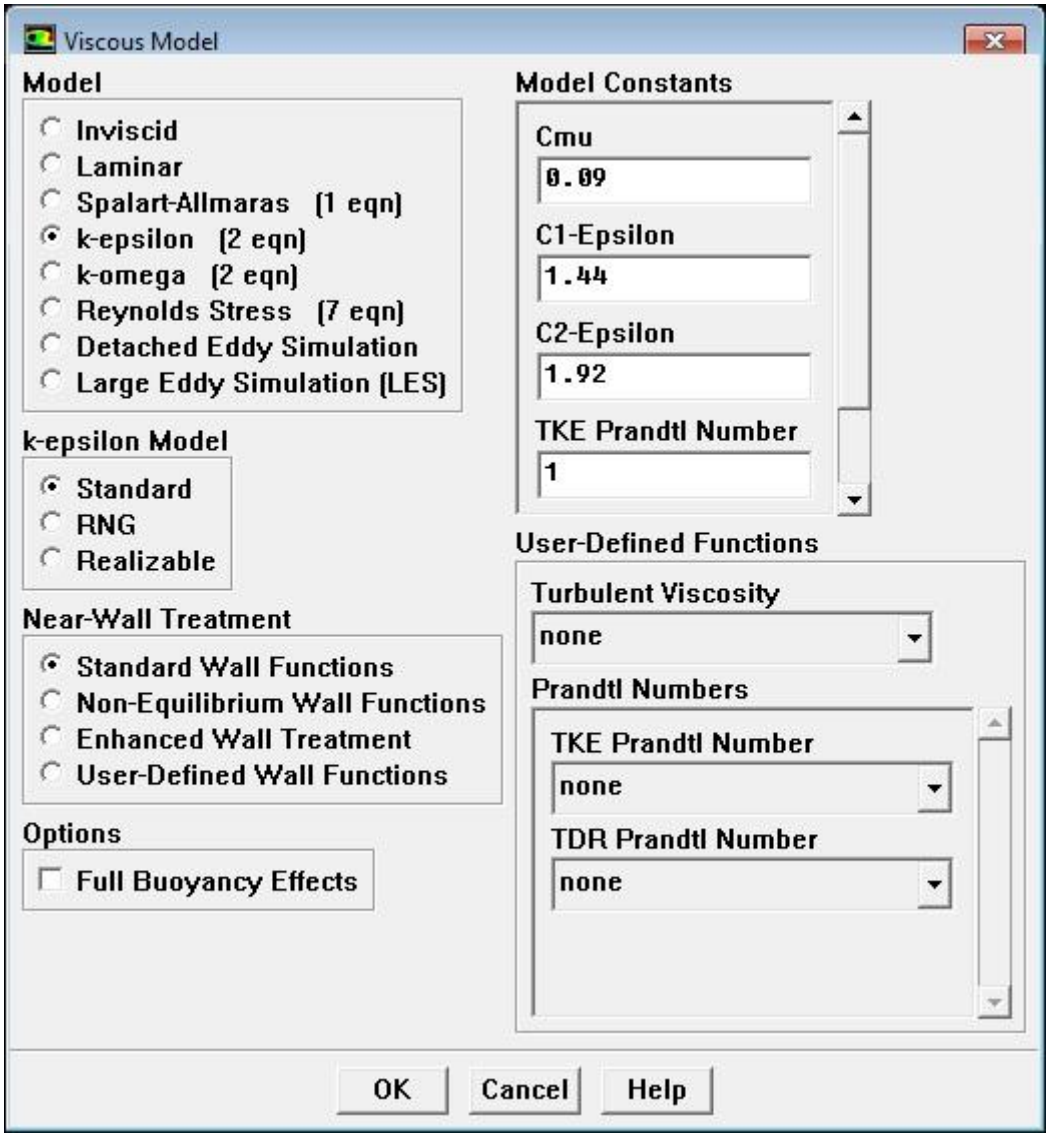

Figure 2-4: Viscous model options in Fluent

But it is a fact that no single turbulence model is universally accepted as being superior for all classes of problems. The choice of turbulence model will depend on considerations such as the physical reality around the flow, the established practice for a specific problem, the level of accuracy required, the available computational resources, and the amount of time available for the simulation. To make the most appropriate choice of model for the application, it is necessary to understand the capabilities and limitations of the various options.[39]

The purpose of choosing turbulence models provided in Fluent is to find the most suitable model that fits the physical reality and gives reliable results. The computational cost in terms of CPU time and memory of the individual models will also be considered. While it is impossible to state which model is best for a specific application, general guidelines are presented to show the advantages of each model.

Selected turbulence model:
In the simulation three different turbulent models has been considered according to literature, physical relevance to the problem and simulation results. The k-ε model with renormalization group (RNG), transition Shear-Stress Transport (SST) k-ω model and the Reynolds stress model (RSM).

The k-ε model needs two additional transport equations, one for the turbulent kinetic energy, k, and another one for the turbulence dissipation rate, ε, to model the turbulences. The advantage of this approach is the relatively low computational cost, but it assumes that the turbulences are isotropic, which is not strictly true. The k-ε RNG, an extension of the standard k-ε model, takes into account the effect of swirl on turbulence, enhancing a higher accuracy for swirling flows which is significant for the centrifuge problem. This model is more reliable for a wider class of flows than the standard k-ε model.

Comparable with the k-ε model the standard k-ω model is an empirical model based on two model transport equations for the turbulence kinetic energy (k) and the specific dissipation rate (ω), which can also be thought of as the ratio of the turbulence dissipation rate, ε to k.[39] The low Reynolds number correction has also been considered. The transition Shear-Stress Transport (SST) k-ω model has incorporated different near wall formulation with far field formulation. A turbulent viscosity calculation has also been modified. The transport equation has also been changed to accommodate transition flows. These features make the SST k-ω model more accurate and reliable for a wider class of flows (e.g., adverse pressure gradient flows, airfoils, transonic shock waves) than the standard k-ω model.

The RSM solves transport equations for each of the terms in the Reynolds stress tensor, st, and, in addition, an equation for the turbulence dissipation rate. This means that five additional transport equations are required in 2D flows and seven additional transport equations must be solved in 3D. The RSM is clearly superior for situations in which the anisotropy of turbulence has a dominant effect on the mean flow, such as highly swirling flows. However, the expensive computational cost of the RSM is often unaffordable.

Although the k-ω model could be regarded as a modified version of a k-ε model, it is rarely seen in literature that k-ω model has been used. One the other hand several test runs for RSM model has been conducted during the model development phase. The result does not show significant difference in flow pattern, pressure and velocity profile or improvements in convergence. The Shear-Stress Transport (SST) k-ω model is taken as the selected turbulence model for the complete model. From the result of simulation these turbulence model works fine with this simulation.

2.4 Numerical solution methods

Fluent has two types of numerical solution methods pressure based solver and density based solver. Historically speaking, the pressure-based approach was developed for low-speed incompressible flows, while the density-based approach was mainly used for high-speed compressible flows. [39] In this project pressure solver is more suitable for a 3D flow simulation in the centrifuge.

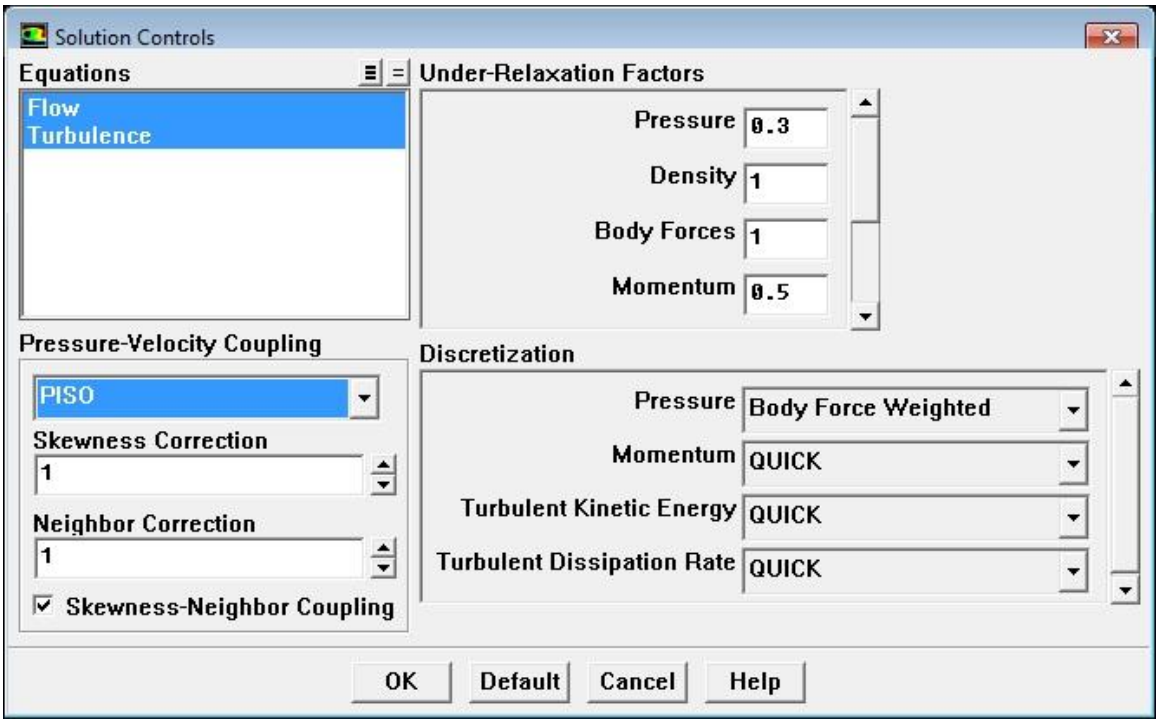

Figure 2-5: Solution control options in Fluent

There are also various solver control options in the pressure solver. As shown in above Figure 2-5 the solution control options has to be determined before the simulation. The pressure-velocity coupling method, under-relaxation factors and discretization method is parameter for the solver.

Pressure based solution with coupling:

Unlike the density solver which solves the governing equations of continuity, momentum, energy and species transport simultaneously (i.e., coupled together). In the pressure solver the velocity field is achieved by solving a pressure (or pressure correction) equation. The pressure equation is derived from the continuity and the momentum equations in such a way that the velocity field, corrected by the pressure, satisfies the continuity. The pressure-based solver uses a solution algorithm where the governing equations are solved sequentially (i.e., segregated from one another). Because the governing equations are non-linear and coupled, the solution loop must be carried out iteratively in order to obtain a converged numerical solution. A typical pressure-based coupled algorithm in Fluent is show below in Figure 2-6.

The Pressure-Implicit with Splitting of Operators (PISO) pressure-velocity coupling scheme has been chosen for the pressure velocity coupling algorithm. PISO algorithm is part of the SIMPLE and SIMPLEC algorithm family and performs two additional corrections: neighbor correction and skewness correction. Those two correction allows better performance under transient conditions and complex geometry conditions (higher screwness for grid cells). Those two corrections is particularly useful for solving this simulation because of the complexity of the geometry and highly curved flow channels of the model.

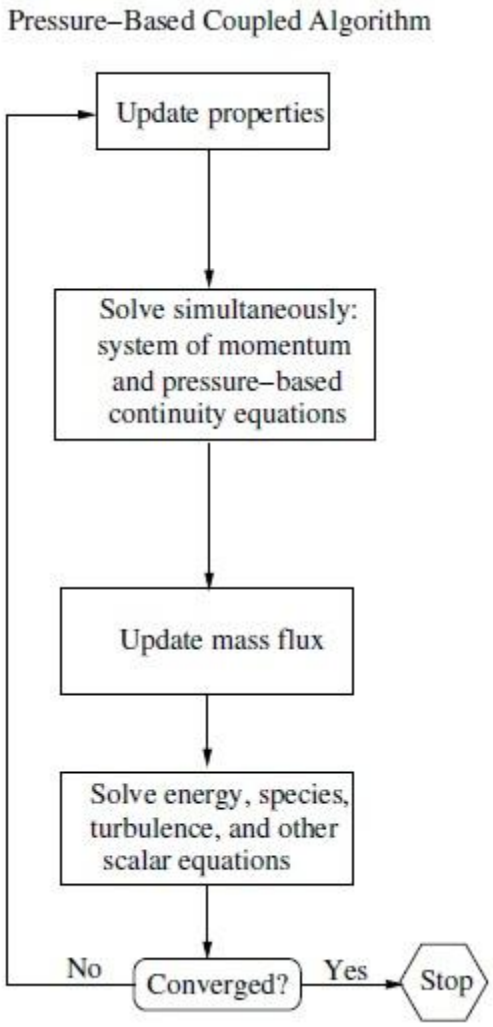

Figure 2-6: Overview of the pressure-based coupled algorithm solution[39]

Discretization method:

The Finite Volume Method (FVM) is one of the most versatile discretization techniques used in CFD, values are calculated at discrete places on a meshed geometry. In the finite volume method, volume integrals in a partial differential equation that contain a divergence term are converted to surface integrals, using the divergence theorem. These terms are then evaluated as fluxes at the surfaces of each finite volume. Conservation laws applied to those fluxes.

FLUENT uses a control-volume-based technique (FVM) to convert a general scalar transport equation to an algebraic equation that can be solved numerically. This control volume technique consists of integrating the transport equation about each control volume, yielding a discrete equation that expresses the conservation law on a control-volume basis. The scalar is including energy, species, turbulence, etc.. The scalar transport equation could be roughly expressed as the accumulation of the scalar plus the convection term is equal to the sum of the diffusion term and source term of the scalar.

$$\int_V \frac{\partial \rho \phi}{\partial t} dV + \oint \rho \phi \vec{v} \bullet d\vec{A} = \oint \Gamma_\phi \nabla \phi \bullet d\vec{A} + \int_V S_\phi dV$$

Equation 2-14

Where,

ϕ is a scalar quantity

ρ is density

$\vec{v}$ is velocity vector

$\vec{A}$ is surface area vector

Γ_ϕ is diffusion coefficient for scalar ϕ

$\nabla\phi$ is gradient of scalar ϕ

S_ϕ is source of scalar ϕ per unit volume

Discretization of Equation 2-14 on a given cell could be written as:

$$\frac{\partial \rho \phi}{\partial t} V + \sum_{f}^{N_{faces}} \rho_f \vec{v}_f \phi_f \bullet \vec{A}_f = \sum_{f}^{N_{faces}} \Gamma_\phi \nabla \phi_f \bullet \vec{A}_f + S_\phi V$$

Equation 2-15

Where,

N_{faces} is number of faces enclosing cell

V is cell volume

ϕ is a scalar quantity

ϕ_f is the value of scalar ϕ convected through face f

$\rho_f \vec{v}_f \phi_f \bullet \vec{A}_f$ is the mass flux through the face f

Γ_ϕ is diffusion coefficient for scalar ϕ

$\nabla\phi_f$ is gradient of scalar ϕ at face f

S_ϕ is source of scalar ϕ per unit volume

The discretization also applies to cells spatially. Fluent stores discrete values of the scalar - at the cell centers (c0 and c1 in Figure 2-7). However, face values -f are required for the convection terms in above mentioned Equation 2-15 and must be interpolated from the cell center values.

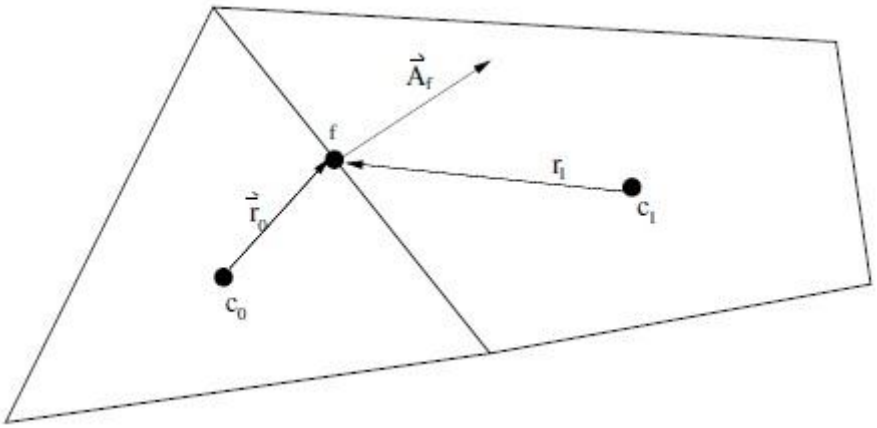

Figure 2-7: Control Volume Used to Illustrate Discretization of a Scalar Transport Equation[39]

Different discretization options such as, First-Order Upwind Scheme, Second-Order Upwind Scheme, QUICK, ect. deals with how the value ϕ_f , scalar ϕ value convected through face f, is being calculated. In this simulation PISO has been selected for pressure-velocity coupling and 1st order upwind spatial discretization scheme is mostly used for momentum, turbulent kinetic energy and turbulent dissipation rate etc.

2.5 Modeling the multiphase fluid: discrete phase model

Two-phase flow is the interacting flow of two phases (gas-liquid, liquid-liquid or three phases) where the interface between the phases is influenced by their motion. The sedimentation of microalgae particle from water in the centrifuge could be regarded as multiphase flow process. The fluid and microalgae particle behave differently in the flow field.

There are two approaches to model the multiphase fluid, namely, the Euler-Lagrange approach and the Euler-Euler approach. The name Euler-Lagrange and Euler-Euler indicates the how the dynamic of the multiphase fluid (liquid phase and solid particle phase) is being handled.

Both Lagrangian and Euler specification is a way to describe the flow filed using mathematical formulations. The Lagrangian specification describes fluid motion where the observer follows an individual fluid parcel as it moves through space and time. It is often visualized as sitting in a boat and drifting down a river. Plotting the position of an individual parcel through time gives the pathline of the parcel. On the other hand the Eulerian specification of the flow field regard the fluid motion on specific locations in the space through which the fluid flows as time passes. This can be visualized by sitting on the bank of a river and watching the water pass a fixed point.

Selection of the multiphase approach:

In the Euler-Euler approach, the different phases are treated mathematically as interpenetrating continua. Since the volume of a phase cannot be occupied by the other phases, the concept of phasic volume fraction is introduced and each phase has its own phasic volume fraction. In the Euler-Euler approach both liquid and microalgae particles will be treated as fluid.

There are three different Euler-Euler multiphase model available in Fluent. VOF model, mixture model and Eularian model.

The Volume of Fluid (VOF) model is a tool to study the interface between two fluids i.e. slug flow, free surface flow, transient tracking of gas liquid interface i.e. air/water interface. A single set of momentum equations is solved for the entire system and the volume fraction of each phase is tracked within each computational cell. There is a rotating air core and air-liquid interface along the axis of the rotor during the centrifugation operation in Evodos SPT centrifuge, as mentioned in section 3.1.1, which is suitable for VOF but add more complexity to the model. The volume fraction and effect of air core could be neglected during simulation. Another disadvantage to consider VOF model for gas-liquid interface is excessive computing time consumption. According to literature transient VOF solution often take days even weeks to form a quasi-steady state solution[30, 31]. Introducing VOF calculation to a model of this scale will need even bigger computing power and longer times.

The mixture model is similar to a VOF model solves for a single set of mixture momentum equation and prescribes relative velocities to describe the dispersed phases .

The Eularian model solves a set of n momentum and continuity equations for each phase. [39] It has been mentioned in the Fluent theory guide that for particle laden flow with a volume fraction

above 10% use mixture or Eularian model. Also the Eularian model is suitable for sedimentation flow.

All of the above mentioned Euler-Euler approaches have been carried out and tried during the beginning of modeling development process but none of them gave desirable results especially for transient conditions. The reason is due to the complexity of the geometry and unavoidable reverse flow at the inlet and outlet.

More over the project has particular interest in the particle behavior and particle separation efficiency based on different particle sized. Therefore according to available literature DPM has been applied to track particle and predict particle studies for centrifugal flows. [30, 33, 37, 43]

DPM:

The Euler-Lagrange approach treat the liquid phase as continuum with Euler specification and algae or starch particle phase as dispersed particles in Lagrange specification. The Fluent Lagrangian discrete phase model (DPM) follows the Euler-Lagrange approach. The fluid phase is treated as a continuum by solving the Navier-Stokes equations, while the dispersed phase is solved by tracking of particles (or bubbles, droplets etc.) through the calculated flow field of the liquid phase. Fluent predicts the trajectory of a discrete phase particle by integrating the force balance on the particle.

The presence of solid particles was ignored during the simulation of the liquid phase, which is an acceptable assumption for low solid concentrations in either microalgae or starch solutions. Once the flow has converged, a finite number of particles (could be massless, inert or droplet) will be injected into the domain from every grid of inlet surface and their trajectories are calculated with an Euler-Lagrange approach, DPM discrete phase model. The DPM can perform steady state or unsteady no matter the calculation of the continuous phase is steady state or transient (for a numerical reason).23.2.2 [40] The iterative process principle to calculate particle track in DPM cloud be visualized in following Figure 2-8.

In this simulation both coupled and non-coupled calculations has been made. The impact of starch or microalgae particles consisting less than 10% mass fraction (approx. 7% for starch test and 0.3% for algae culture) is not very significant on the overall momentum balance of the continuous phase.

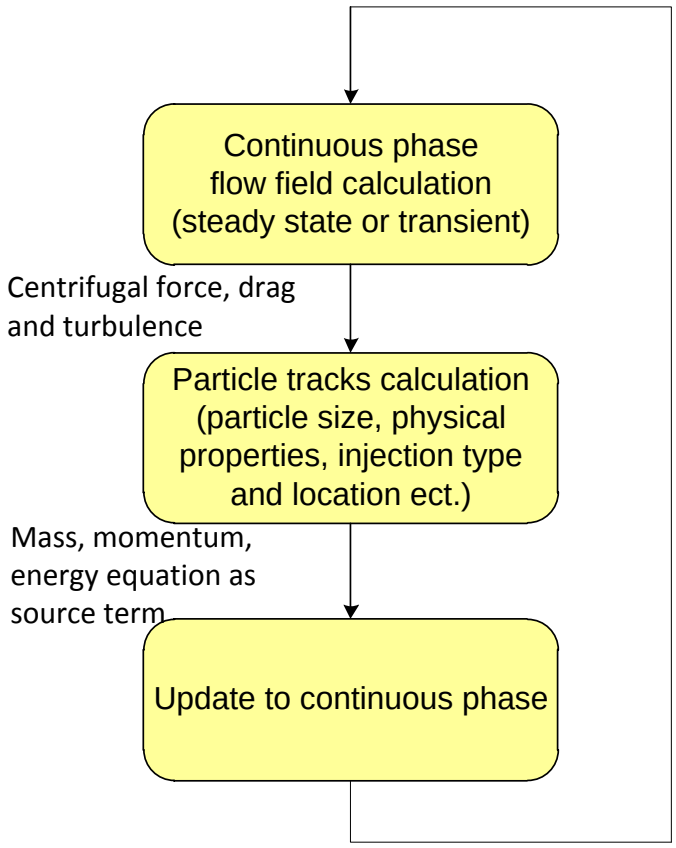

Figure 2-8: Flow chart of how DPM calculation particle track couple with continuous phase

One of the underlining assumption for DPM is the volume fraction of the disperse phase should not exceed 10% of the whole volume although the mass fraction can be large (100%). The typical volume fraction of microalgae in water is less than 0.3% and for starch test the volume fraction of starch particle is less than 5% which is suitable for the application of DPM. Other restrictions in DPM including there should be no particle-particle interaction or break up.

The dispersed phase can exchange momentum, mass, and energy with the fluid phase. Each of the particle trajectories are calculated. The behavior of each particle could be recorded and visualized by Fluent post processor. The turbulent dispersion of individual particle can be modeled in DPM but is not included in this modeling work.

This is the previously mentioned force balance for single particle:

$$\frac{d\vec{V}_P}{dt} = F_D\left(\vec{v} + \vec{v}_P\right) + \frac{g(\rho_P - \rho)}{\rho_P} + F_x / \rho_P$$

Equation 2-16

In Equation 2-16, $\vec{v}$ and ρ are the fluid velocity and fluid density, respectively, and $\vec{v}_P$ and ρ_P the particle velocity and particle density, respectively. The first term on the right hand side is the drag force per unit of mass F_D, the second term is the gravitational force and the third term is additional force which is including the rotational force. The rotational force consist of centrifugal force and Coriolis force, which arises in the moving reference frame. The other additional force

i.e. Brownian force, thermo-phoretic force and Saffman's lift force is comparably insignificant and neglected during simulation. The drag force could be express as:

$$F_D = \frac{18\mu}{\rho_P d_P^2}\frac{C_D \mathrm{Re}}{24}$$

Equation 2-17

Where, μ is the molecular viscosity of the fluid, ρ_P is the density of the particle, and d_P is the particle diameter. A drag coefficient C_D for spherical particles described by Morsi and Alexander [39] was chosen for the drag force. Re is the relative Reynolds number, which is defined as:

$$\mathrm{Re} = \frac{\rho d_P |v_P - v|}{\mu}$$

Equation 2-18

The model computes the trajectory of inert particles (for microcalgae and starch particle) released from each grid center of the desired inlet surface by integrating the force balance Equation 2-16 until they reach the bowl wall or leave the flow field. There are basically four interaction types between particles and boundaries shown in Figure 2-9. Escape, as the particles leave the domain via the designed (pressure) outlet surface; Reflect, as the particles bounce back from the wall; Trap, as the particles retained by striking some part of the spiral plate or outer rim of the drum wall; and incomplete as the complete trajectory of the particles is hard to calculate inside the flow field. In FLUENT most of the wall faces have been set as reflect while some certain wall faces i.e. the outer rim of the drum have been set as trap surface.

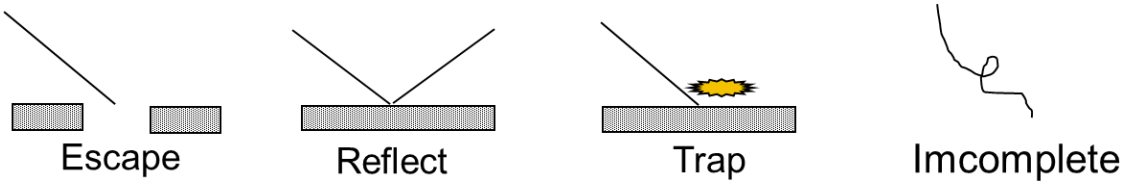

Figure 2-9: Type of fates of particles in DPM calculation

The fate of each individual particle could be tracked, visualized, counted and summarized by FLUENT. In section 4.5 the DPM simulation result for separation efficiency for different particle size will be presented.

This chapter has talked about the theory behind the CFD modeling tool Fluent and different options used in the model. The basic sedimentation centrifuge principles is presented in section 2.1. The theory behind calculate the mass, momentum and energy balance used in the CFD simulation has been briefly described in section 2.2 while the turbulence model, numerical solution methods and discrete phase model have been shown in section 2.3, 2.4, 2.5 respectively.

In the next chapter the geometry of model and boundary conditions for developing the model will be presented in detail. Parameter and condition for solving the model will also be introduced.

CHAPTER 3: MODEL DEVELOPMENT

The geometry of the Evodos SPT centrifuge is very unique and together boundary conditions and other specifications forms an essential part of the Fluent model setup. The geometry and parameters of the model will affect the result of flow field, particle track etc. of the model Results. A brief introduction of the working principle of the Evodos SPT centrifuge could be found in section 3.1.1. The proposed 3D design and general approach of CFD modeling methods are also shown in section 3.1.2 and 3.1.3.

Section 3.2 of this chapter will present the complete geometry model of the centrifuge and the information on meshing of the different components. Later the operation conditions, boundary conditions, material properties and mesh interface used in the model will be discussed in section 3.3, 3.4, 3.5 and 3.6. Section 3.7 elaborate on the specifications and parameters used in DPM model. Last but not least solver conditions is presented in section 3.8. The results of the model will be discussed in detail in chapter 4.

3.1 Modeling approach

3.1.1 Evodos SPT centrifuge design

Evodos SPT centrifuge is a belt driven batch type self-balancing pendant separator. Drive head and intermediate drive are mounted in a silencer suspended sub-frame. The drive head carries the hollow main shaft and rotor. The main motor is mounted directly to the machine frame and is connected to the intermediate drive via a flexible shaft.[28] The machine could be hang, mounted or stand along according to process needs. The centrifugation process is semi continuous. The feed and effluent is running continuously while the solid paste is discharged after certain time intervals triggered by the weight sensor in the machine.

The Evodos SPT centrifuge, standing on the ground as shown in the left side of Figure 3-1 consists of a frame, control box, motor, shaft which is hollow to carry feed and effluent from feed inlet and inner/outer outlet, sliding inner drum, splash screen and discharge bin to collect solid discharge. A schematic of the components inside the drum with the sliding inner drum, hollow shaft, inlet feed slots, two plate stack stages, 2 paring wheels etc. is shown in the right side of Figure 3-1 below.

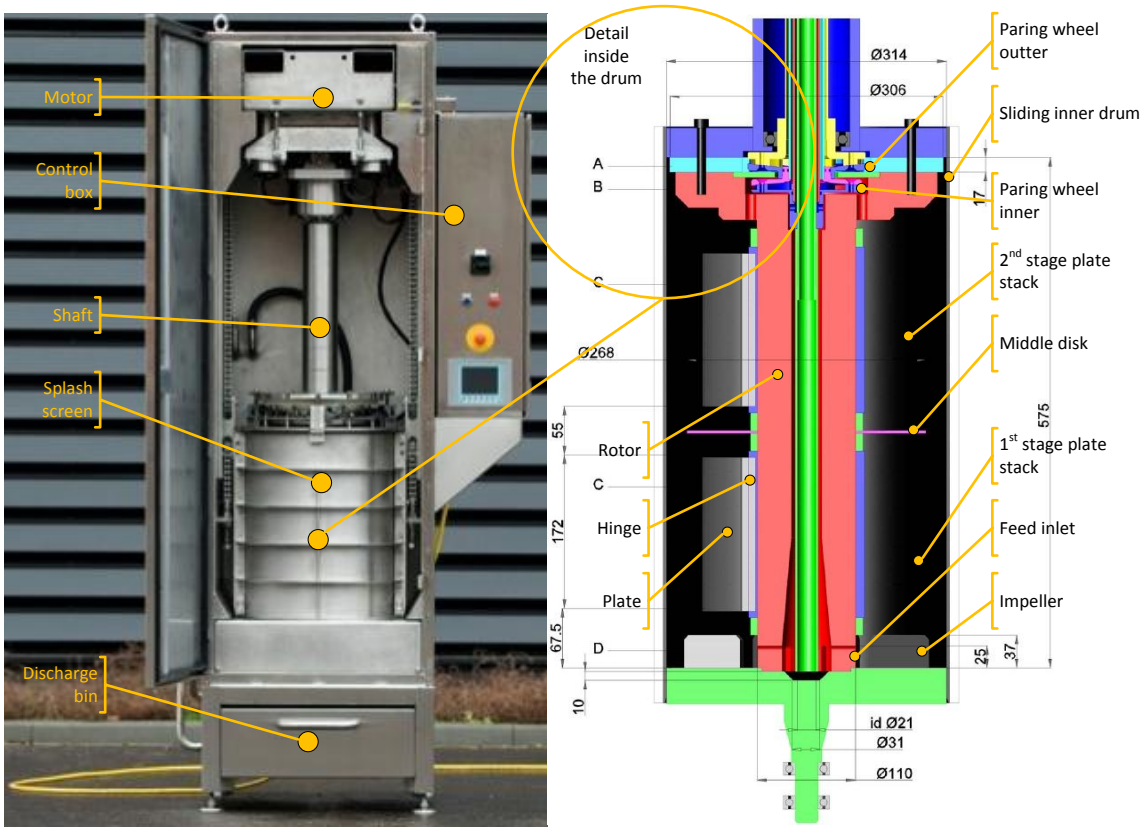

Figure 3-1: Schematic of Evodos SPT centrifuge with key elements of the drum shown

The feed flow is pumped with a frequency-controlled mono-pump by at a pressure slightly higher than the atmosphere pressure. The feed flow enters the centrifuge from the inlet nozzle on the side wall of the frame. The feed enters to the centrifuge drum via the stationary hollow shaft from the top and flows downward. There are 8 rectangular shaped slots at the bottom of the rotor to let the inlet feed flow from the hollow shaft to the impeller chamber. The flow from the stationary hollow shaft will form a jet stream to the drum via 8 rectangular feed inlet slots. During normal operation when the drum is filled with liquid there will be a free surface parallel and very close to the rotating axis.

As shown in Figure 3-2: Schematic of cross section plate stack and spiral plate [28], curved plates (normally with configuration of 40, 80, 120 or 30 90 plates) are hinged to the core (rotor), and rest with their free end touch against the drum. The stationary hollow shaft is in the middle. During spinning the rotor together with plates and sliding inner drum are turning at the same rotational speed of around 4500 rpm and an artificial gravity of 3000G. Two neighboring plates form an enclosed vertical curved flow channel. These channels run almost from bottom to top of the relevant plate stack. In the above shown right side of Figure 3-1 the mixture flows upward along those channels. While passing these channels, the heavier liquid moves away from the axis of rotation, the lighter liquid moves into the direction of the axis. Heavier particles travel away from the axis of rotation and build a layer of compressed solid deposit paste like cake.

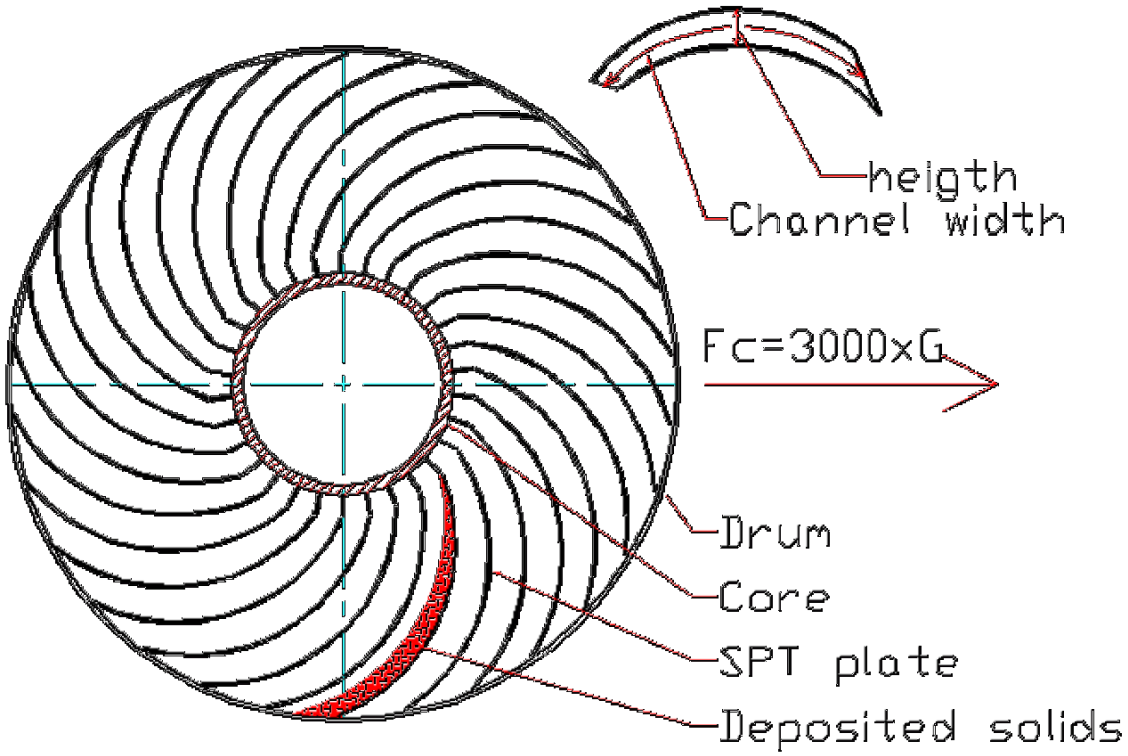

Figure 3-2: Schematic of cross section plate stack and spiral plate

The flow coming out of the 1st stage plate stack will be mixed at the top end. A middle disk is used to divert the flow inside the centrifuge and introduce the flow to the outer rim of the 2nd stage plate stack. This special configuration of the middle disk is to divert the flow to the large centrifugal force area when the flow enters 2nd stage plate stack.

The effluent of the centrifuge is discharged via the inner and outer outlet at the top of the drum via two stationary paring wheels. Figure 3-3: Cross section A (left) and B (right) showing outer and inner paring wheels. The effluent to the inner paring wheel will come through 12 ϕ12mm weirs and effluent to the outer paring wheel will come through the channel between 12 guided vanes(cyan color). The stationary paring wheel converts the kinetic energy of the outlet flow to pressure of the effluent. For liquid/liquid/solid three phase separation the light component will be discharged via the inner outlet and the heavier component will be discharged via the outer outlet. Before discharging the consolidated cake, the remaining liquid is pumped out of the drum via the supply tube.

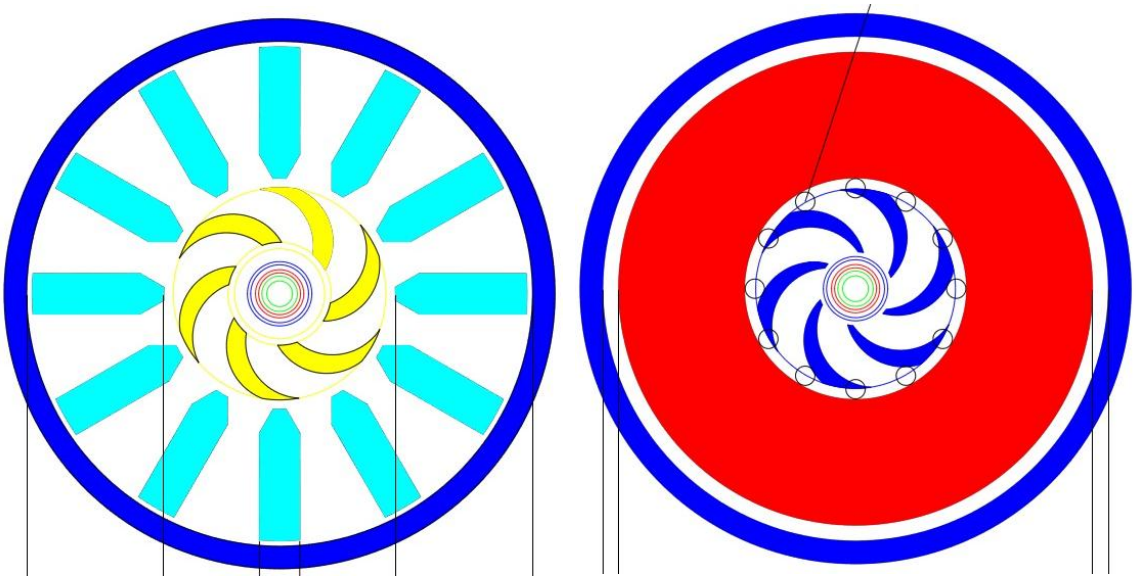

Figure 3-3: Cross section A (left) and B (right) showing outer and inner paring wheels

The collected cake will be removed at intervals. During solid cake discharge the sliding inner drum is moved upward and downwards via a lift with a grabber. The rotor is still turning and the hinge is change to open position and the cake is spinned off from the plates to the splash screen. The discharged material will be removed by the scraper, at the outside of the sliding inner drum, from the splash screen to the discharge bin during its downward stroke. The patented method to discharge the collected material leads to high dry solid content of the discharged material.

The maximum volume of collected cake per discharge is fixed by the dimension of the drum. The number of discharge cycles per hour is determined by feed flow, type of feed and other operating conditions. The collected cake may be discharged in a discharge bin, a big-bag or on a conveyor adapted to downstream process needs. Figure 3-4 has shown nanochloropsis culture from microscope and the final solid discharge cake from Evodos STP centrifuge. It is clear to see that very high concentration factor has been achieved.

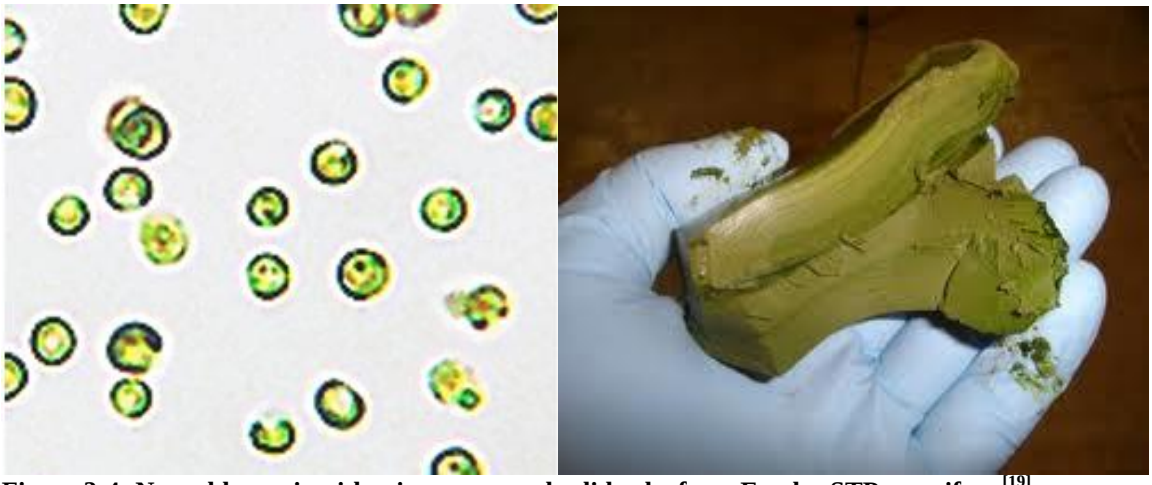

Figure 3-4: Nanochloropsis with microscope and solid cake from Evodos STP centrifuge[19]

3.1.2 Proposed centrifuge geometry 3D model design

The 3D geometry model of the flow channel of the Evodos SPT centrifuge will be made by the Fluent pre-processor GAMBIT and contains the geometry of feed inlet, impeller chamber, 1st stage plate stack, middle disk, 2nd stage plate stack to the inner outlet and outer outlet. The flow channel between hollow shaft via rotor to the feed inlet, inner paring wheel and outer paring wheel will not be modeled because the major focus of the project is to understand the flow field

There are several unique aspects of the model need to be clarified for the proposed geometry 3D GAMBIT centrifuge model design. The first is due to the asymmetrical nature of the centrifuge and improving computing speed, (less grid number therefore less computing power) only 1/8 of the complete geometry will be modeled. The complete flow field will be derived from the 1/8 model results. The second aspect is due to the meshing capabilities of the GAMBIT and the complexity of the geometry, the complete model geometry cannot be meshed in a single volume. Five distinct and simpler component (sub volumes) have been divided according to their functions and meshed respectively. The complete model mesh will be connected using the Fluent "grid interface" function to calculate the non-conformal mesh boundaries(detailed methods could be seen in Fluent users guide [40] 6.4.1 to 6.4.4. As mentioned above the five sub volumes are feed inlet, impeller chamber, 1st stage plate stack, middle disk, 2nd stage plate stack to the inner outlet and outer outlet. Last but not least a rotating reference frame has been used to simulate the rotation and artificial gravity field in the centrifuge.

The detailed description of complete geometry model will be presented in chapter 3.2 Complete 1/8 geometry model. A schematic of the proposed design 3D GAMBIT geometry model and the divide of sub volume is shown below in Figure 3-5.

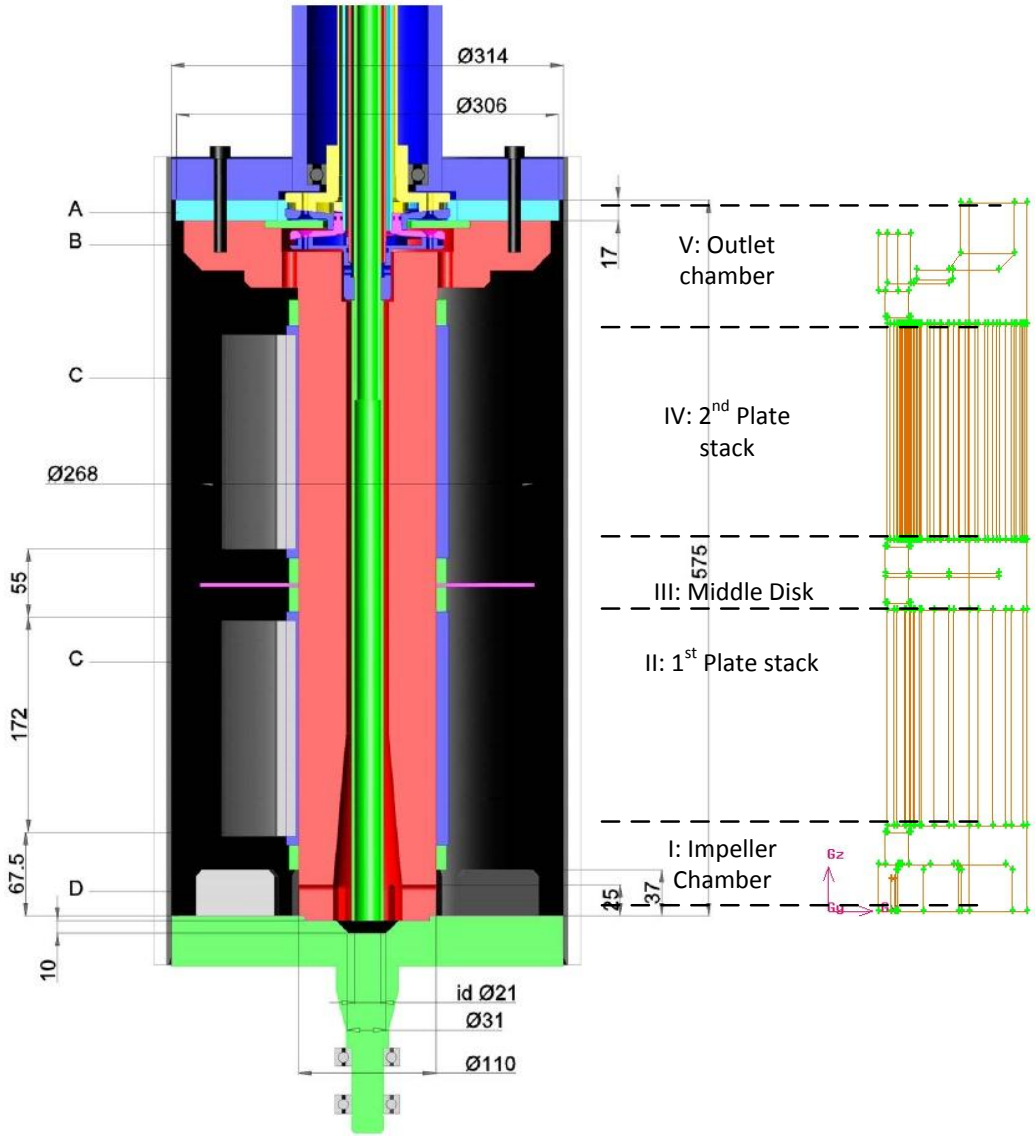

Figure 3-5: Proposed design 3D GAMBIT geometry model and the divide of sub volume

3.1.3 General approach for CFD modeling method

The modeling of the 3D CFD model of the parallel plate centrifuge has been done with the world-wide used commercial software package Fluent™. Fluent is a general-purpose CFD software that could be used in a wide range of industrial applications.

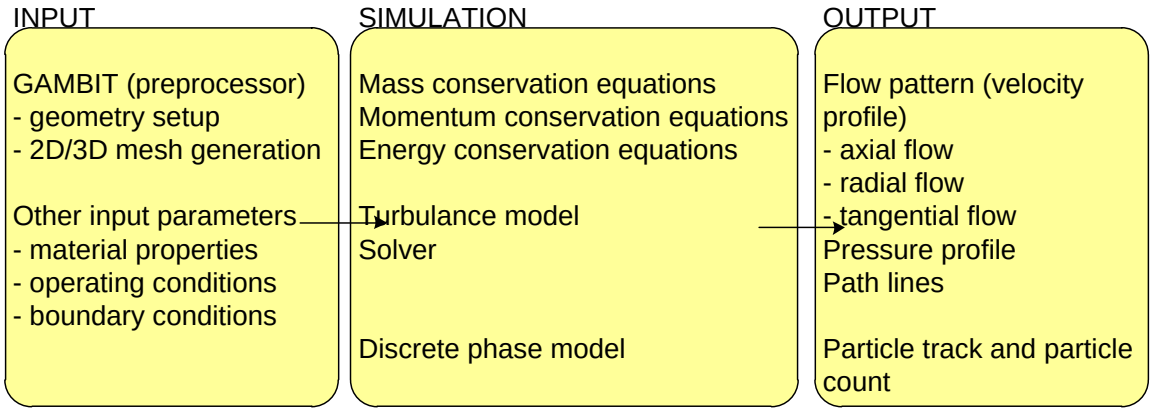

Figure 3-6: General approach for Fluent CFD modeling of this project

Figure 3-6: General approach for Fluent CFD modeling of this project represents the general modeling method with input and output variables for the simulation of Evodos SPT centrifuge. For Fluent simulation the geometry of the model has to be setup and converted to 2D/3D mesh using GAMBIT, the build in preprocessor of Fluent. The know inputs are material properties of both liquid and solid phase, operating conditions (rotational speed) and boundary conditions (flow rate, pressure and temperature). A detailed description of the geometry and input parameters will be presented in chapter 3.

During simulation, the mass, momentum and energy conservation equations will be iterated across the divided cells in liquid phase and the discrete phase model for particle track, viscous model and solver will be considered. The discrete phase model calculated the particle movement in the flow after the flow field calculated from the liquid phase. Chapter 2 will focused on the theory and modeling methods over conservation equations, viscous model, discretization methods and discrete phase model.

After simulation, the result of simulated flow pattern will be given by their velocity profile, pressure profile and path lines. The particle behavior of the solid phase will be given by the result of discrete phase calculation. Furthermore, the calculated results could be visualized by fluent post-processor.

Depending on the size (number of grids) of the 3D geometry the single flow path model is run on Fluent 6.3.26 with a desktop and complete model on Fluent 12.0.7 with a work station. It is described in APPENDIX B: Fluent computing environment in detail. The result of the 3D simulation will be validated by particle size distribution and flow concentration test results.

3.2 Complete 1/8 geometry model

The complete three-dimensional 1/8 geometry model of the has been made using the Fluent pre-processor GAMBIT Figure 3-7. The detailed design and size information has been derived from simplified mechanical drawing provided by Evodos.

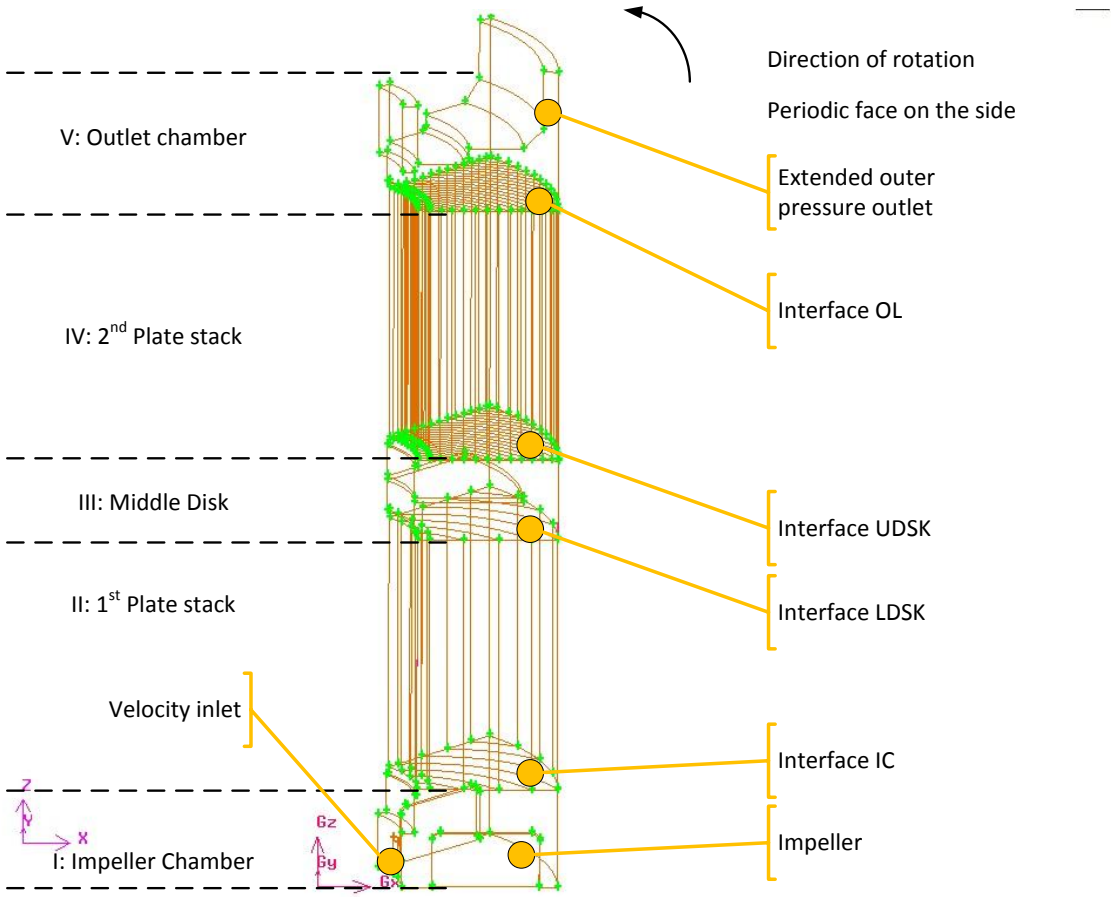

Figure 3-7: Isometric of 1/8 complete 3D GAMBIT geometry model of Evodos SPT centrifuge

The feed enters the model from the velocity inlet at the impeller chamber. The complete model is assumed to be filled with liquid and rotating under the rotational reference frame of 4500 rpm. The near stationary liquid is accelerated by the impeller and flows upward through 1st stage plate stack, middle disk, 2nd plate stack to the outlet chamber. The effluent will leave the model from the pressure outlet at the outer rim of the outlet chamber.

As briefly mentioned in section 3.1.2 there are several unique aspects of the model need to be stressed for the proposed geometry 3D GAMBIT centrifuge model design;

- Only 1/8 of the complete geometry is modeled due to asymmetrical design;
- The complete model consists of five distinct and simpler components (sub volumes);
- The five components (sub volumes) are feed inlet, impeller chamber, 1st stage plate stack, middle disk, 2nd stage plate stack and the outer outlet chamber;
- The model does not include the flow of hollow shaft, inlet feed slots, inner and outer outlet paring wheels;
- "Grid/mesh interface" function is used between bordering components, four interfaces;
- Periodic face and conditions is used on the side (1/8 cut boarder) of each component;
- Rotational reference frame of 4500 rpm is used to simulation centrifugal force.

The dimension and mesh data of the model is summarized below. Another reason to divide the complete model into five sub volumes is for the convenience of meshing. Different meshing methods has been used to mesh the sub volumes. The number of parallel spiral plates is model as 32 and 96 for 1st and 2nd plate stack. Both the inner and outer pressure outlet has been extended to ensure a well-developed flow field at the outlet. During the modeling only the outer pressure outlet is used as outlet. The dimension and mesh information of the complete model is summarized in Table 3-1.

It is also interesting to notice the number of grid in the complete 1/8 geometry model is almost five million which give great challenge on the computing power and calculation time needed to run the simulation.

	Abbreviation	Value
Dimensions [mm]	X*Y*Z	157*111*562.5
Angle of the sector [°]	α	45 (1/8 of the circle)
Volume [L]	*V*	4.153
Number of parallel spiral plates 1st plate stack for complete geometry [-]		32
Number of parallel spiral plates 2nd plate stack for complete geometry [-]		96
Number of impellers for complete geometry [-]		8
Number of velocity inlets for complete geometry [-]		8
Number of meshed cells [-]	*n*	4440594

Table 3-1: Summary of dimension and mesh data for complete model

3.2.1 Component I: Impeller chamber

Impeller chamber is located at the bottom of the drum near the feed slots. One of the important function of the impeller chamber is to accelerate the flow from nearly stationary to a very high rotational speed around 4500 rpm. The feed enters to the centrifuge drum via the stationary hollow shaft from the top and flows downward. There are 8 rectangular shaped slots at the bottom of the rotor to let the inlet feed flow from the hollow shaft to the impeller chamber. The flow from the stationary hollow shaft will form a jet stream to the drum and impeller chamber via the 8 rectangular feed slots. The velocity inlet in the impeller chamber is the opening of 1 of the 8 slots.

As shown in Figure 3-8 the dimension of velocity inlet slot is 8*25 mm. In the impeller chamber model the actual impeller is cut in half and located on both side of the periodic face. The thickness of the impeller is 8.25 mm. The geometry with 8 slots and 8 impellers is also shown in Figure 3-9 broken-out section view on the impeller chamber. The inner and outer wall of the drum is wall and periodic condition is set at side. The impeller is also located at both side and set as wall. The dimension information is summarized in Table 3-2.

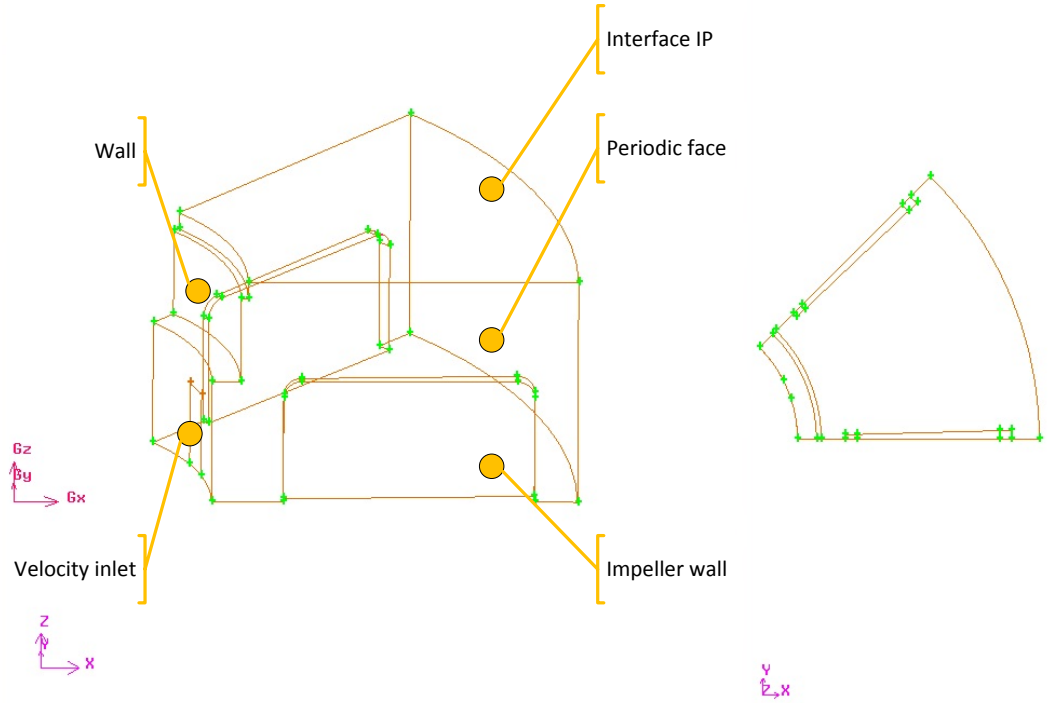

Figure 3-8: Isometric and apical view of component I impeller chamber in GAMBIT model

	Abbreviation	Value
Outer diameter [mm]	D_o	314
Inner diameter [mm]	D_i	130
Dimension of the Impeller [mm]	w*h*t	75*37*4.125
Distance of the Impeller from rotor edge[mm]	d	20
Dimension of the velocity inlet [mm]	w*h	8.25*25
Location of the velocity inlet		Centered at 22.5°
Volume [L]	V	4.153
Number of cells [-]	n	4440594

Table 3-2: Summary of dimension component I impeller chamber

The meshing of the impeller chamber is using quad (quadrilateral) mesh and “pave” on one periodic (side) face of the impeller chamber first than mesh the body with “cooper” swiped from one side face to another side face. The mesh interval is set to 1 mm.

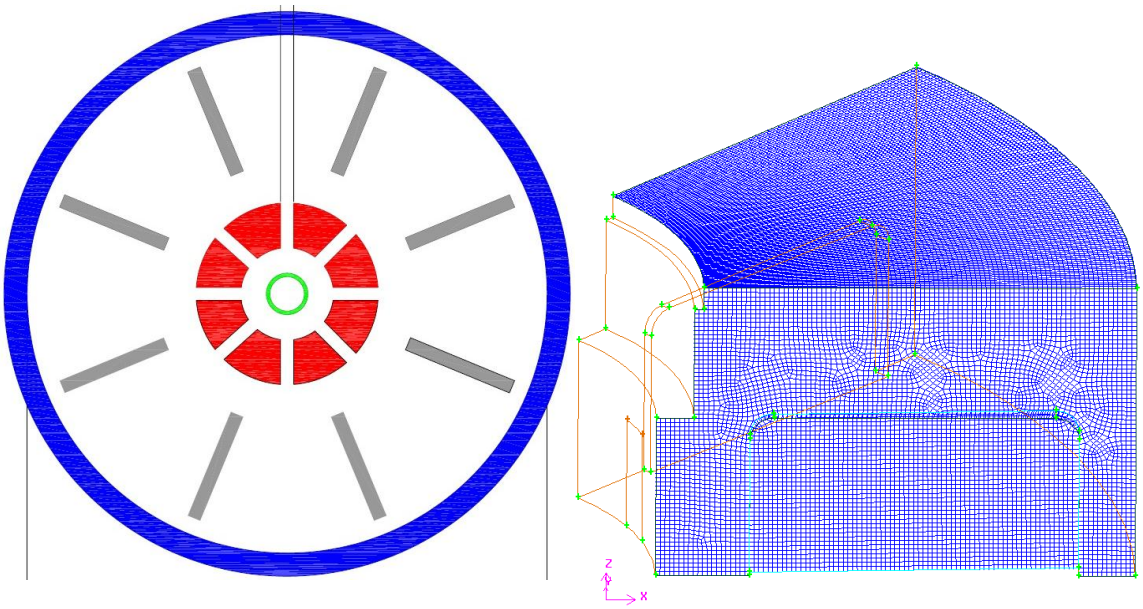

Figure 3-9: Broken-out section view and meshing of component I impeller chamber

3.2.2 Component II: 1st stage plate stack 1/8 geometry 32 plate configuration

The separation will take place at the 1st and 2nd stage plate stack. The isometric and meshing of component II 1st stage plate stack in GAMBIT model is shown in Figure 3-10. The strange geometry is the 1/8 of the complete geometry of the 1st stage plate stack. The spiral plates in the middle divide the geometry into 8 sub volumes or flow channels. The 8 sub volumes have been linked from the side face and by adapting periodic conditions on the linked face the 8 sub volumes forms 4 complete flow channels. The 1/8 geometry of 1st stage plate stack cut the complete model from 0° to 45°. As a complete model there are all together 32 spiral plates and 32 flow channel between those plates.

The top and bottom surface of the plate stack is the interface to be connected with impeller chamber and middle disk respectively. The flow enters from the interface IP at the bottom, flow through the different channels and leave through interface LDSK. The wall surface is set on inner and outer part of the rim of the drum. One important aspect of creating the flow channels in GAMBIT between the spiral plates is the shared real edge of the flow channel faces should be disconnected before the sweep surface operation being made and volume created. It makes the 2 neighboring flow channels do not share the same wall but have 2 separate wall faces.

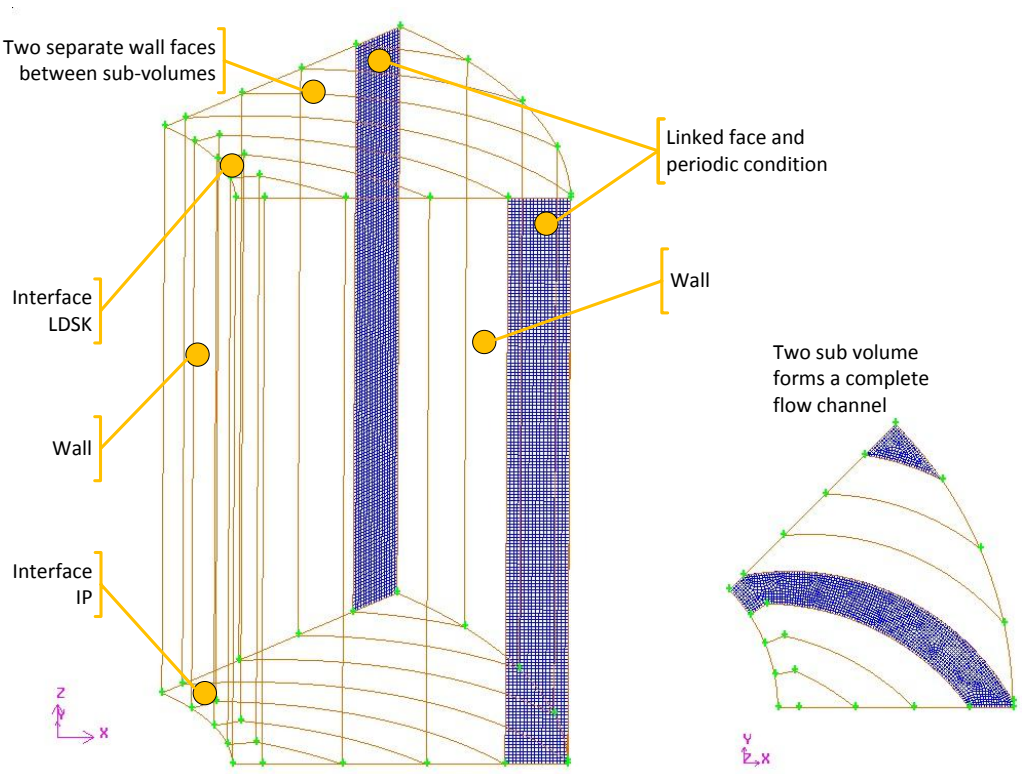

Figure 3-10: Isometric and meshing of component II 1st stage plate stack in GAMBIT model

The dimensions of the spiral plate is summarized in Table 3-3 and the schematic of the position and geometry for one spiral plate is shown in Figure 3-11. The red part in the middle is the rotor with a green hollow stationary shaft in the middle. The spiral plate is hinged to the rotor by the sleeve of the rotor. During discharge operation the hinge is opened to remove solid deposits.

During operation the spiral plate will be pressed against the drum wall and make each of the flow channel enclosed. Flat plates tend to bend due to the centrifugal forces and become curbed with the shape of the arc of a circle[44]. Therefore from mechanically stable point of view the plate shape has been defined as an arc of a circle. The radius of the arch shaped stainless steel spiral plate curvature is 100mm and the center of the curvature is at (16.3, -82.5). The flow channel angle between the chord and the tangential line of the hinge is 20°. By changing the number of plates, channel angle and chord length the geometry of the flow channel could be changed to meet the need for various feed streams.

The meshing of the flow channel between spiral plate is rather simple as partly shown in Figure 3-10: Isometric and meshing of component II 1st stage plate stack in GAMBIT model. First use quad (quadrilateral) and tri (triangular) mesh with “pave” on the bottom faces of the plate stack than mesh the body with “cooper” swiped from bottom to top. 8 sub volumes divide the plate stack geometry and by linked faces they form 4 flow channels. The mesh interval is set to 1 mm.

Dimensions	Abbreviation	Value
Outer diameter [mm]	D_o	314
Inner diameter [mm]	D_i	130
Radius for plate curvature [mm]	R_P	100

Center of plate curvature [mm]	*A0(x,y)*	16.3, -82.5
Cord length [mm]	*l*	115
Channel angle [°]	β	20
Plate thickness [mm]	*d*	1 (0 is used for modeling purpose)
Number of plates [-]	*n*	32
Length from inner wall to hinge [mm]	*h*	8
Height of plate stack [mm]	*H*	172

Table 3-3: Summary of dimension component II 1st stage plate stack

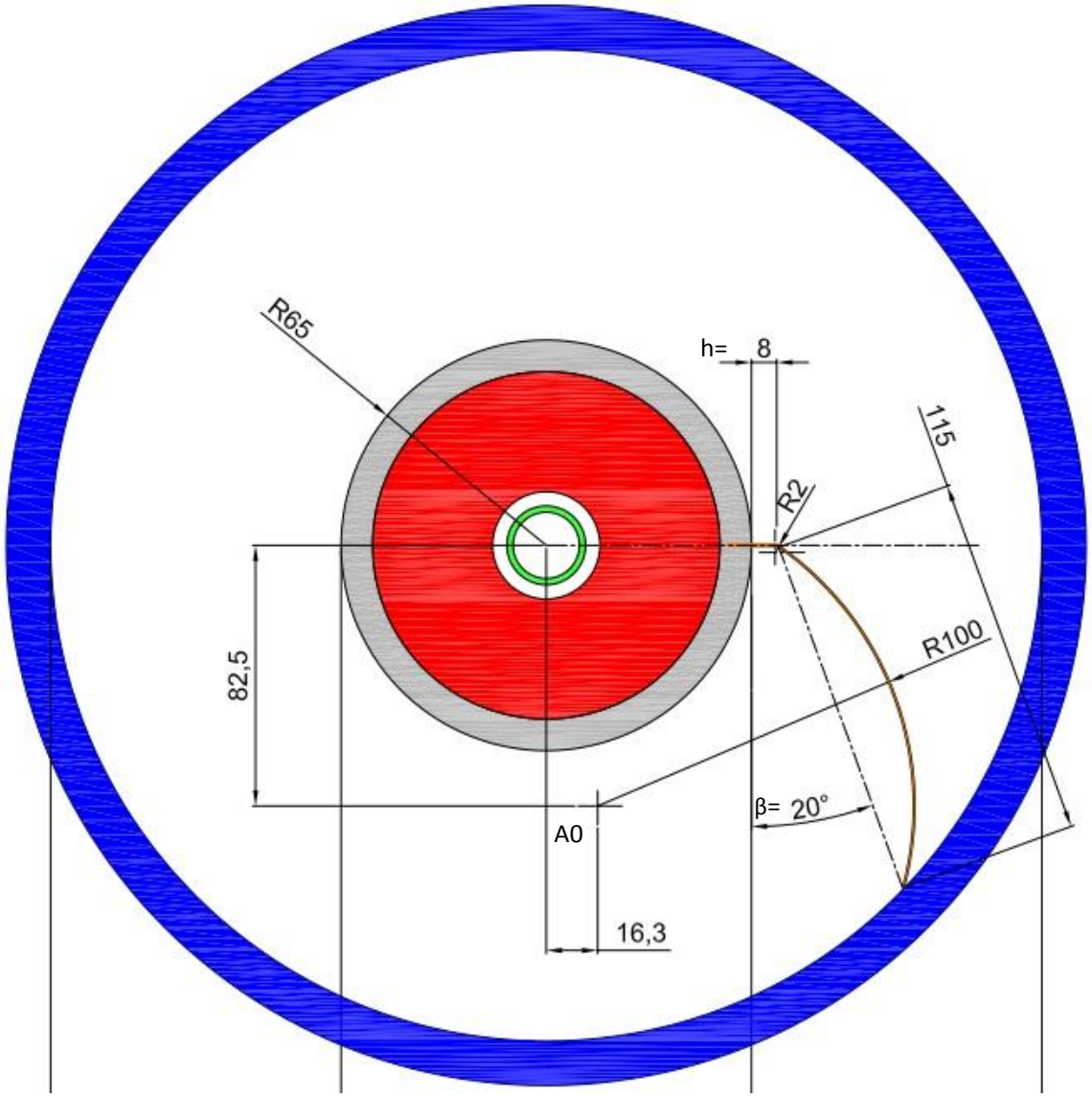

Figure 3-11: Schematic shown geometry and position of 1 spiral plate in plate stack

3.2.3 Component III: Middle disk

The middle disk is the most simple component of the complete model. It is basically a stainless steel disk located in the middle of the drum between two plate stack stages, shown in Figure 3-12. The flow leaving the 1st plate stack will enter the space between 1st and 2nd plate stack and flow around the middle disk. The purpose of the disk is to divert the flow from the flow to enter the 2nd

plate stack from the high pressure region near the rim of the drum. This is especially useful for microalgae liquid separation due to the microalgae particle behavior at the high pressure region.

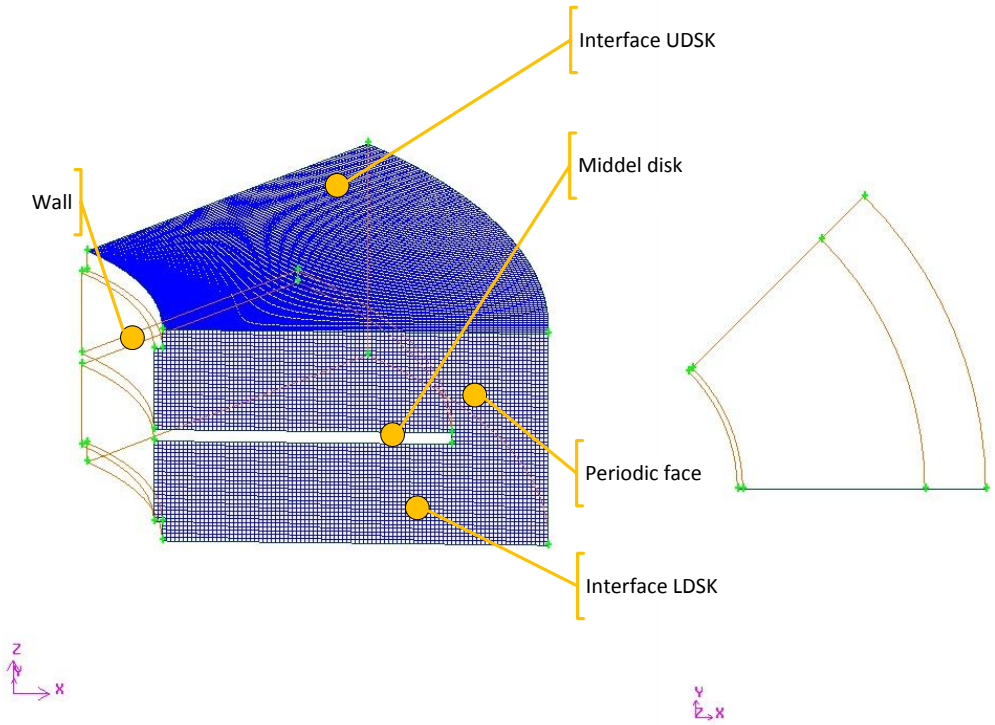

Figure 3-12: Isometric and meshing of component III middle disk in GAMBIT model

The geometry and location of the middle disk is shown in Table 3-4. The disk is 268 mm diameter and 3 mm thick.

Dimensions	Abbreviation	Value
Outer diameter [mm]	D_o	314
Inner diameter [mm]	D_i	126
Middle disk diameter [mm]	D_m	268
Middle thickness [mm]	d	3
Height of middle disk chamber [mm]	H	55

Table 3-4: Summary of dimension component III middle disk

Similar to the impeller chamber meshing of the middle disk is using quad (quadrilateral) mesh using "pave" on one side of the impeller chamber first than mesh the body with "cooper" swiped from one side to another. The mesh interval is set to 1 mm.

3.2.4 Component IV: 2nd stage plate stack 1/8 geometry 96 plate configuration

The isometric and meshing of component IV 2nd stage plate stack in GAMBIT model is shown in Figure 3-13. The 1/8 of the complete geometry of the 2nd stage plate stack look very similar to the 1st stage plate stack. The geometry of every single plate is the same as the plate shown in Figure 3-11. The only difference is there are 96 plates in the complete 2nd stage plate stack model which

means the 1/8 model geometry has been divided into 24 separate flow channels and with the linked face and periodic condition forms 12 complete flow channel.

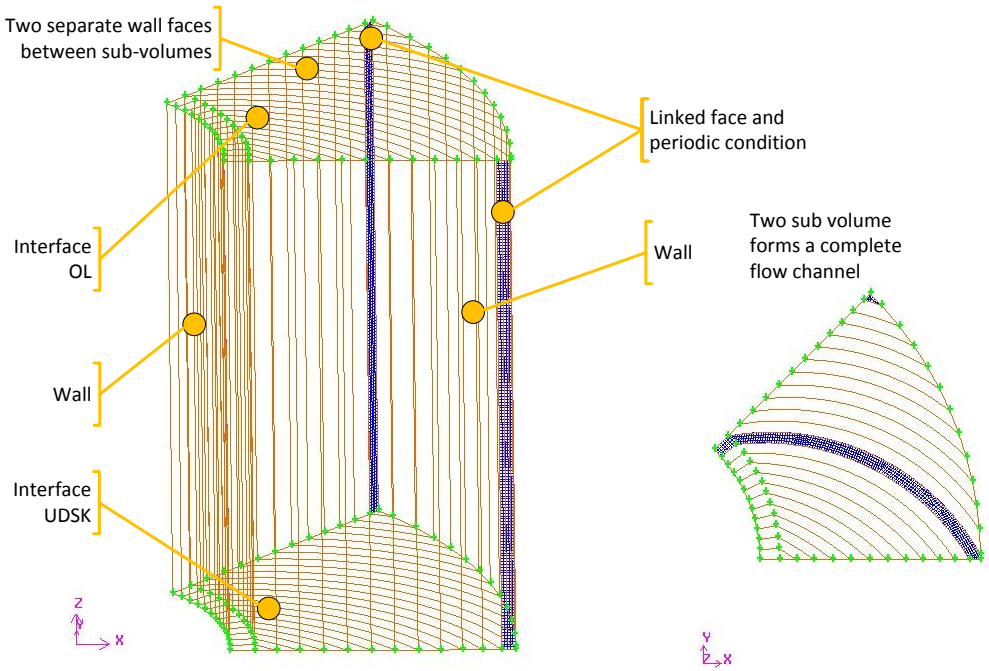

Figure 3-13: Isometric and meshing of component IV 2nd stage plate stack in GAMBIT model

The upper and bottom faces are interface connection with interface UDSK of the component III middle disk and interface OL of the component V outlet chamber. The summary of dimension of the 2nd stage plate stack is shown in Table 3-5. Only the number of plates is different.

Dimensions	Abbreviation	Value
Outer diameter [mm]	D_o	314
Inner diameter [mm]	D_i	130
Radius for plate curvature [mm]	R_P	100
Center of plate curvature [mm]	*A0(x,y)*	16.3, -82.5
Cord length [mm]	*l*	115
Channel angle [°]	β	20
Plate thickness [mm]	*d*	1 (0 is used for modeling purpose)
Number of plates [-]	*n*	96
Length from inner wall to hinge [mm]	*h*	8
Height of plate stack [mm]	*H*	172

Table 3-5: Summary of dimension component IV 2nd stage plate stack

The meshing of the 2nd stage plate stack is also partly shown in Figure 3-13 and the method used in meshing is similar to that of the 1st stage plate stack. The meshing interval is set to 1mm which means for every flow channel there are around 6 cells between two walls. The calculation of near the wall is not very rough.

3.2.5 Component V: Outlet chamber

The isometric and meshing of component V outlet chamber in GAMBIT model is shown in Figure 3-14. The outlet chamber is the place where the effluent from the two plate stack join together and leaves the drum. As briefly discussed in section 3.1.1 the effluent is discharged via the inner and outer outlet at the top of the drum via two stationary paring wheels. Figure 3-3: Cross section A (left) and B (right) showing outer and inner paring wheels. The light effluent to the inner paring wheel will come through 12 ϕ12mm weirs and the heavier effluent to the outer paring wheel will come through the channel between 12 guided vanes(cyan color). The stationary paring wheel converts the kinetic energy of the outlet flow to pressure of the effluent.

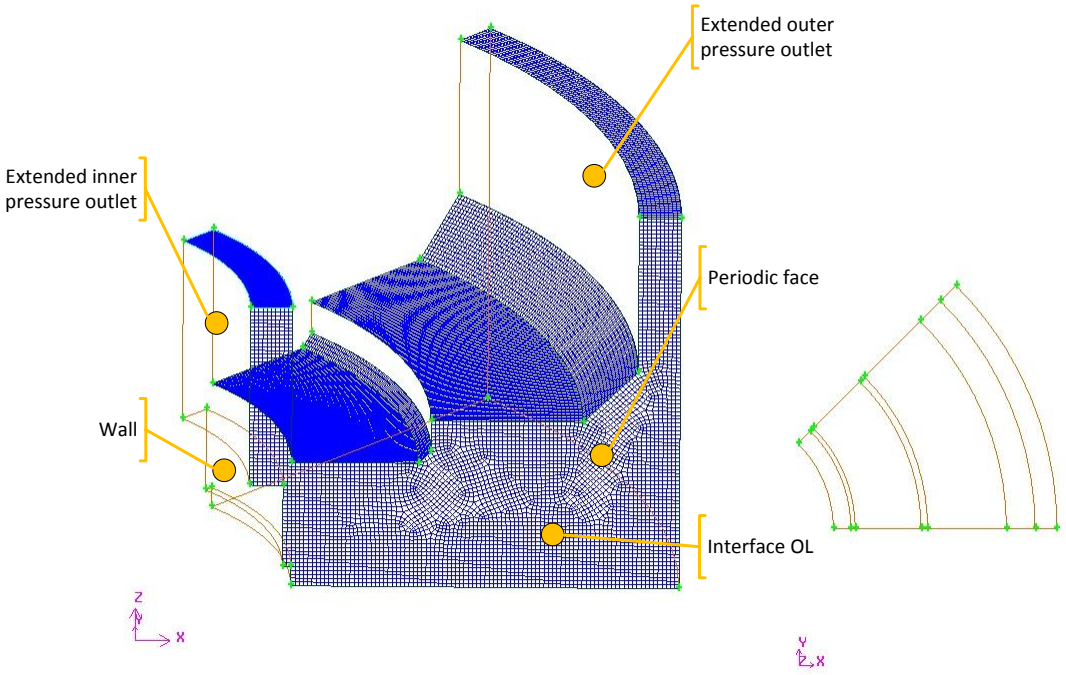

Figure 3-14: Isometric and meshing of component V outlet chamber in GAMBIT model

The geometry and location of the outlet chamber is shown in Table 3-6. The geometry does not include the model of inner and outer outlet paring wheels. With geometry estimated from simple mechanical drawing provided by Evodos.

Dimensions	Abbreviation	Value
Outer diameter [mm]	D_o	314
Inner diameter [mm]	D_i	110
Center line of inner outlet diameter [mm]		122
Center line of outer outlet diameter [mm]		304
Inner outlet width [mm]		12
Outer diameter width [mm]		10

Table 3-6: Summary of dimension component V outlet chamber

3.3 General parameters operation conditions and viscosity model

The general parameters and operation conditions has been summarized in Table 3-7. The general parameters includes solver type and velocity formulation. A pressure based solver has been chosen based on the incompressible nature of the flow. For high speed aero dynamics a density based solver is preferred.

The operation conditions describe the gravitational acceleration and relative movements of the fluid continuum. A rotational velocity of 432.9575 rad/s has been selected based on the 3000G artificial gravity and 4500 rpm for the Evodos machine described in section 3.1.1.

		Value	Remarks
General parameters	Scale setting	In millimeter	
	Solver type	Pressure based	Suitable for incompressible flow based problems
	Velocity formulation	Relative	Suitable for rotating reference frame
Gravity	Gravitational acceleration (X, Y, Z)	(0, 0, -9.81)[m/s^2]	
Fluid	Montion type	Moving reference frame	
	Transitional velocity	(0, 0, 0)	
	Rotational velocity	432.9575 [rad/s]	4500 rpm, 3000G
	Rotation-axis direction	(0, 0, 0); (0, 0, 1)	

Table 3-7: Summary of general parameters and operation conditions

A summary of viscosity model settings has been summarized in Table 3-8. For a standard two equation k-ω model.

		Value	Remarks
Model type	k-ε Near wall treatment	RNG Standard wall functions	Base case
Model type	k-ω SST	SST With low Reynolds number correction	Used in the model
	Specification method	k-ω	Default setting constant 1

Table 3-8: Summary of viscosity model settings

3.4 Boundary conditions

Boundary conditions defines the conditions of the fluid enters and leaves the model at model inlet/outlet at specific faces of the GAMBIT model. The location of the boundary face can be found in Figure 3-7. The velocity inlet is set to 0.503 m/s based on the 3000 l/hr flow rate. A pressure outlet boundary condition is set for the outer outlet. The pressure at the outer outlet is

estimated to be approx. 19 bar gauge. The outlet pressure value works only as a reference point of the model. All the other static pressure value is calculated with relative values.

The interface between components as the periodic conditions for each components is described in section 3.6 of this chapter. Rotational periodic condition has to be set for all periodic faces and wall condition is set for all other faces.

	Type	Value	Remarks
Inlet	Flow rate	3000[l/hr]	
	Velocity inlet	0.503 [m/s]	normal to adjacent cell
Outlet inner	Wall		
Outlet outer	Pressure outlet	190000 [pascal]	gauge

Table 3-9: Summary of boundary conditions

3.5 Material properties

The material properties used in the model is for fluid and solid particles. The fluid properties is used in Fluent calculation of continuum and solid particle properties used in DPM calculation. The summary of material properties could be found in Table 3-10: Material properties liquid and Table 3-11: Material properties solid particles.

		Value	Remarks
Fluid	Pure water liquid		
	Density	998.2 [kg/m^3]	
	Viscosity	0.001003 [kg/ms]	
Fluid	Starch liquid		
	Density	998.2 [kg/m^3]	
	Viscosity	0.001003 [kg/ms]	
Fluid	Microalgae liquid		
	Density	998.2 [kg/m^3]	
	Viscosity	0.001003 [kg/ms]	

Table 3-10: Material properties liquid

		Value	Remarks
Solid particle	Starch particle		
	Density	1540 [kg/m^3]	[45]
	Diameter	Various	5-40 μm and up to100 μm
Solid particle	Microalgae particle		
	Density	1100 [kg/m^3]	Feycon internal estimation
	Diameter	Various	2-4 μm for microalgae

Table 3-11: Material properties solid particles

3.6 Mesh interface

The interface between sub components has to be specified under the option mesh/grid interface. As indicated in Figure 3-7: Isometric of 1/8 complete 3D GAMBIT geometry model of Evodos SPT centrifuge, there are four interface between the five sub components namely:

Interface IC: Between the surface of outlet chamber and the 8 surface of inlet to the 1st stage plate stack;

Interface LDSK: Between the surface of 8 outlet to the 1st stage plate stack and the surface of lower middle disk;

Interface UDSK: Between the surface of higher middle disk and the surface of 24 inlet to the 2nd stage plate stack;

Interface IC: Between the surface of 24 outlet to the 2nd stage plate stack and the surface enters the outlet chamber.

3.7 Model specifications viscosity and DPM

After the material properties for solid particles is set the parameters for DPM can be also filled in. The selected solid particles has to be injected to the already calculated fluid flow field determined by the injection properties. In this model the inert solid particles starch or microalgae is injected to the system via the inlet surface at the impeller chamber. Their initial velocity is the same as the fluid and perpendicular to the surface.

For DPM settings the particle track of the injected particle is steady state in a transient flow field. The drag law to calculate the particle is set to spherical. A brief introduction to the theory behind DPM could be found in section 2.5. The effect of hindered sedimentation is not considered.

Injection properties	Injection type	surface	
	Particle type Particle diameter Initial point properties Initial turbulence properties	Inert Various Same as fluid Same as fluid	Also refer to Table 3-11
DPM settings	Particle treatment Drag law	Steady state Spherical	Steady state particle track with in transient flow field
Boundary condition settings	Wall surface	Trap Reflect Escape	Wall faces on the outer rim of the drum All other wall faces Pressure outlet

Table 3-12: Summary of injection properties and DPM settings

3.8 Solver conditions

The last step before running the model is to determine the solver condition which includes the numerical settings for solver type and calculation settings for transient calculation.

The solution methods consist of pressure-velocity coupling scheme and spatial discretization methods for the most important variants i.e. pressure, flow, turbulent kinetic energy and turbulent dissipation rate etc.. A brief theory behind those schemes and methods can be found in 2.4. The summary of solution methods are shown below in Table 3-13.

Solution methods			
	Scheme	PISO	Pressure-velocity coupling
	Gradient	LSCB	Spatial discretization
	Pressure	PRESTO!	Spatial discretization
	Momentum	1st order upwind	Spatial discretization
	Turbulent kinetic energy	1st order upwind	Spatial discretization
	Turbulent dissipation rate	1st order upwind	Spatial discretization
	Transient formulation	1st order implicit	

Table 3-13: Summary of solution methods

The transient calculation settings dealt with how many steps and time step size of the transient calculation. The final setting is shown in Table 3-14 with 2 adaptive time steps of 0.05 mili seconds which each time step has 100 iterations.

Calculation settings for transient calculation		
	Time stepping method	Adaptive
	Time step size	5e-5 [s]
	Number of time steps	2 [-]
	Max iteration per time-step	100 [-]

Table 3-14: Summary of calculation settings for transient calculation

The convergence of the desired solution could be indicated by the residual of key variants i.e. continuity, velocity components and turbulence parameters etc. Fluent consider the solution is converged when the residual value is less than 1e-3. Another well accepted indicator for solution convergence is the mass flow at the system boundary which has to be stable and correspond well with the steady state value of the inlet/outlet flow. In this case 0.103 kg/s. Figure 3-15 shows a Typical residual and mass flow rate for a converged solution.

To help with the converging process, the model could be run first for 2 time steps under the base case k-ε RNG turbulence model followed by 2 time steps of k-ω SST turbulence model. Another way to help with the model is to run the simulation with lower rotational velocity and gradually increasing the rotational velocity to the desired value. The simulation converge quite good under transient calculations.

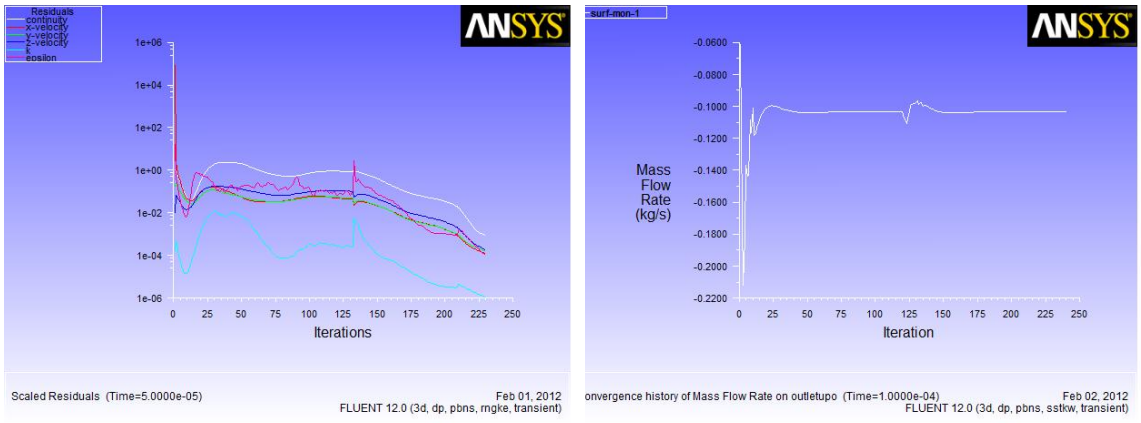

Figure 3-15: Typical residual and mass flow rate for a converged solution

The details of model development and parameters for simulation has been presented in this chapter. The results of the model will be discussed in detail in chapter 4.

CHAPTER 4: SIMULATION RESULTS AND DISCUSSIONS

In this chapter the simulation result of 3D CFD modeling of the complete model will be presented. Firstly, in 4.1 the result of path-lines are shown followed by the visual impression of the algae test. Flow pattern, velocity components and pressure profile for each of the model components have been presented in 4.3 and 4.4 with the location of reference surface shown in 4.2. The results of DPM calculation will be presented together with the theoretical separation efficiency and particle size distribution in 4.5. And last 4.6 the effects of change operation parameters will be discussed.

4.1 Path lines and visual validagtion

Pathlines are used to visualize the flow of massless particles in the problem domain. The particles are released from one or more surfaces. As shown in Figure 4-1 a pathline colored by particle ID is released from the InletIP surface at the lower left corner, made a detour around the middle disk and leaves the calculation domain from the outer outlet at the top right corner of the figure.

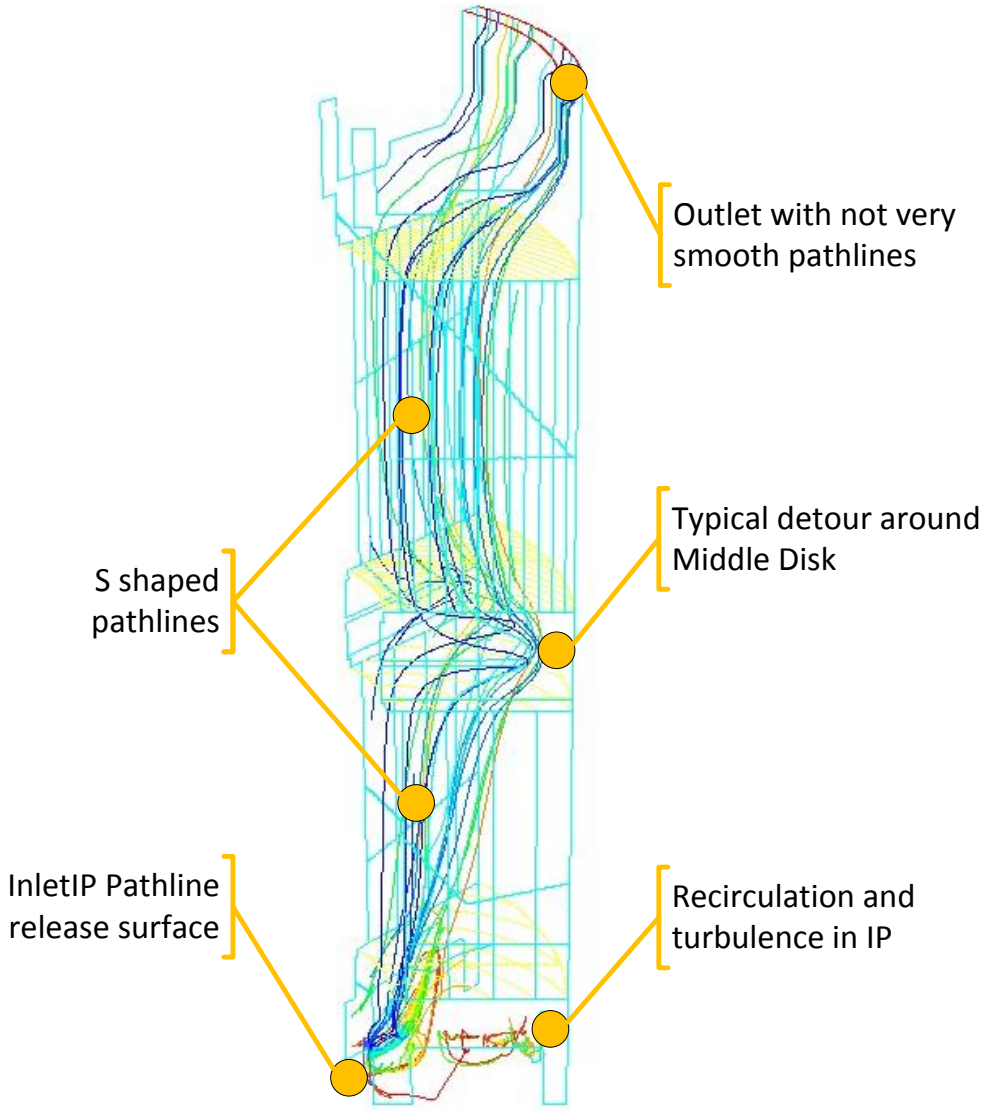

Figure 4-1: Pathlines colored by particle ID released from InletIP

The pathlines visualized the flow field inside the Evodos centrifuge. For better visual effect only 10% of the particle pathlines have been shown in the figure. The particles released from InletIP surface will be accelerated by the impellers and flow upwards. A small portion of the particles will be wander a bit in the outer side of the impeller chamber. The condition at this part of the impeller chamber is relatively turbulent. Some recirculation could also be observed at the impeller chamber.

Most of the particle flow through the 1st plate stack in a "S" shape from the inner part of the impeller chamber because of the lower pressure value and relative higher pressure gradient. In the middle disk the pathlines made a clear detour around the disk and the pathlines seems to be compressed because of the higher pressure and pressure gradient at this region. A similar "S" shaped pathline could be seen from the flow channels of the 2nd plate stack. Because of the different configuration of the 1st and 2nd plate stack of 32 and 96 plates the shape of the "S" showed to be more round and smooth for the 2nd plate stack configuration and more flat for the 1st plate stack configuration..

The pathline leaves the 2nd plate stack merges in the outlet chamber and leaves the calculation domain from the outer outlet.

It can be clearly observed from Figure 4-2: Photo of solid deposition line Evodos SPT centrifuge microalgae test a more flat "S" shaped curve between plates of the 1st plate stack and a more smooth and curved "S" shape at the 2nd plate stack. In the model does not take into account of the solid deposition and changes in the flow channel. But the high pressure area and pathlines correspond well with the solid deposition line shown in experiment photos.

To some extent it visually validate the 3D CFD model of the Evodos SPT centrifuge describes well with the real physics inside the centrifuge.

Figure 4-2: Photo of solid deposition line Evodos SPT centrifuge microalgae test

4.2 Reference iso, line and rake surfaces for pressure and velocity field

To study the pressure field and velocity field inside the complete centrifuge model there are several iso surface, line surface and rake surface drawn to give better understanding at certain important locations of the model. Iso surface is the those surface with the same height, or Z value. For example Z150, Figure 4-3, means the iso surface at z=150mm which is the surface at the middle of the 1st plate stack.

Line/rake surface is a line drawn with given starting point and end point. Rake surface will show data on certain number of points on a line. For example lz020line is the line surface with z value of 020mm and is a line between inner side and outer side of the drum, shown in Figure 4-3. Lz020rake10 is the rake surface representing 10 points of the line lz020line from P01 to P10. Also the axial (vertical) P line surfaces are shown in Figure 4-3 and Table 4-2. It stretch from z=0 mm to z=500 mm.

Components	IP		1st stage	MD			2nd stage	OL	
Location Z [mm]	20	40	150	247	267	287	380	490	575
Iso surface name	Z020	Z040	Z150	Z247	Z267	Z287	Z380	Z490	Z575
Line surface name	lz 020 line	lz 040 line	lz 150 line	lz 247 line	lz 267 line	lz 287 line	lz 380 line	lz 490 line	lz 575 line
Rake surface name	lz 020 rake10	lz 040 rake10	lz 150 rake10	lz 247 rake10	lz 267 rake10	lz 287 rake10	lz 380 rake10	lz 490 rake10	lz 575 rake10

Table 4-1: Name and location of iso surfaces and line/rake surfaces

	P00	P01	P02	P03	P04	P05	P06	P07	P08	P09	P10
Radial location	55,00	64,27	73,55	82,82	92,09	101,36	110,64	119,91	129,18	138,45	147,73
X	50,81	59,38	67,95	76,51	85,08	93,65	102,21	110,78	119,35	127,92	136,48
Y	21,05	24,60	28,14	31,69	35,24	38,79	42,34	45,89	49,44	52,98	56,53

Table 4-2: Name and location for P line surfaces

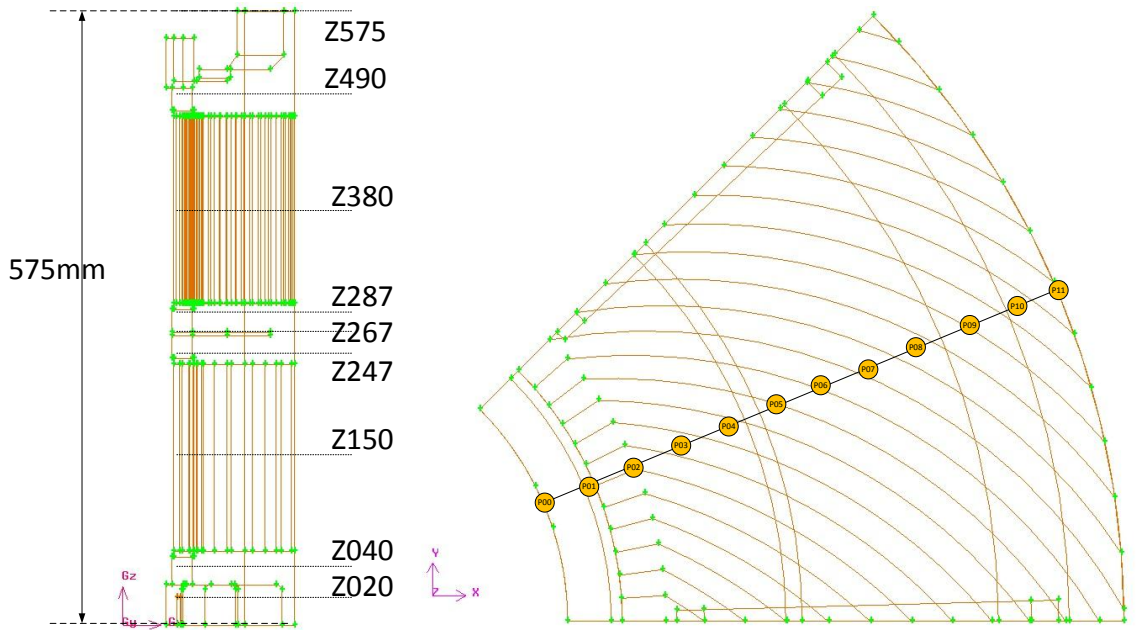

Figure 4-3: Location of the Z and P surfaces

The name and location of the 9 broken-out section view are shown in Table 4-1, Table 4-2 and drawn on Figure 4-3 below. The iso and line Z surface is indicated as dashed line and rake P surface as big orange dots. There are 12 p rake surfaces, 10 of them (from P01 to P10) could be regarded as located in the same long flow channel The result of pressure and velocity field of those sections will be compared and discussed.

4.3 Flow patterns

4.3.1 Velocity magnitude

The velocity magnitude along the radial position for different z rake surfaces are shown in Figure 4-4. The velocity magnitude along radial position is linear and differs very little with the theoretical tangential velocity. This is because the tangential velocity is 2 orders of magnitude larger than the axial or radial velocity and is the main component of the velocity magnitude. The flow inside the parallel plates differs very slightly with the height z value. The most divert velocity happened in lz040rake which is the most turbulent area with recirculation.

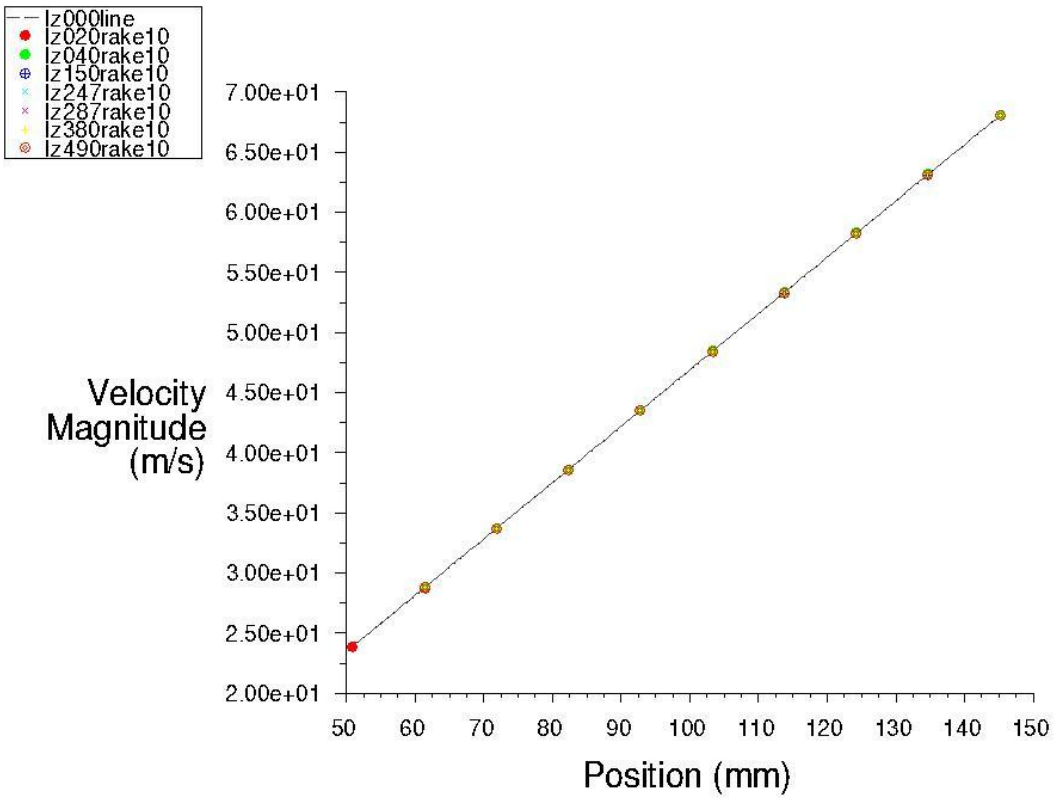

Figure 4-4: Velocity magnitude of liquid versus radial position for different Z rake surfaces

The velocity magnitude profile of the complete model and at different iso surfaces (height) are shown in Figure 4-5. Z020 and Z040 is located in the impeller chamber. It is clear from the figure that the shape of the velocity profile has been extorted from the lower right corner where the fluid is pushed by the impeller blade and kinetic energy has been transported to the fluid. It is clear that the velocity in Z040 is slightly higher compare to Z020 at the same radial position.

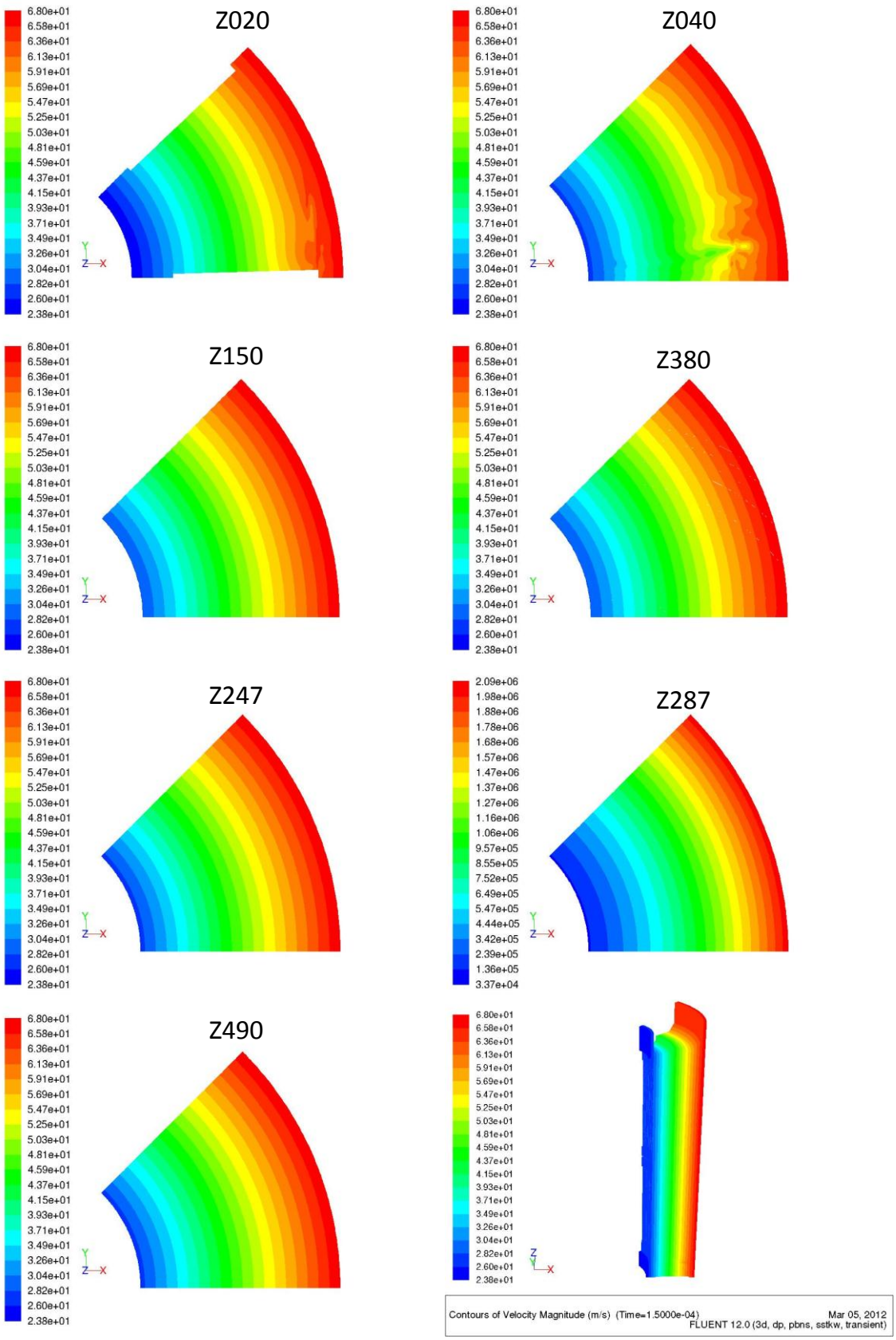

Figure 4-5: Velocity magnitude profile of the complete model and at different iso surfaces

Z150 and Z380 is the velocity profile at the middle of the 1st and 2nd plate stacks. The shape looks exactly the same although if look closely the shape of the flow channel could be seen. The velocity profiles in both plate stacks look like the velocity profile of a rigid body.

Z247 and Z287 is the velocity profile at the lower and higher part of the middle disk. Z490 is the velocity profile in the middle of the outlet chamber. The profiles show similar pater with each other and at plate stacks.

The complete velocity profile also show conformity of the velocity along z axis. The biggest velocity component is the tangential velocity.

4.3.2 Axial flow

The axial velocity is the velocity component along the axis of the centrifuge. For an positive axial velocity value the flow component is upward toward the outlet of the centrifuge and for a negative axial velocity value the flow component is downward toward the bottom of the centrifuge. An axial velocity profile along different height the z line surfaces has been shown in Figure 4-6. The figure in the right is a zoom-in version of the figure in the left excluding lz020line and lz040line.

From the left part of Figure 4-6 the lz020line and lz040line indicate a strong axial velocity component both positive and negative. The magnitude of axial velocity component is about 0.2 m/s, 1% of the magnitude of the tangential velocity component. The lz040line showed a unsteady whirls vertically and a reverse flow at the radial position of 110mm which is roughly the location at the middle of the impeller blade. On the contrary at the rest of the height from lz150line above to lz490line the axial velocity is nearly zero and showing an increasing trend.

The right part of Figure 4-6 is a zoom-in version of the left part. For the line surface lz150line and lz380line are located in the middle of the plate stack. The pattern of the axial velocity has shown a clearly boundary layer inside the flow channels. The gray dashed lz150line has four peaks indicating the four complete flow channel in the 1st plate stack while the blue dotted lz380line has 12 peaks indicating the 12 complete flow channel in the 2nd plate stack. The axial velocity in the plate stack is about 0.015 m/s gradually increasing toward the outer rim of the drum.

The red, green and cyan line surface lz247line, lz287line and lz490line is the line surfaces of the lower/upper middle disk and of the outlet chamber. Those axial velocity profile has shown a similar pattern of a “S” shaped velocity profile with the highest axial velocity near the outer edge of the centrifuge.

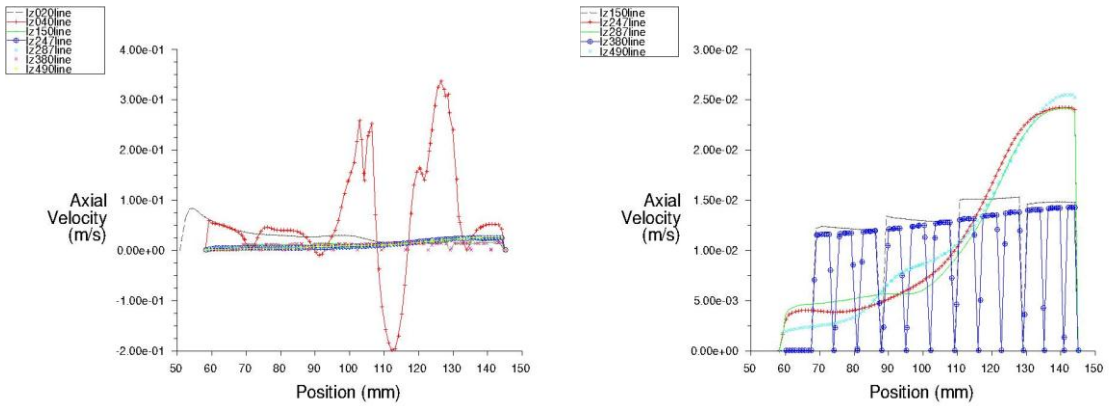

Figure 4-6: Axial velocity of liquid versus radial position for different Z line surfaces

4.3.3 Tangential flow

The tangential velocity is the velocity component tangential to the radius. For a rigid body the tangential velocity is proportional to the radial position as Vt=ω*r. The tangential velocity profile along different height the z line surfaces has been shown in Figure 4-7. The tangential velocity profile correspond very well with the rigid body tangential speed which is the lz000line and velocity magnitude profile Figure 4-4. The tangential velocity also is the biggest and determining component of the velocity magnitude.

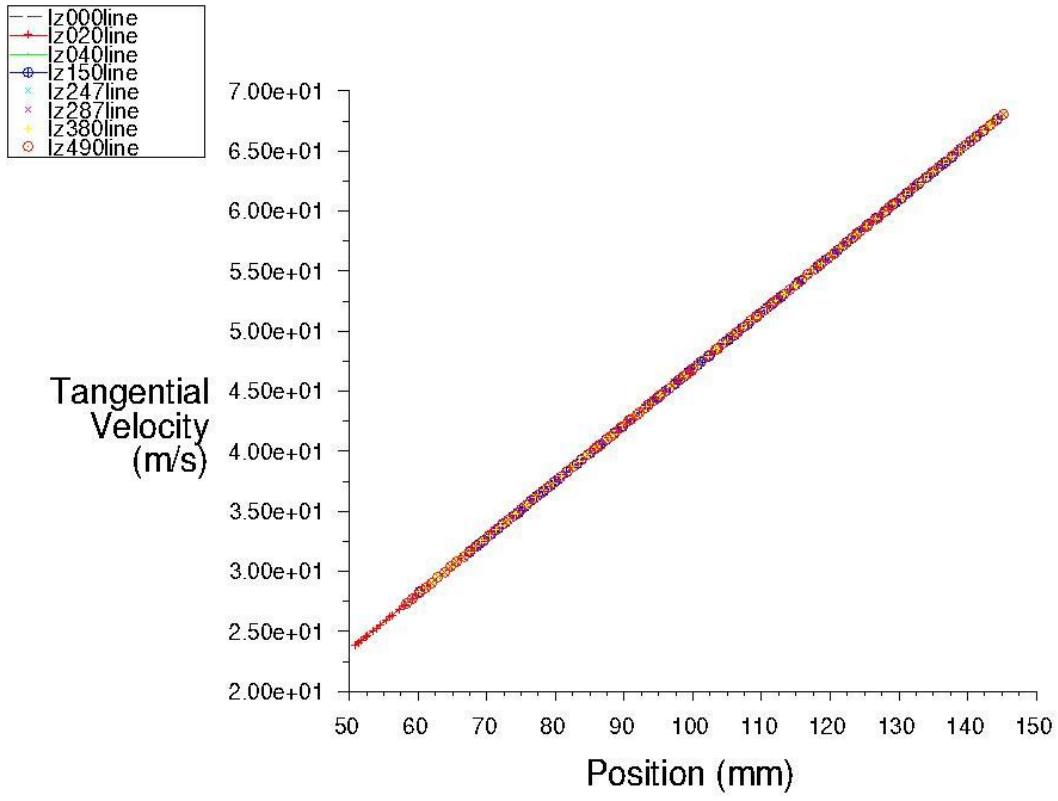

Figure 4-7: Tangential velocity of liquid versus radial position for different Z line surfaces

4.3.4 Radial flow

The radial velocity profile along different height the z line surfaces has been shown in Figure 4-8. The radial velocity is the velocity component along the radial direction of the centrifuge. For an positive radial velocity value the flow component is outward toward the outer rim of the centrifuge and for a negative radial velocity value the flow component is inward toward the inner rim of the centrifuge.

From the left part of Figure 4-8 the red lz040line indicate a strong radial velocity component both positive and negative. The peak of the radial velocity is near the peak of axial velocity peak and at the radial position of 110mm which is roughly the location at the middle of the impeller blade. It represents in this unsteady whirl both recirculation and high turbulence intensity, shown in Figure 4-9. The magnitude of radial velocity component is about 0.2 m/s, 1% of the magnitude of the tangential velocity component. The lz020line showed a decreasing trend of radial velocity of 0.5m/s which is set in the boundary condition of the surface inletIP, please refer to Table 3-9. The rest of the height from lz150line above to lz490line the radial velocity is nearly zero.

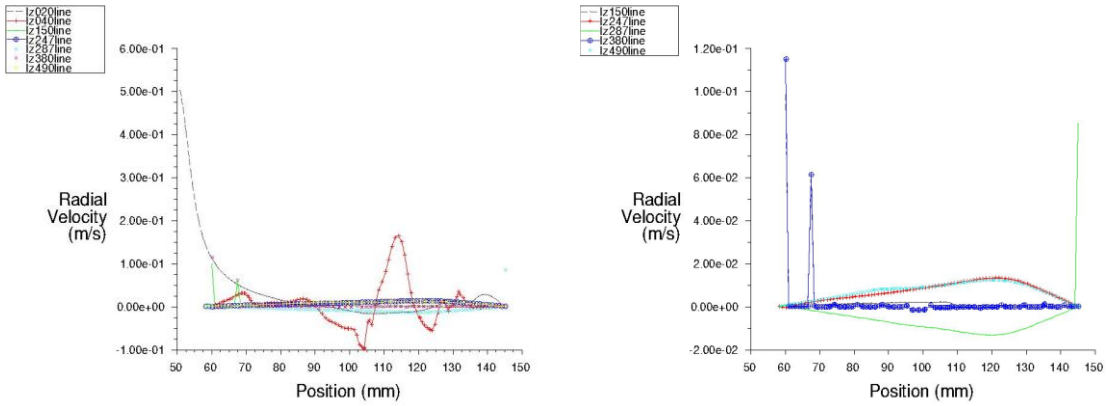

Figure 4-8: Radial velocity of liquid versus radial position for different Z line surfaces

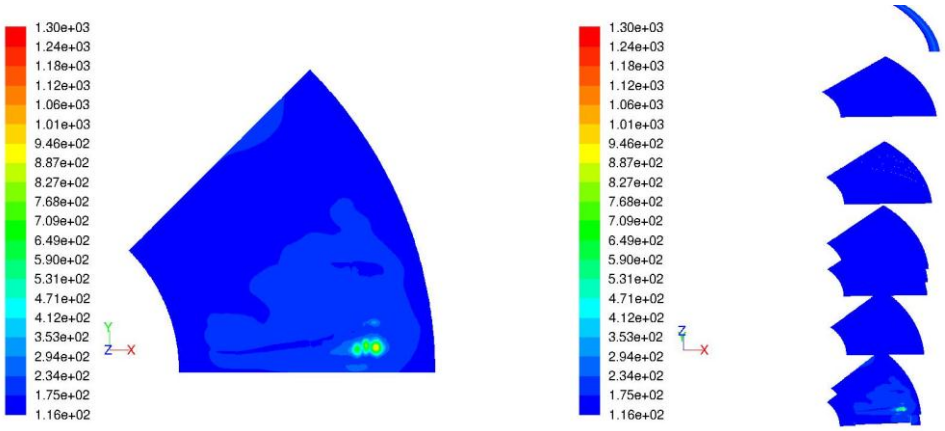

Figure 4-9: Turbulence intensity for z040 (left) and complete model

The right part of Figure 4-8 is a zoom-in version of the left part. For the line surface lz150line and lz380line are located in the middle of the plate stack. The pattern of the radial velocity between parallel plates is almost zero because the radial flow has been restrained by the plate walls.

The red, green and cyan line surface lz247line, lz287line and lz490line is the line surfaces of the lower/upper middle disk and of the outlet chamber. Those radial velocity profile of red lz247 and green lz287 showed a reversed shaped to each other. Because of the flow is detoured by the disk in the middle the radial velocity component of the lower disk, lz247line is toward outer rim and in the upper disk, lz287line the direction is toward inner rim. The cyan lz490line of the outlet chamber showed a similar pattern as lz287 because the outlet is near the outer rim of the centrifuge. There are three strange points showing strong positive radial velocity in the blue lz380line and green lz287line.

4.4 Pressure profile

4.4.1 Static pressure profile

The static pressure along the radial position for different z rake surfaces are shown in Figure 4-11. The static pressure along radial position is linear and differs very little with the theoretical static pressure based on Bernoulli's equation as $Ps=\rho\omega^2(r_0^2-r_L^2)/2g$ [46] shown in Figure 4-10.

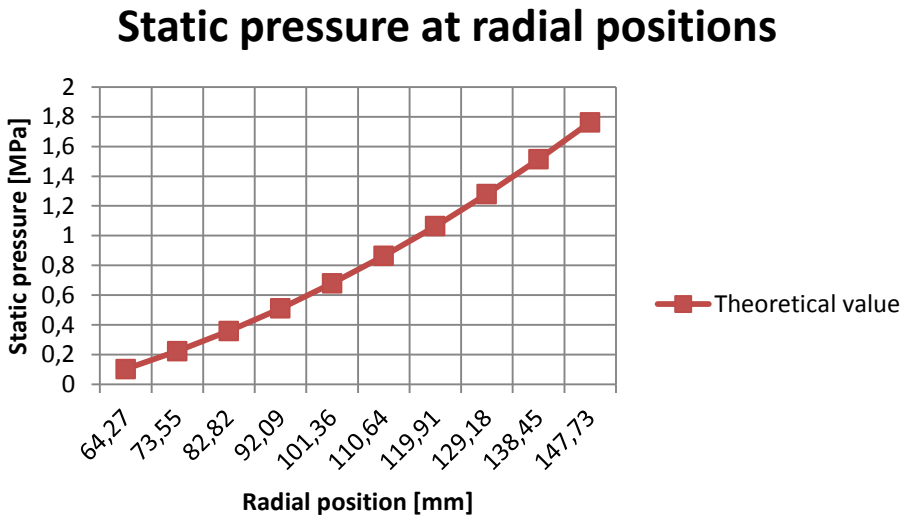

Figure 4-10: Static pressure of liquid versus radial position for different Z rake surfaces

The static pressure in Figure 4-11 differs very slightly with the height z value along the same radial position. It correspond quite well with the theoretical static pressure value. The biggest static pressure divergence happened in lz040rake which is the most turbulent area with recirculation.

Similar to the velocity magnitude profile, the static pressure of the complete model and at different iso surfaces (height) are shown in Figure 4-12. Because the velocity and pressure are coupled parameters as explained in 2.4, the static pressure profile of the complete model and at different iso surfaces shows great similarity compare to the velocity magnitude profile. The bid unsteady whirl can be seen in the inlet chamber iso surface z020 and z040. In the rest of the iso surface the pressure profile showed conformity along the vertical range of the centrifuge.

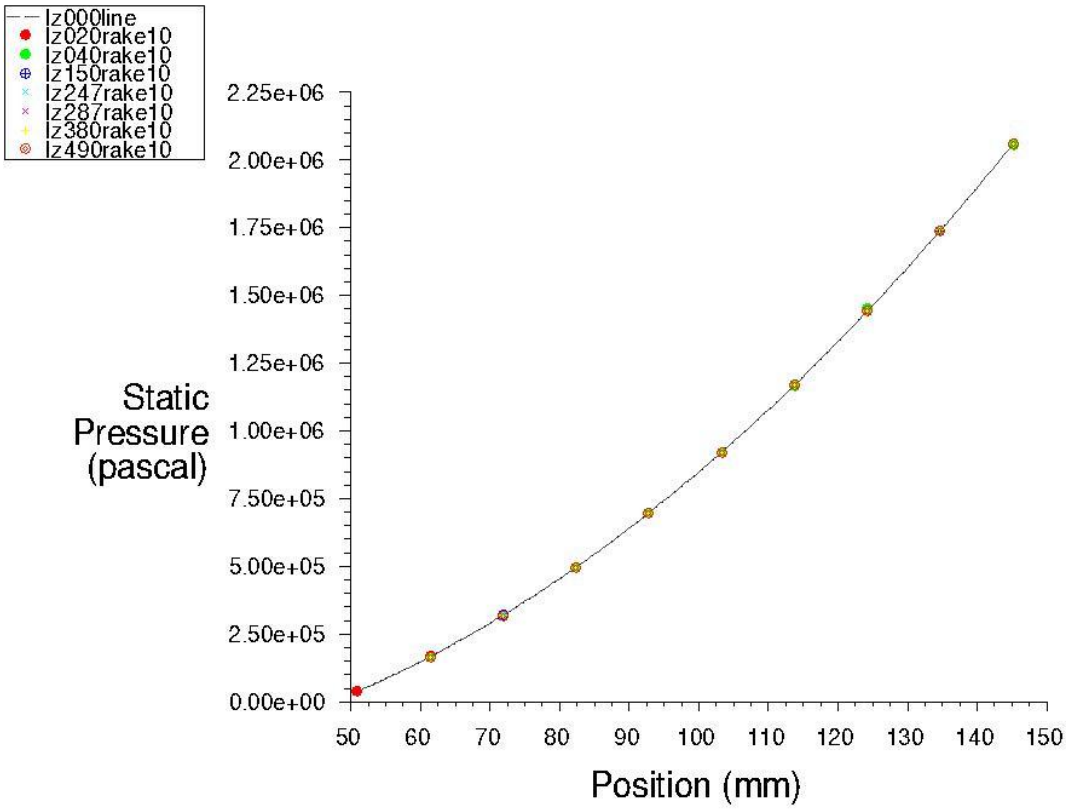

Figure 4-11: Static pressure of liquid versus radial position for different Z rake surfaces

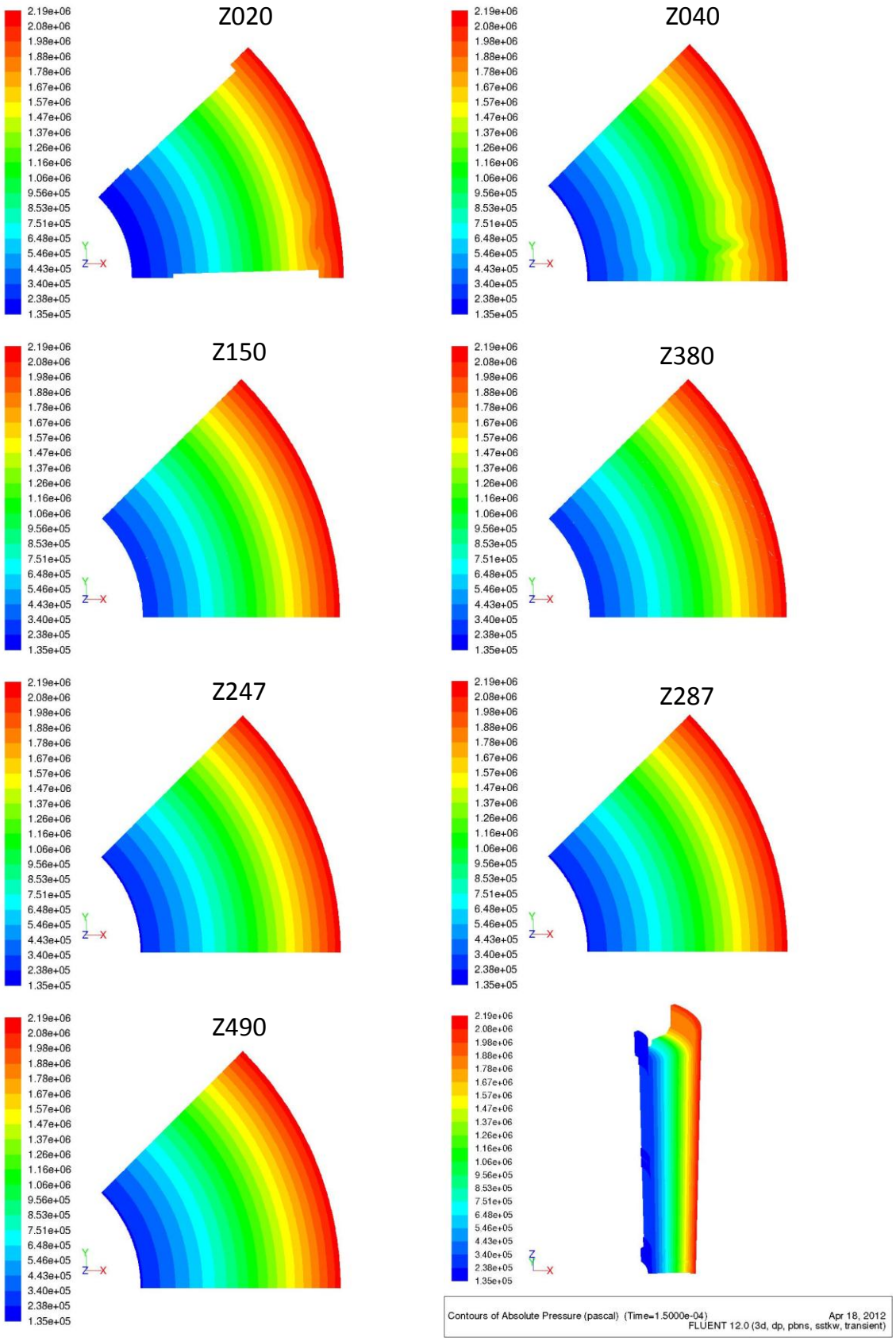

Figure 4-12: Static pressure profile of the complete model and at different iso surfaces

4.4.2 Vertical static pressure

When the focus is put on the static pressure versus vertical position for different P line surfaces, the vertical pressure difference is the driving force of the flow to go upwards. Some of the vertical static pressure profile of certain line surfaces, namely lrp02, lrp04, lrp 06 and lrp09 are shown below in Figure 4-13. The location of those P line surfaces is along a typical flow channel between two parallel plates along the two plate stacks, shown in Figure 4-3. Lrp02 is near the root of the flow channel and lrp09 is near the tip.

The overall pressure difference for different vertical position is small compare to the pressure difference at different P line surfaces along a typical flow channel. It is a common sense that the static pressure near the root is smaller than the static pressure near the tip. The difference is nearly 20 bar.

For the vertical height position below 67.5 mm, in the inlet chamber, the pressure has a big vibration for all P line surfaces indicating the effect of the big unsteady whirl in the impeller chamber caused by the impeller blades.

From height 67.5 to height 239.5 is the 1st plate stack and from height 294.5 to 466.5 is the 2nd plate stack. For all P line surfaces the static pressure in the 1st plate stack is higher than the 2nd plate stack. It is easy to explain that it is due to the gravity of the vertical arrangement of the centrifuge and the driving force to make fluid flow upward along the axis.

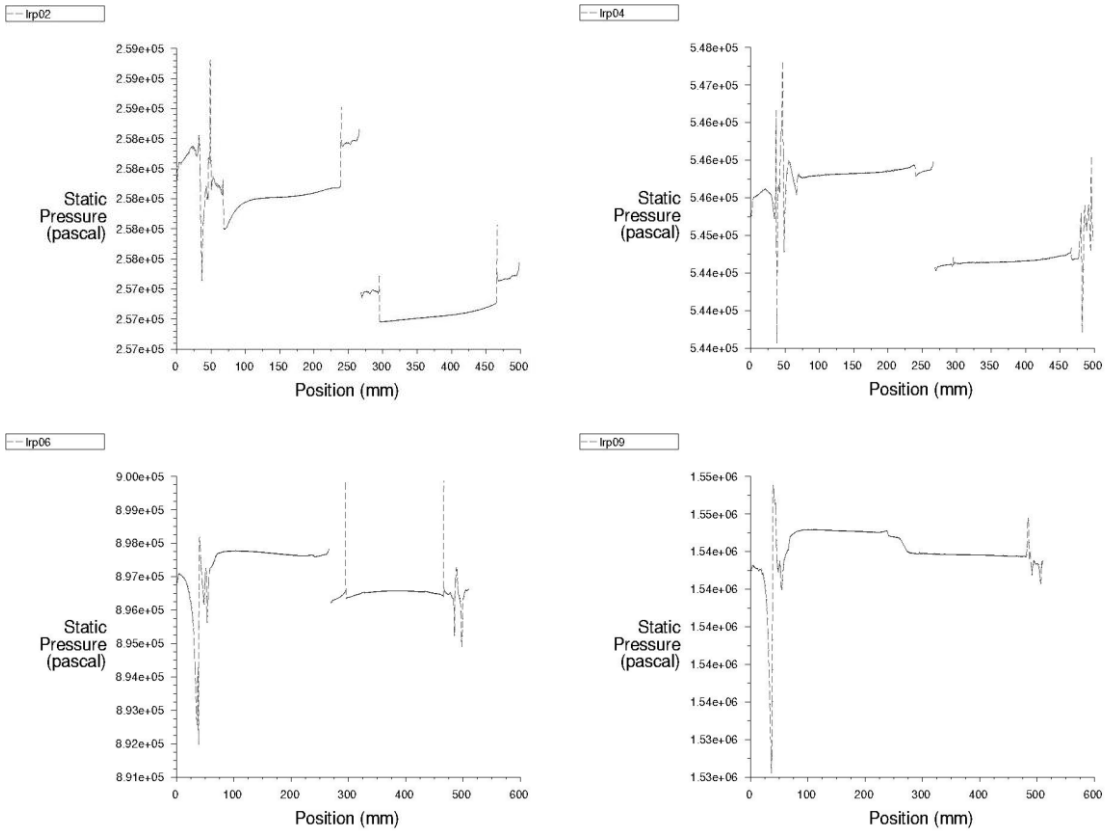

Figure 4-13: Static pressure of liquid versus vertical position for different P line surface

An interesting finding for the P line surfaces lrp02 and lrp04 near the root of the flow channel along the height of two plate stacks is that the pressure inside the plate stack showed a reverse trend indicating a relative reverse flow from up to bottom. While on the line surfaces lrp06 and lrp09 near the tip of the flow channel the pressure inside the plate stack showed a higher value at lower vertical positions. But looking closely at the axial velocity at the same region no reverse flow has been recognized. It is regarded as a pressure build up in this corner area of the plate stack.

The vertical pressure profile in the middle disk chamber has shown a higher pressure below the disk and lower pressure above the disk. A smaller vibration of pressure at the outlet chamber have been also noticed indicating potential unsteady flow.

4.5 Particle distribution and separation efficiency

As mentioned in 3.6 modeling of DPM, a separation efficiency calculation has been done for the complete 3D CFD model for particles with different sizes.

	00	01	02	03	04	05	06	07	08	09	10
Particle size [µm]	1184	497.8	104.7	52.33	5.5	3.27	2.312	1.945	1.635	1.375	1.156
Escaped [%]	0	0	0	0	0	0	9	26.9	39.1	44.2	48.7
Trapped [%]	99.4	100	95.5	75.6	76.3	76.9	66.7	48.1	34	30.1	23.7
Incom-plete [%]	0	0	4.5	24.4	23.7	23.1	24.4	25	26.9	25.6	27.6
Total [%]	100	100	100	100	100	100	100	100	100	100	100

Table 4-3: Summary of DPM calculation results on particle size for starch particles

	00	01	02	03	04	05	06	07	08	09	10
Particle size [µm]	1184	497.8	104.7	52.33	5.5	3.27	2.312	1.945	1.635	1.375	1.156
Escaped [%]	0	0	0	0	7.7	30.8	51.3	54.5	57.7	62.8	62.2
Trapped [%]	100	100	78.2	80.8	67.3	43.6	23.1	16.7	14.1	11.5	9.6
Incom-plete [%]	0	0	21.8	19.2	25	25.6	25.6	28.8	28.2	25.6	28.2
Total [%]	100	100	100	100	100	100	100	100	100	100	100

Table 4-4: Summary of DPM calculation results on particle size for microalgae particles

The results of particle size DPM calculation has been summarized in Table 4-3 and Table 4-4. 10 typical particle size frm 1184 µm to 1.156 µm has been chosen to run for the DPM calculation under the calculated flow field described in the previous sections of this chapter. The fate of the particle is categorized in escaped, trapped and incomplete as described in 2.5 modeling of DPM.

The result of the DPM calculation has been shown in Figure 4-14 along with the Evodos Expected performance of the Evodos SPT centrifuge, a typical test result 21On of the starch test and the Fluent CFD modeling with DPM calculation based on the particle with different particle sizes for both starch and microalgae particles.

The cut-off size expected by Evodos is shown in light blue, the starch test results is shown in purple. The test measurements validate the claim held my Evodos that their SPT centrifuge can separate 50% of the particles at a particle size of 1 µm. The test measure shows an even better cut-off size of 0.5 µm.

On the other hand the CFD result for starch particle separation is shown in dark blue and the CFD results for microalgae particle is shown in red. The CFD simulation shown a cut-off size of 1.5 µm for starch particle and approx. 3 µm for microalgae particles. It is easy to understand physically that the starch particle is easier to separate compare to the microalgae particle due to the particle size distribution and the density difference from the liquid phase.

According to literature computational simulations frequently obtained larger cut-sizes than measured for different flow conditions, which is clearly a signal of the complexity of the flow and the approximate nature of the models.[36] In this simulation this phenomena is clearly evident through the results.

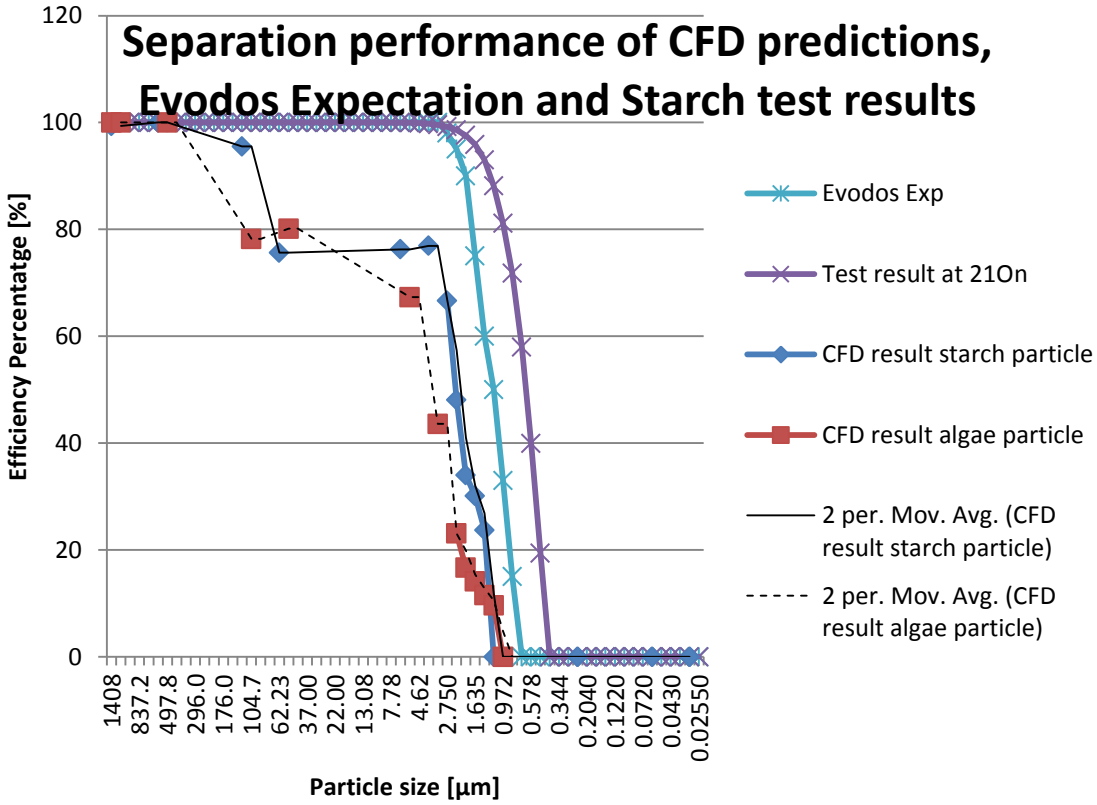

Figure 4-14: Separation performance of CFD predictions, Evodos Expectation and Starch test results

The separation performance of some of the medium to large size particles have shown less desired value. The difference could be due to the complexity of the problem and the approximation of the model.

Also bear in mind only particles of large size will behave as exclusively influenced by the time-averaged gas flow. Very small particles will tend to fluctuate following turbulent fluctuations of the liquid velocity, and there will be a complete range of intermediate behaviors between these two extremes.

In chapter 4, the simulation results for the complete model will be presented. Firstly, the result of pathlines, flow pattern, pressure profile, velocity profiles is shown followed by the result of separation efficiency by different particle sizes. The modeling results has been validated partly by visual inspection with test results, theory prediction and measurements. In chapter 5 the starch test run and measurement results will be discussed.

CHAPTER 5: STARCH TEST FOR EVODOS SPT CENTRIFUGE

5.1 Sample taking of Evodos SPT centrifuge: starch test

A starch test has been carried out on 10-01-2011 on the Raton site in Breda by Bowen Yu from TU Delft and Remko van Dam from Evodos.

The purpose of the starch test is to use starch suspension in water as centrifuge feed fluid to see test the working conditions of the centrifuge. Samples were taken from the inlet and outlet of the Evodos SPT centrifuge at certain time intervals during a complete centrifugation cycle.

The samples collected during the test will be used for measurement of the particle distribution with laser particle sizer and solid concentration with turbidity measurement by spectrophotometry. The result and detail description of those measurements will be elaborated in appendix C and D respectively.

As shown in below Figure 5-1. The test setup consist of an open tank with mixer as feed tank to make the starch suspension. The sampling point inlet is located near the bottom of the open tank. The sampling point outlet is located at the top of the open tank. Samples from both locations were taken by plastic bottle and bear hand. The feed pump will pump the feed from the open tank to the centrifuge. The pump head is slightly higher than the atmospheric pressure (around 0.3 barg) and will be shown from the pressure indicator and the inlet connection. The inlet and outlet connection of the centrifuge is located at the lower side of the centrifuge.

All of the sequence could be set and controlled through the control box of the Evodos SPT centrifuge. First the centrifuge will be running from stand still to rotational speed of 4200 rpm without feed pump working. After the working rotational speed of 4200 rpm has been reached the feed pump start to feed fluid to the centrifuge and sampling could start.

The starch suspension is continuously taken from the open mixing tank and starch will be separated from the Evodos STP centrifuge. The outlet pure liquid will be send back to the tank and dilute the starch suspension in the tank. There is a time discrepancy between inlet feed to the centrifuge and outlet effluent coming out from the centrifuge because it took some time to fill up the drum of the centrifuge. The time discrepancy is 60 seconds for 3000 l/hr test and 110 seconds for 1500 l/hr test.

After certain time the centrifuge will be discharged when the plate stack are filled with starch and the suspension in the open tank is clean. Samples were taken from the inlet and outlet during the whole process. The set time is around 7 mins for feed pump running at 3000 l/hr and 14 mins for feed pump running at 1500 l/hr. The solid discharge will be collected from the discharge bin, weighted and put back to the open mixing tank for next test.

Altogether two test runs on feed pump 3000 l/hr and 1500 l/hr were run and 21 samples (10 for each test runs and 1 for solid deposites) were taken. The following table Table 5-1 and Table 5-2 shows the conditions of the sample with their ID.

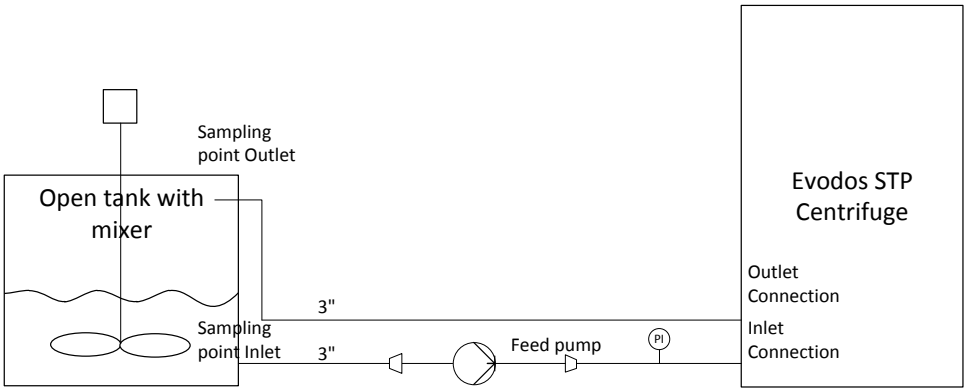

Figure 5-1: Picture of starch test environment and schematic of test setup

Other observations of the starch test and sample taking:

- The open mixing that has a dimension of 73x110x100 cm (WxLxH) the liquid depth is 40 cm;
- There are 20 kg of starch (5kg bag potato starch each bought from supermarket) and around 30 L of water used to make the testing starch suspension;
- The Evodos SPT centrifuge works efficiently, steadily and quietly;
- All the process steps is controlled through the control box;
- The solid discharge is rather dry; (see photo)
- The inlet sample has obvious starch deposition in the bottle;
- The inlet sample taking earlier during the sample test has more starch deposition than those of later; (see photo)
- The outlet effluent is clean and without recognizable starch deposition; (see photo)

- The flow of effluent coming out of the outlet is fluctuating rhythmically due to the position of the interface inside the centrifuge and efficiency of the pairing wheel;
- There was a minor technical problem with the electric motor and it was solved in around 1 hr.

Sample ID	Location [-]	Time at [s]	Remarks
1BI	Inlet	0	
1BO	Outlet	60	
11I	Inlet	90	
11O	Outlet	150	
12I	Inlet	180	
12O	Outlet	240	
13I	Inlet	270	
13O	Outlet	330	
1EI	Inlet	360	
1EO	Outlet	420	
Test run No. 1, conditions: - The lower 1st plate stack consist of 30 plates and the higher 2nd plate stack consist of 90 plates; - Feed pump work at 3000 l/hr; - Pressure indicator at 0.3 barg; - Centrifuge running at 4200 rpm ; - Time discrepancy (time to fill up the centrifuge) 60s			

Table 5-1: Sample ID, information and timing for test run No. 1

Sample ID	Location [-]	Time at [s]	Remarks
2BI	Inlet	0	
2BO	Outlet	110	
21I	Inlet	180	
21O	Outlet	290	
22I	Inlet	360	
22O	Outlet	470	
23I	Inlet	540	
23O	Outlet	650	
2EI	Inlet	720	
2EO	Outlet	830	
2Solid	Solid	>830	Solid discharge sample taken from discharge bin
Test run No. 2, conditions: - The lower 1st plate stack consist of 30 plates and the higher 2nd plate stack consist of 90 plates; - Feed pump work at 1500 l/hr; - Pressure indicator at 0.3 barg; - Centrifuge running at 4200 rpm ; - Time discrepancy (time to fill up the centrifuge) 110s			

Table 5-2: Sample ID, information and timing for test run No. 2

Measurement of the particle distribution with laser particle sizer and solid concentration with turbidity measurement by spectrophotometry will be shown in appendix C and D

The following photos below is showing the sample bottles of test 1, test 2, solid discharge and open mixing tank with mixer and starch suspension.


130
121
110
131
111


210
220
230
260
260
260
21C
23C
22C

5.2 Measurement of particle distribution with laser particle size analyzer

The particle size distribution is measured with an laser particle size analyzer. The cut off size of the Evodos SPT centrifuge could be estimated from the particle size distribution measurement.

Introduction to starch

Starch, a white, granular, organic chemical that is produced by all green plants. Starch is a soft, white, tasteless powder that is insoluble in cold water, alcohol, or other solvents. The basic chemical formula of the starch molecule is (C6H10O5)n. comprising glucose monomers joined in α 1,4 linkages. Starch is a polysaccharide although in absolute mass only about one quarter of the starch granules in plants consist of amylose, there are about 150 times more amylose molecules than amylopectin molecules. Amylose is a much smaller molecule than amylopectin.[47] The simplest form of starch is the linear polymer amylose; amylopectin is the branched form.[48, 49] A schematic of the molecule structure is shown in Figure 5-2 below with a microscopic photo of iodine stained starch granule.

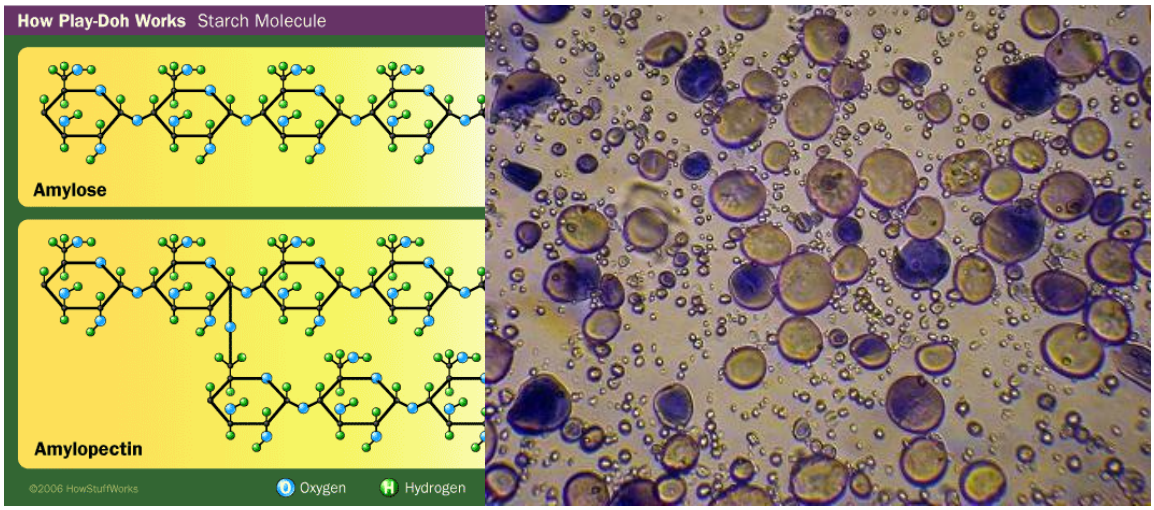

Figure 5-2: Granules of wheat starch, stained with iodine, photographed through a light microscope

Starch molecules arrange themselves in the plant in semi-crystalline granules. Starch has a form of discrete granules ranging from about 5 to 40 μm in average particle size, depending on the source[48] i.e. rice starch is relatively small (about 2μm) while potato starches have larger granules (up to 100μm).[47] The density of potato starch is considered 1.54 kg/l. [45]

Introduction to Mictrotrac S3500 particle size analyzer (PSA)

A Microtrac S3500 series particle size analyzer has been used to determine the particle side distribution of the centrifuge inlet/outlet fluid samples. The principle of the laser particle size analyzer is laser diffraction method.

The method depend upon analysis of the "halo" of diffracted light produced when a laser beam passes through a dispersion of particles in air or in a liquid. The angle of diffraction increases as particle size decreases, so that this method is particularly good for measuring sizes between 0.1 and 3,000 μm. The resultant scatter pattern can be measured electronically and then deconvulated mathematically to infer a particle size distribution.[50] Advances in sophisticated data processing and automation have allowed this to become the dominant method used in industrial PSD determination. A particular advantage is that the technique can generate a continuous

measurement for analyzing process streams. The working principle of Microtrac S3500 series particle size analyzer shown below is from their website.[51]

The TRI-LASER Diffraction System developed by MICROTRAC allows light scattering measurements to be made from the forward low angle region to almost the entire angular spectrum (approximately zero to 160 degrees). It does so by a combination of three lasers and two detector arrays, all in fixed positions. The primary laser (onaxis) produces scatter from nearly on-axis to about 60 degrees, detected by a forward array and a high-angle array, both of which have logarithmic spacing of the detector segments. The second laser (off-axis) is positioned to produce scatter beyond the 60 degree level which is detected using the same detector arrays. The third laser (off-axis) is positioned to produce backscatter, again using the same detector arrays. This technique effectively multiplies the number of sensors that are available for detection of scattered light.

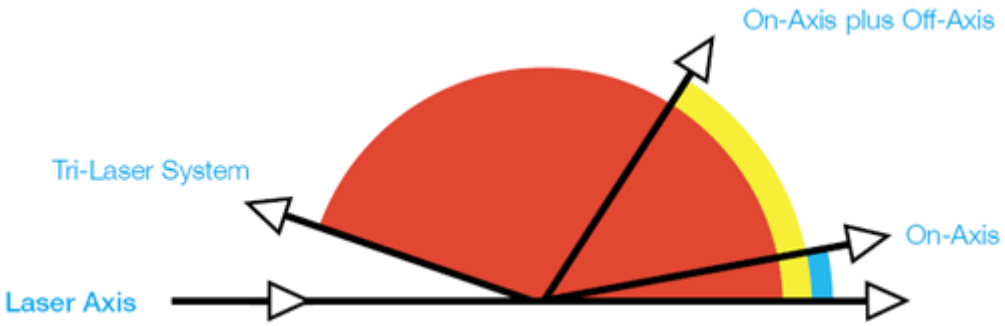

Figure 5-3: Schematic showing laser beams scattered at different angles

During a measurement cycle, Laser 1 is switched on while Lasers 2 and 3 remain inactivated. The sample to be measured scatters light in an angular pattern depending on the material size. The scattered light from Laser 1 is detected by the on axis, forward detector and the off axis, high angle detector. Laser 1 is then switched off and Laser 2 is activated. Laser 2 is directed at the sample at a different angle of incidence providing a different optical axis. Light scattered by the sample is detected by the same fixed detectors. Laser 2 is then switched off and Laser 3 is activated. Again the angle of incidence and optical axis is different. In this case the fixed detectors detect light that is back–scattered by the sample. The resultant scattered light information from all three lasers is combined to generate particle size distributions with unsurpassed resolution. Tri laser diffraction technology is proprietary and is patented by Microtrac.

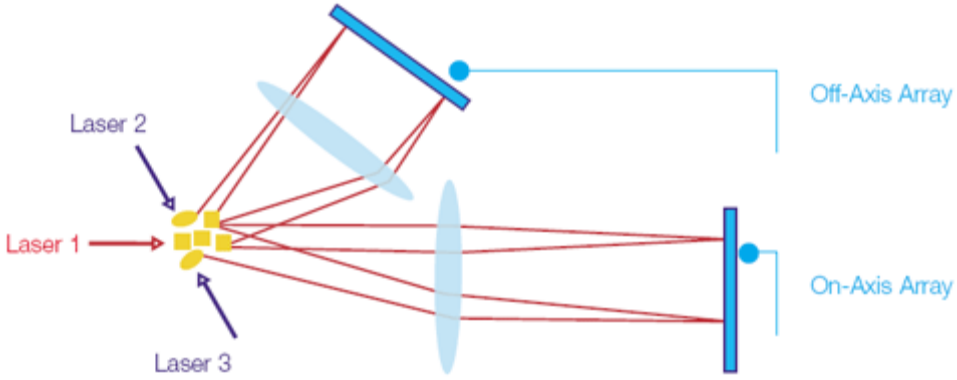

Figure 5-4: Schematic showing 3 laser beams scattered by the particles

The Microtrac Automated Sample Delivery Controller (SDC) is used for delivers WET suspensions to increases the accuracy and consistency of your particle-sizing operation. Inside SDC automated filling, de-aerating, pre-circulating, and circulating operation means each sample is handled consistently, to improve the repeatability and linearity of the results. It has in-line ultrasonic probe disperses agglomerated particles more effectively than the ultrasonic baths used by most competitive instruments. The below Figure 5-5 is the lab photo showing the Microtrac S3500 particle size analyzer in the middle, automated sample delivery controller for wet suspension to the left and sample deliver point (ofter open the lid of SDC) to the right.

Figure 5-5: Photo showing SDC (left), Microtrac S3500 PSA (middle) and deliver point (right)

During measurement the

Result of particle size analyzer (PSA) measurement

The results of particle size analyzer (PSA) measurement over samples taken from inlet and outlet flow of Evodos SPT centrifuge are shown below. The results are shown separately for rest run No. 1 and test run No. 2 with different flow velocity and other conditions please refer to **Error! Reference source not found.**.

Result of particle size analyzer (PSA) measurement for test run No. 1

In Figure 5-6 the number based cumulative percentage particle size distribution for test 1 inlet and solid discharge is shown. The horizontal axis is the size of the particles and the vertical axis shows the number based cumulative percentage of the particle according to their particle size. It can be seen that the cumulative number percentage with particle size of 7 μm and below is negligible. The percentage with particle size of 30 μm and below consist roughly 50% of the number of particles in those samples.

The percentage particle size distribution for test 1 inlet and solid discharge in Figure 5-7 is more easy to read. The particle size distribution has a curve curve shape close to normal distribution with a peak of 12% particle at the size of 30 μm.

It can be seen clearly from the measurement result of inlet flow cumulative and percentage particle size distribution from Figure 5-6 and Figure 5-7 that:

- The particle size distribution from solid discharge sample and inlet flow samples (taken at different time interval) shows more or less the same pattern of distribution.
- The pattern of inlet flow samples is also has similar. The pattern does not change in particle size and shape. It means the starch suspension is homogeneous and concentration of the flow does not affect particle size distribution within the flow.
- The size distribution of starch particles is ranging from 7 μm to 100 μm which corresponds quite well to previous mentioned statement that starch has a form of discrete granules ranging from about 5 to 40 μm in average particle size while potato starches have larger granules (up to 100μm).

Figure 5-8 and Figure 5-9 represents the measurement result of outlet flow cumulative and percentage particle size distribution for test run No. 1:

- The samples of solid discharge is show as the base line among particle size distribution of sample of outlet flow taken at different time interval.
- The outlet flow samples shows a significant difference in particle size distribution compare to the base line solid discharge particle size distribution. The shape of the particle size distribution is similar to each other and to the solid discharge particle size distribution pattern.
- The size distribution of particles from outlet samples has an average size of 1 μm. The particle size distribution has a curve similar to normal distribution.
- The number of those small particles around the size 1 μm is significantly smaller than that of bigger particles with size 7 μm to 100 μm because the majority of particles in the inlet from are from this range. Those small particles could be the particles which does not separated during the centrifugation process.
- The remaining particle size of around 1 μm correspond to the cut off rate of 2-37 μm claimed by the Evodos SPT centrifuge.
- The particle size distribution of sample 1EO and 12O for both outlet flow shows a different pattern with the rest of the samples. It could be errors from the sample taken or from the measurement device. The hypothesis of this behavior will be checked for test run No. 2 samples.

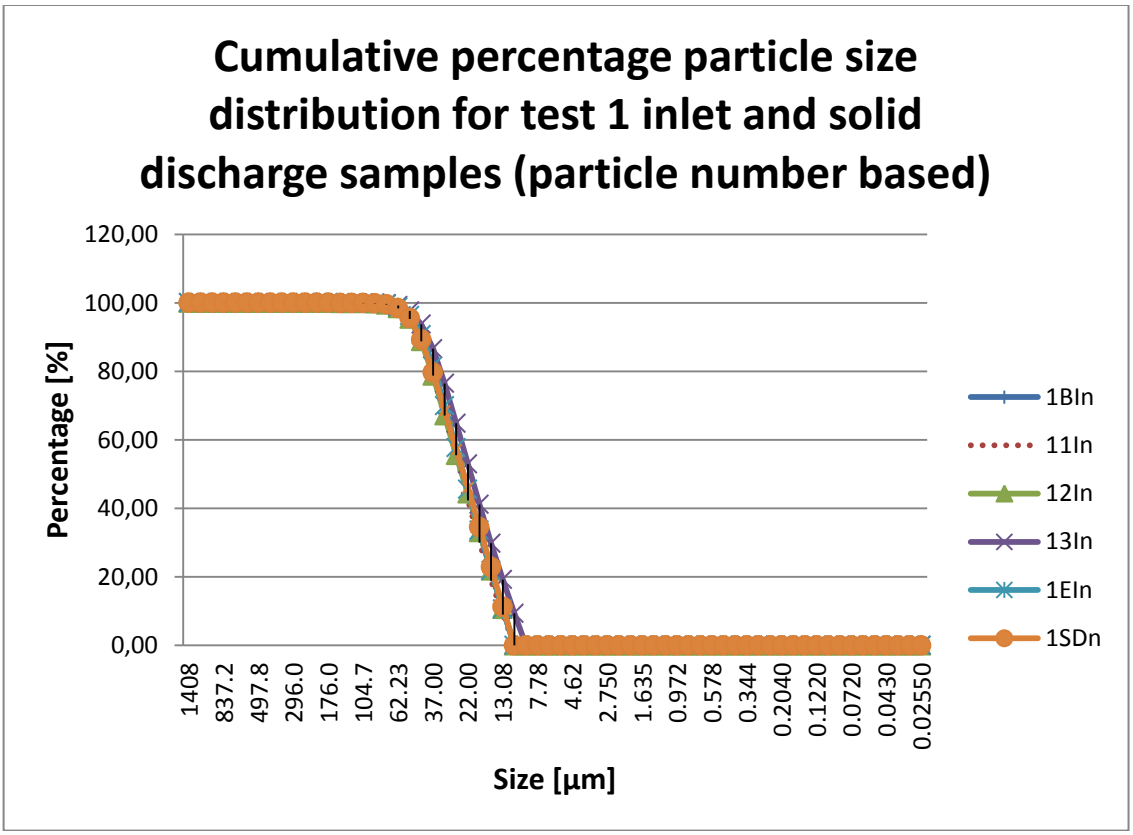

Figure 5-6: Cumulative percentage particle size distribution for test 1 inlet

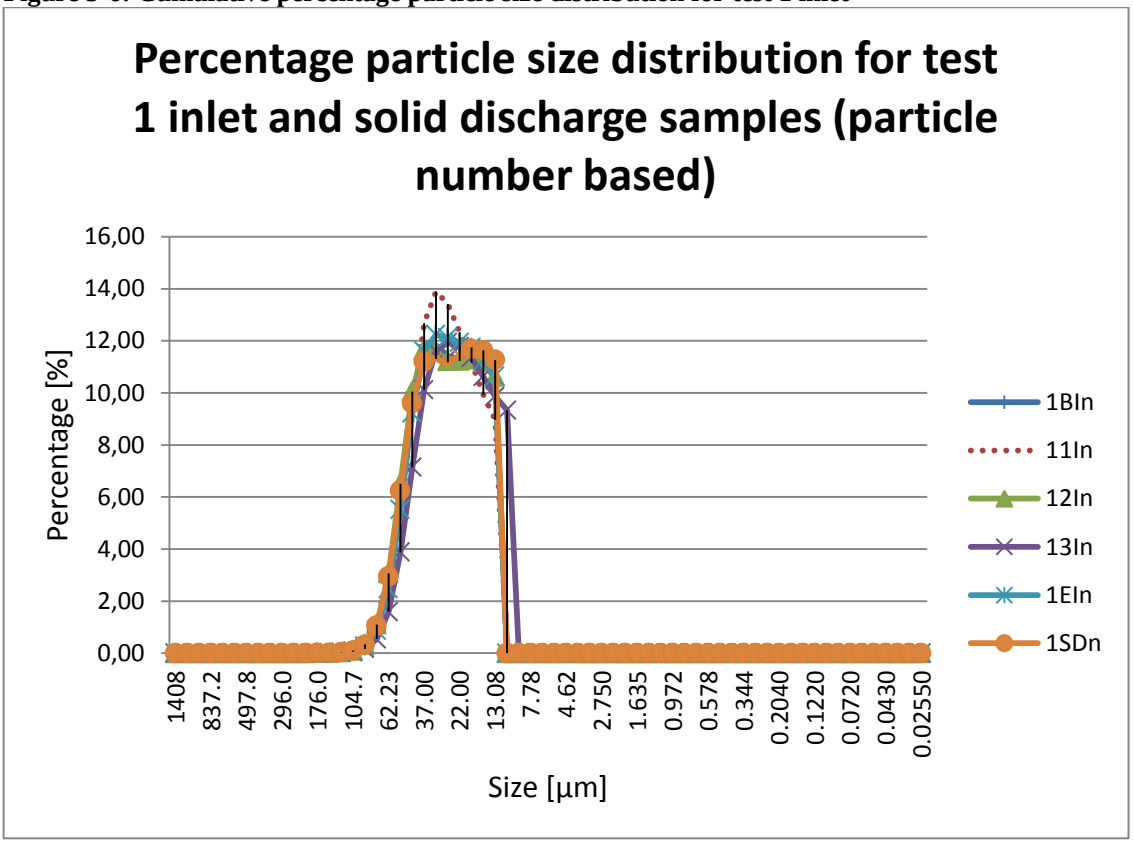

Figure 5-7: Percentage particle size distribution for test 1 inlet

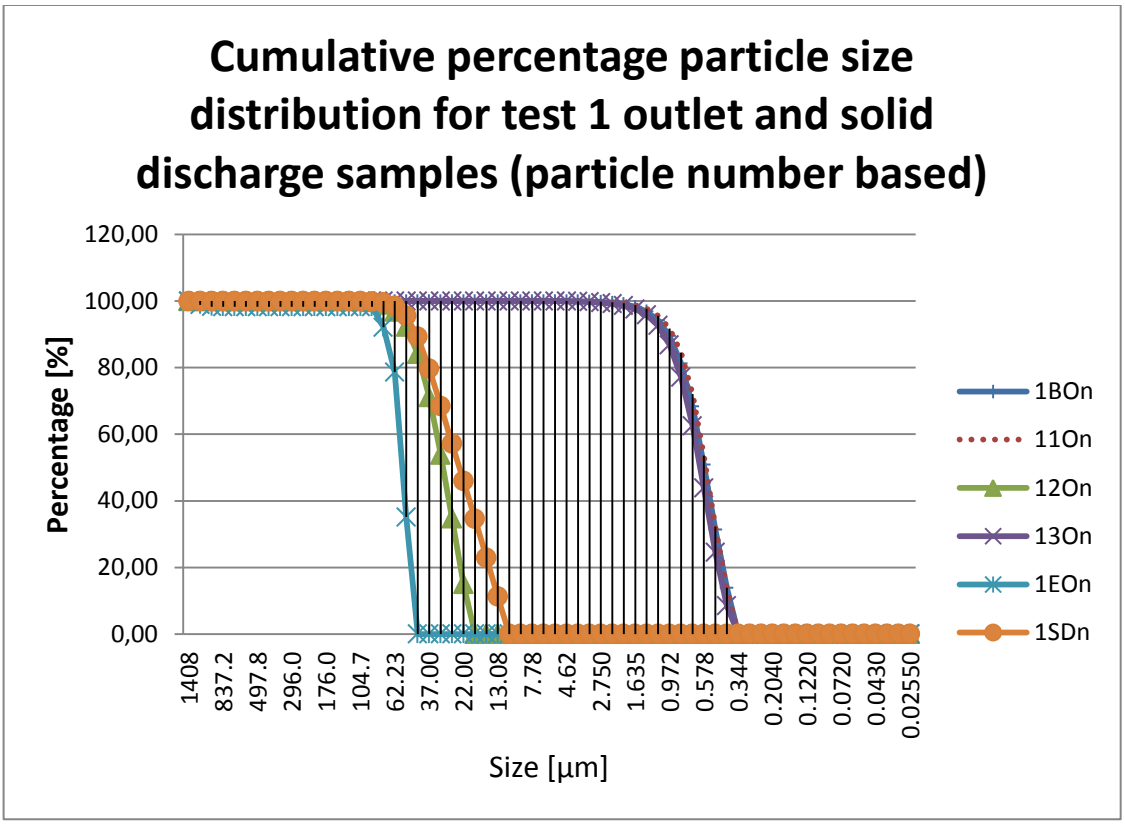

Figure 5-8: Cumulative percentage particle size distribution for test 1 outlet

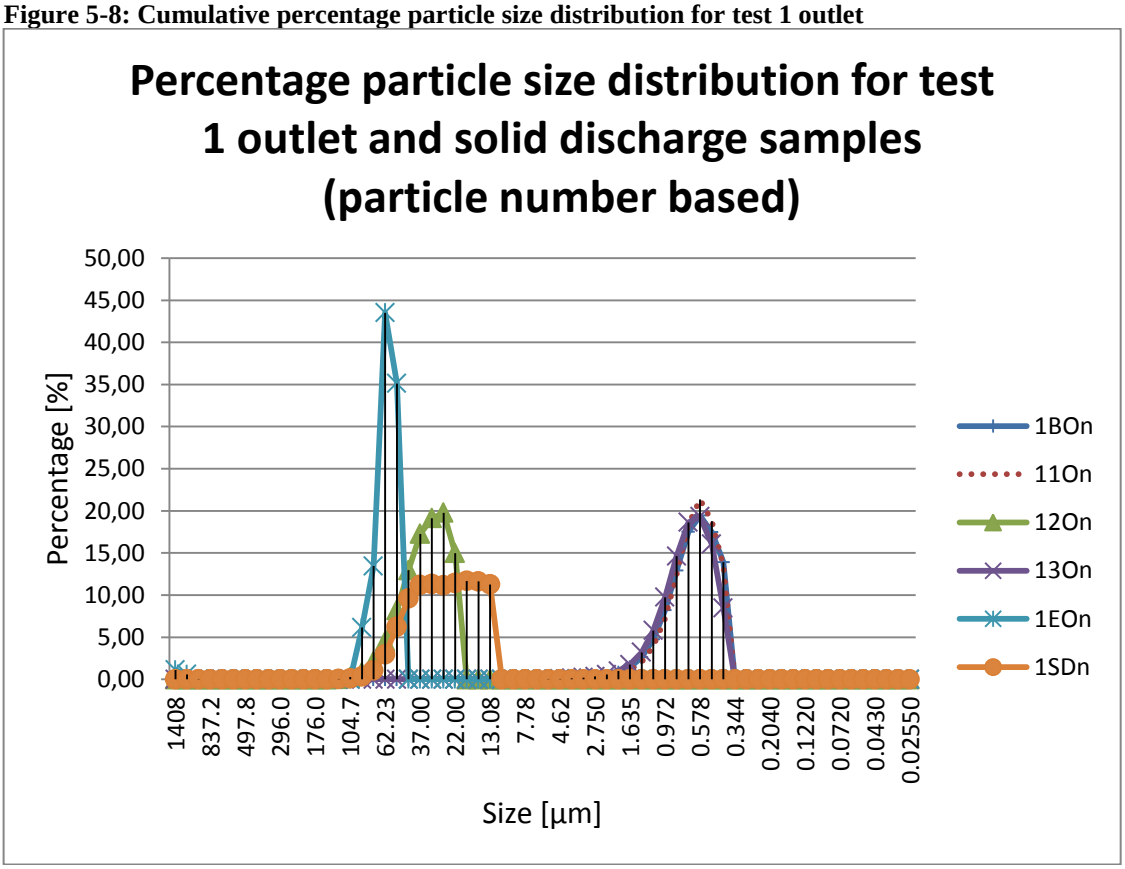

Figure 5-9: Percentage particle size distribution for test 1 outlet

Result of particle size analyzer (PSA) measurement for test run No. 2

In Figure 5-10 the number based cumulative percentage particle size distribution for test 2 inlet and solid discharge is shown. The horizontal axis is the size of the particles and the vertical axis shows the number based cumulative percentage of the particle according to their particle size. The particle distribution result is almost the same compare to Figure 5-6. The particle size of 7 μm and below is negligible. The percentage with particle size of 30 μm and below consist roughly 50% of the number of particles in those samples.

The percentage particle size distribution for test 2 inlet and solid discharge in Figure 5-11 is also similar to that of Figure 5-7 for test run No. 1. The particle size distribution has a curve shape close to normal distribution with a peak of 12% particle at the size of 30 μm.

Comparable with the test run No. 1, the test No.2 results indicates from the measurement result of inlet flow cumulative and percentage particle size distribution in Figure 5-10 and Figure 5-11 that:

- The particle size distribution from solid discharge sample and inlet flow samples (taken at different time interval) shows more or less the same pattern of distribution.
- The pattern of inlet flow samples is also has similar. The pattern does not change in particle size and shape. It means the starch suspension is homogeneous and concentration of the flow does not affect particle size distribution within the flow.
- The particle distribution result is almost the same compare to Figure 5-6.

Figure 5-12and Figure 5-13 represents the measurement result of outlet flow cumulative and percentage particle size distribution for test run No. 2:

- The samples of solid discharge is show as the base line among particle size distribution of sample of outlet flow taken at different time interval.
- The outlet flow samples shows a significant difference in particle size distribution compare to the base line solid discharge particle size distribution. The shape of the particle size distribution is similar to each other and to the solid discharge particle size distribution pattern.
- The size distribution of particles from outlet samples has an average size of 1 μm. The particle size distribution has a curve similar to normal distribution.
- The number of those small particles around the size 1 μm is significantly smaller than that of bigger particles with size 7 μm to 100 μm because the majority of particles in the inlet from are from this range. Those small particles could be the particles which does not separated during the centrifugation process.
- The remaining particle size of around 1 μm correspond to the 2-3 μm cut off rate of SPT centrifuge claimed by Evodos BV.
- The particle size distribution of all outlet samples stays very close to each other. It suggest the measurement result of outlet sample 1EO and 12O from test run No.1 could be contaminated with bigger particles.

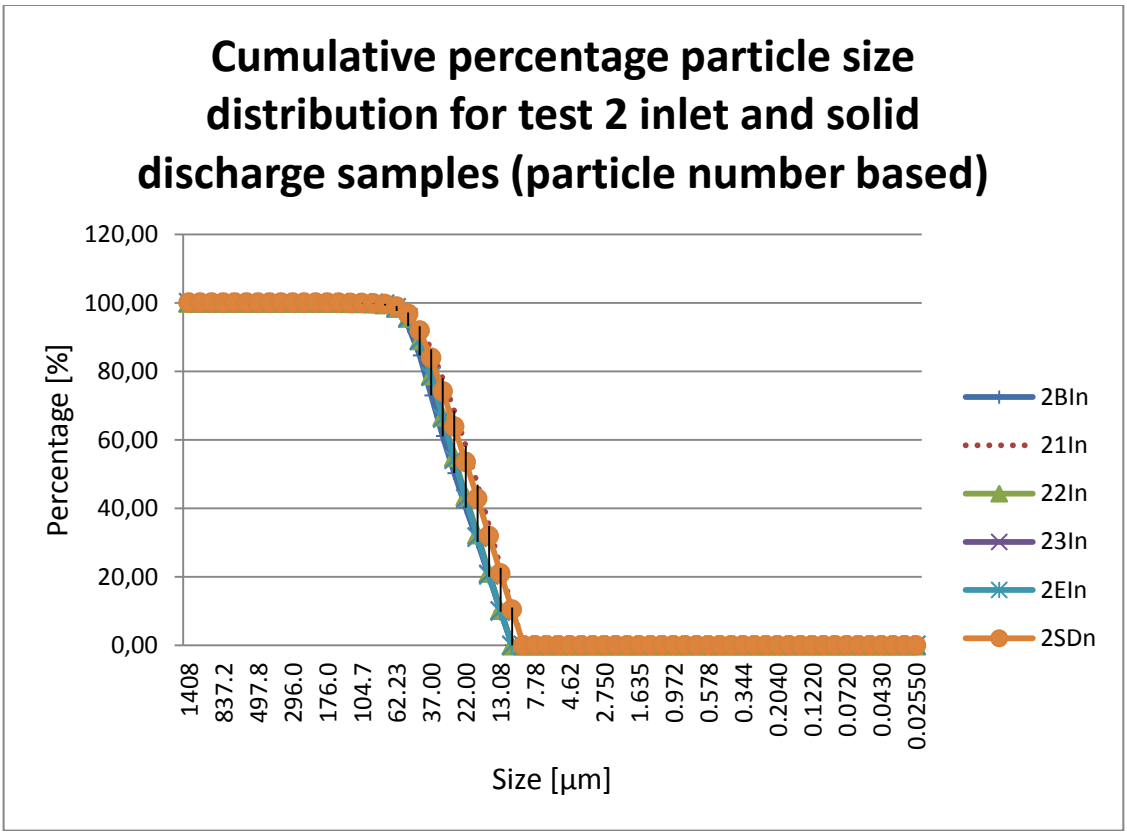

Figure 5-10: Cumulative percentage particle size distribution for test 2 inlet

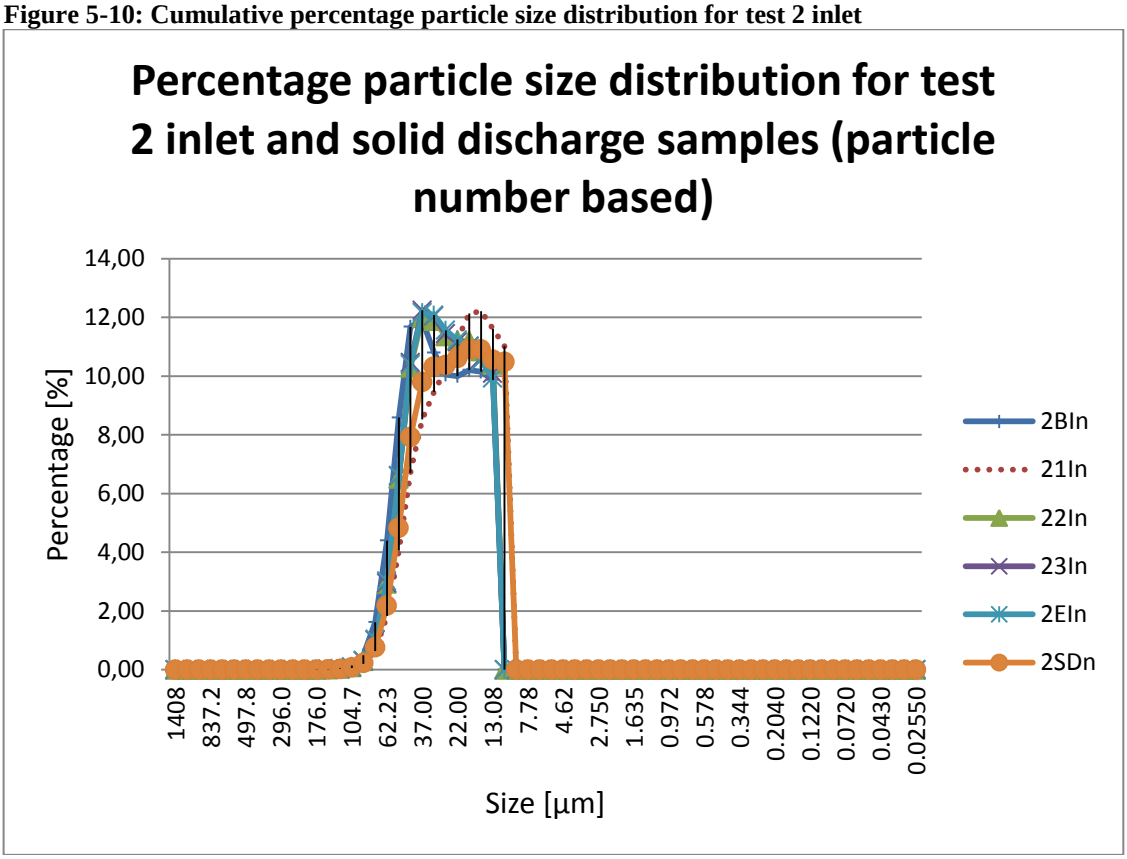

Figure 5-11: Percentage particle size distribution for test 2 inlet

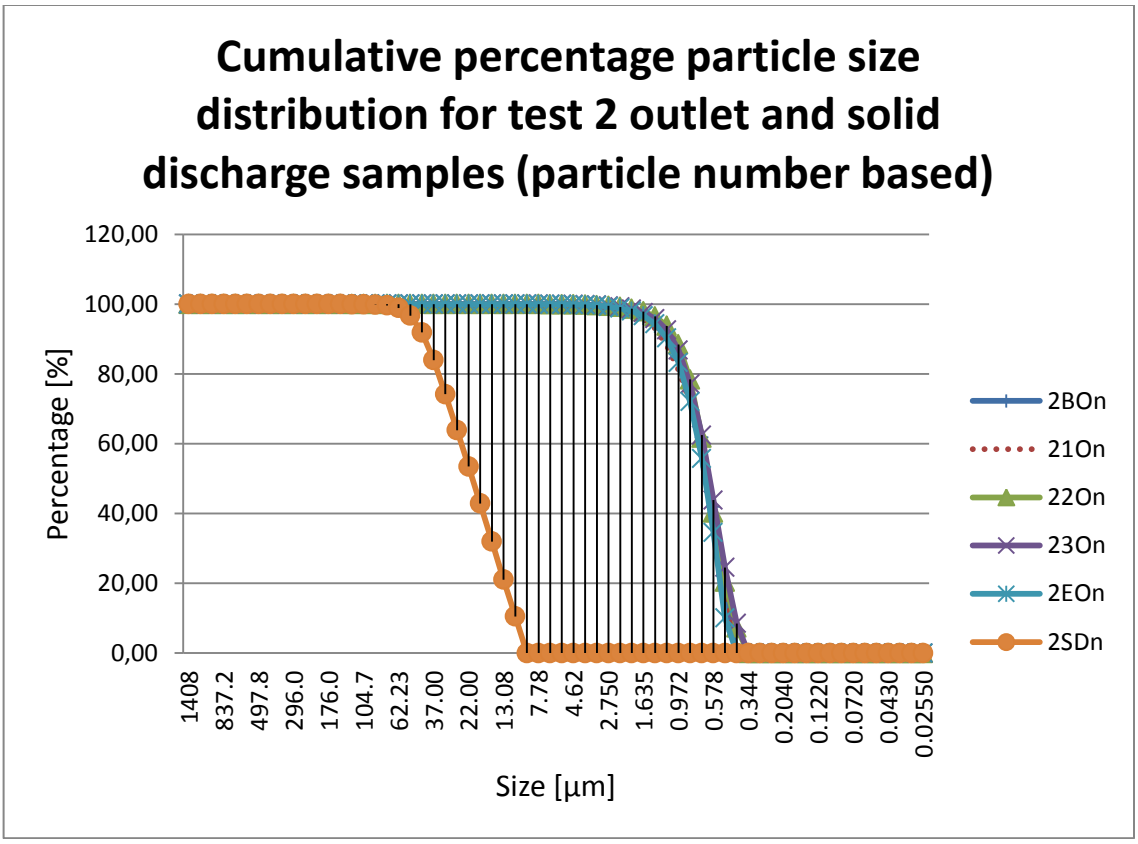

Figure 5-12: Cumulative percentage particle size distribution for test 2 outlet

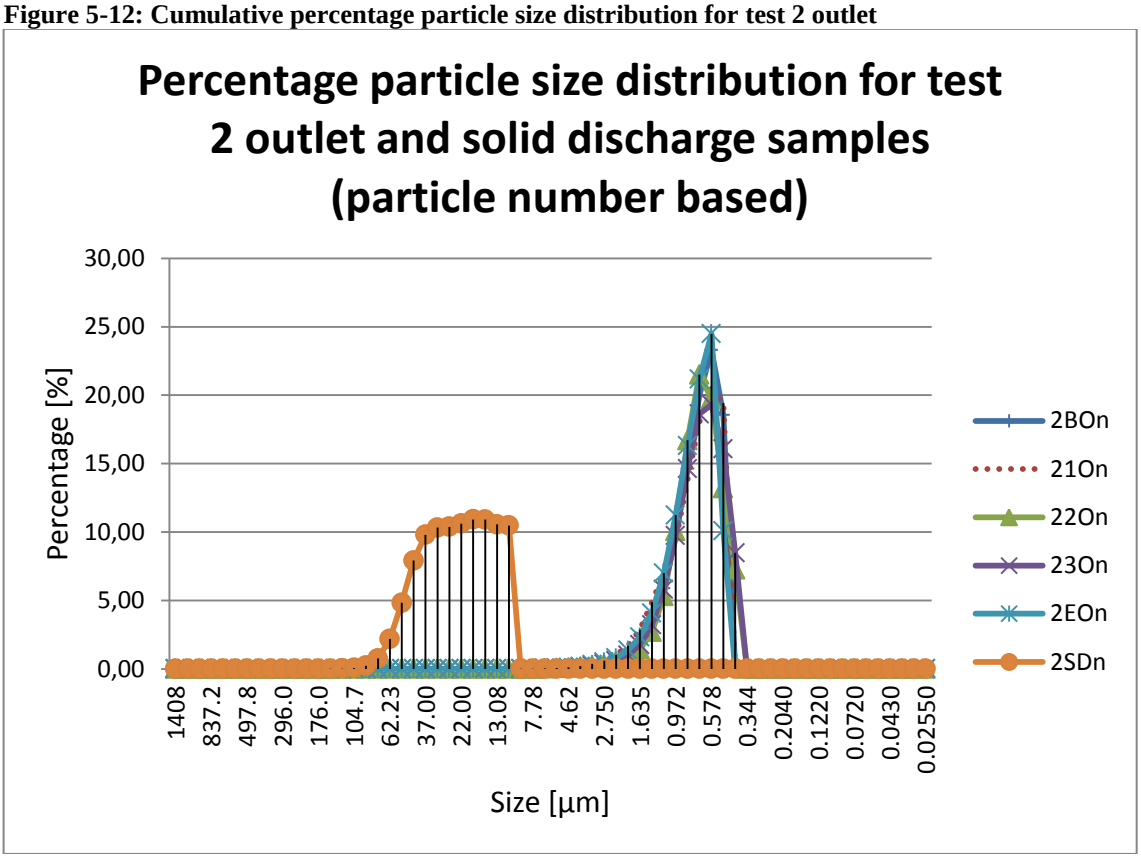

Figure 5-13: Percentage particle size distribution for test 2 outlet

5.3 Measurement of starch granule concentration in suspension by spectrophotometry

Spectrophotometric techniques are used to measure the concentration of solutes in solution by measuring the amount of light that is absorbed by the solution in a cuvette placed in the spectrophotometer. Light passes into a monochromator where only the desired wavelength, or a very narrow range of wavelengths, can pass through. From there, light passes through the sample cuvette, and on to a phototube where the light energy is converted to an electrical current that is registered on a meter.

For the starch suspension the concentration of the suspended starch granules (particles) is measured using spectrophotometry. The spectrophotometry measurement of starch suspension is different compared to measurement of concentration in normal solutions. The concentration of the suspended starch has to be partly calculated with initial data and partly derived from the turbidy measurement from the spectrophotometry.

Turbidity is the cloudiness or haziness of a fluid caused by individual particles (suspended solids). Sometimes they are generally invisible to the naked eye. Fluids can contain suspended solid matter consisting of particles of many different sizes. While some suspended material will be large enough and heavy enough to settle rapidly to the bottom of the container if a liquid sample is left to stand (the settable solids), very small particles will settle only very slowly or not at all if the sample is regularly agitated or the particles are colloidal. These small solid particles cause the liquid to appear turbid.[52] This also held true for starch suspension from the test run samples. For the inlet samples there are a layer of settled starch while the remaining liquid looks turbid.

Spectrophotometry measure light transmission rather than light scattering using a narrow, short-wavelength light source. For turbidity measurement it is also called light attenuation. The spectrophotometry is considered inaccurate for absolute turbidity measurement with highly susceptible to interferences. It is suggested to apply at low to medium turbidity levels for better result. The typical and suggested application rage is from 20 to 1,000 nm wave length.[53]

Introduction to Hitachi U-2900 Double Beam Spectrophotometer

The Hitachi High-Tech U-2900 double beam spectrophotometer is used to measure the turbidity of the starch samples. First the find the characteristic absorption spectrum and measure the absorbance in the sample.

As shown in Figure 5-14 light having wavelengths from 200-400 nm is called ultraviolet (UV), from 400-800 nm is called visible (VIS), from 800 nm – near 1mm is called infrared, and from 800 nm – 2500nm is called near infrared (NIR). The U-2900 is a double beam UV/VIS/NIR spectrophotometer which has the light range from 190nm to 1100nm.

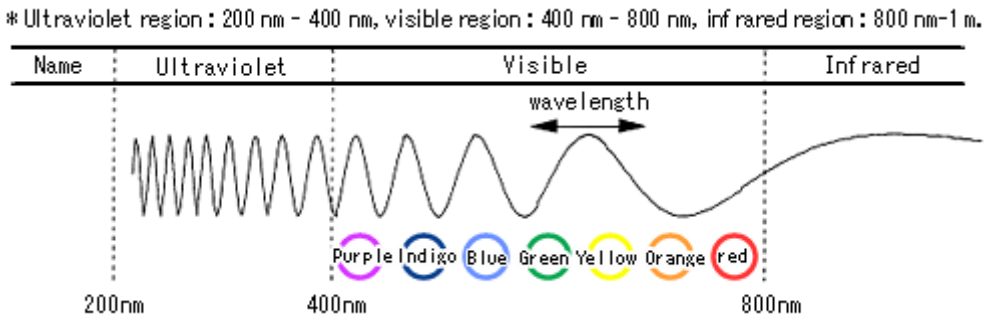

Figure 5-14: Name of light with wavelength range

The Figure 5-15 shows the schematic of light beam, overview and sample cuvette of the Hitachi U-2900 spectrophotometry. Inside the spectrophotometry, the energy of the light source is divided into two with a half mirror so that one passes through the reference side, and the other through the sample side. The chamber for the reference and sample cuvette is at the right side of the machine under the blue hatch.

Since the reference-side energy is also incident on a detector, photometry is carried out on the basis of this signal. Therefore, an energy change in the light source can be compensated to ensure stable measurement for a long time. This is unique for double beam design and unavailable with the single beam design.

Figure 5-15: U-2900 spectrophotometry schematic (left), overview (middle) and sample cuvette (right)

As mentioned earlier spectrophotometry measure light transmission rather than light scattering. Of the light that comes in from the lamp, the percent of light that comes in through the sample is called transmittance (T). Generally, transmittance is more commonly expressed as a percentage transmittance (%T). The part of the light that comes in from the window and is absorbed into the water of the aquarium is calls absorbance (Abs).

Result of spectrophotometry measurement inlet samples

From the Figure 5-16 and Figure 5-17 below shown spectrophotometry of the inlet sample from the two test runs. It is impossible to tell the difference between the turbidity or absorbance value from the inlet test run samples (1BI, 11I, etc.) because there are visible deposits of starch in the sample cuvette and the Abs value from the spectrometry is beyond the resolution range.

An alternative has to be found to determine or estimate the absolute and relative concentration value of the inlet samples.

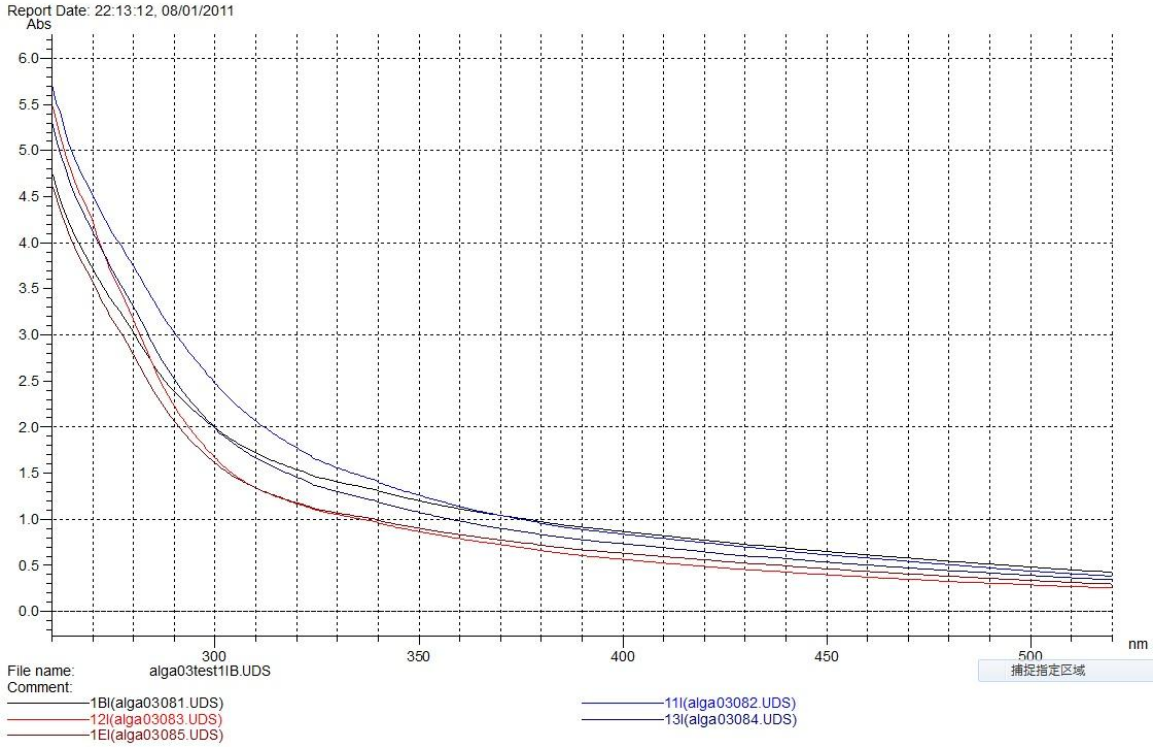

Figure 5-16: Wave length scan for test run No.1 Inlet samples

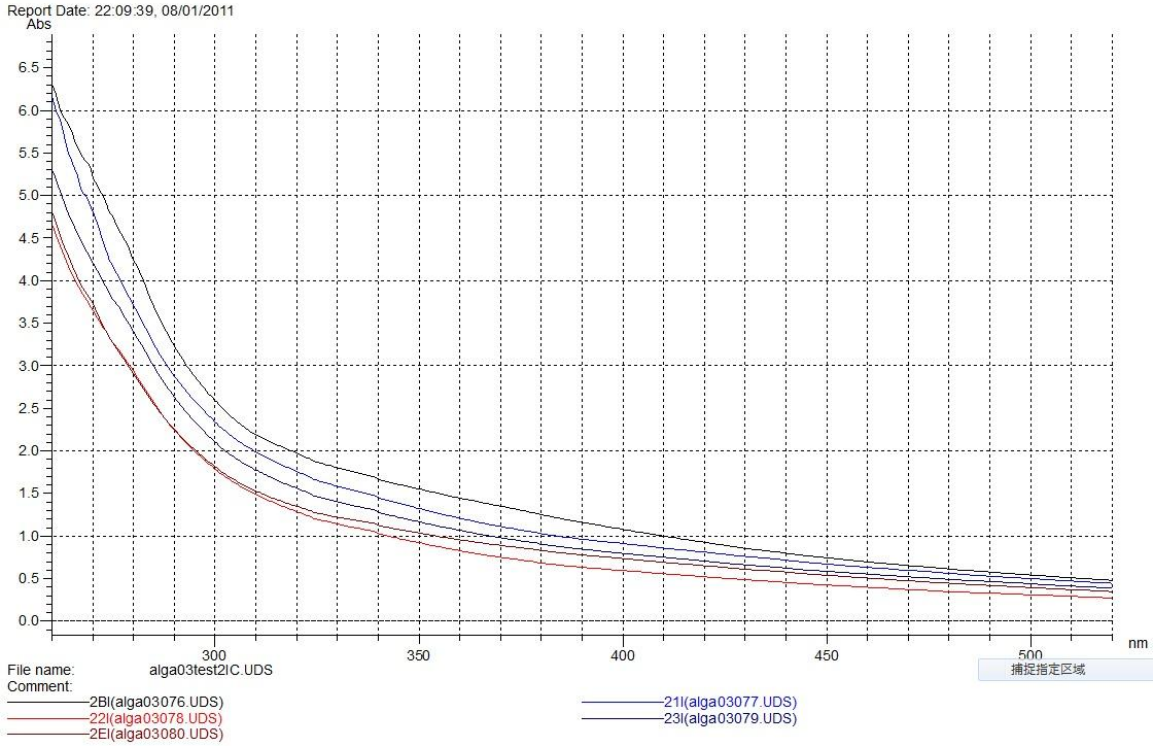

Figure 5-17: Wave length scan for test run No.2 Inlet samples

By visual inspection a certain level of deposit in cuvette for each inlet samples in Figure 5-18 the deposition level could be measured and a rough estimation of the weight concentration could be made.

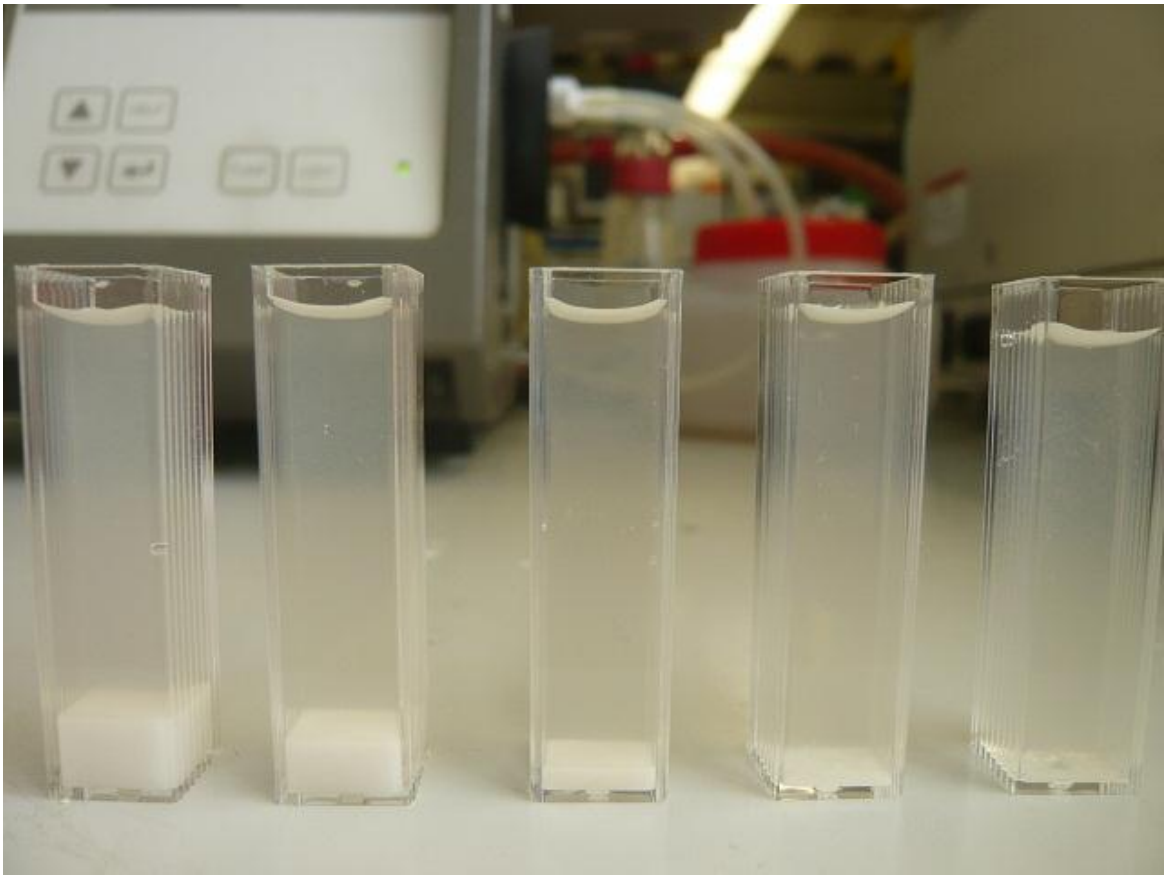

Figure 5-18: Solid deposit in cuvette for inlet samples test run NO.1

Estimated starch particle concentration with solid deposition level in cuvette is summarized in Table 5-3 and Table 5-4. It is clear to see that with the recirculation configuration of the starch test run the concentration of starch inside the inlet sample has been significantly reduced. The inlet sample concentration at the end of the test run is estimated to be 30 dilute then of the beginning.

Sample ID	1BI	11I	12I	13I	1EI
Solid deposition in cuvette [mm]	6.0	4.2	2.0	0.6	0.2
Estimated weight concentration [%]	6.67[1]	4.67	2.22	0.67	0.22
Test run No. 1, conditions: - Feed pump work at 3000 l/hr; - Pressure indicator at 0.3 barg; - Centrifuge running at 4200 rpm ; - Time discrepancy (time to fill up the centrifuge) 60s					

Table 5-3: Estimated concentration for inlet samples from test run No. 1

[1] : Concentration estimated from 20kg of starch in 300 litre of water.

Sample ID	2BI	21I	22I	23I	2EI
Solid deposition in cuvette [mm]	6	4.6	2.2	1.0	0.2
Estimated weight concentration [%]	6.67[1]	5.11	2.45	1.11	0.22
Test run No. 2, conditions: - Feed pump work at 1500 l/hr; - Pressure indicator at 0.3 barg; - Centrifuge running at 4200 rpm ; - Time discrepancy (time to fill up the centrifuge) 110s					

Table 5-4: Estimated concentration for inlet samples from test run No. 2

Result of spectrophotometry measurement outlet samples

The spectrophotometry results for outlet samples is shown below in Figure 5-19 and Figure 5-20. The Abs value is from 0.065 to 0.09 which indicates the concentration factor of approx. 60 to 70. Combined with the Abs value of the 1EI, the concentration factor for starch separation is over 2000.

A concentration value of 200 for algae culture (0.3% weight) has been claimed by Evodos. Convert it to the starch test results a concentration factor for starch particle of 100 has been achieved. Considering the difficulty of separating algae particles the converted concentration factor should be below 100.

It is also could be seen from Figure 5-19 and Figure 5-20 that the difference of Abs values between different outlet samples is not obvious. It is to say with higher inlet concentration the Evodos SPT centrifuge will provide more or less the same result as the lower inlet concentration cases.

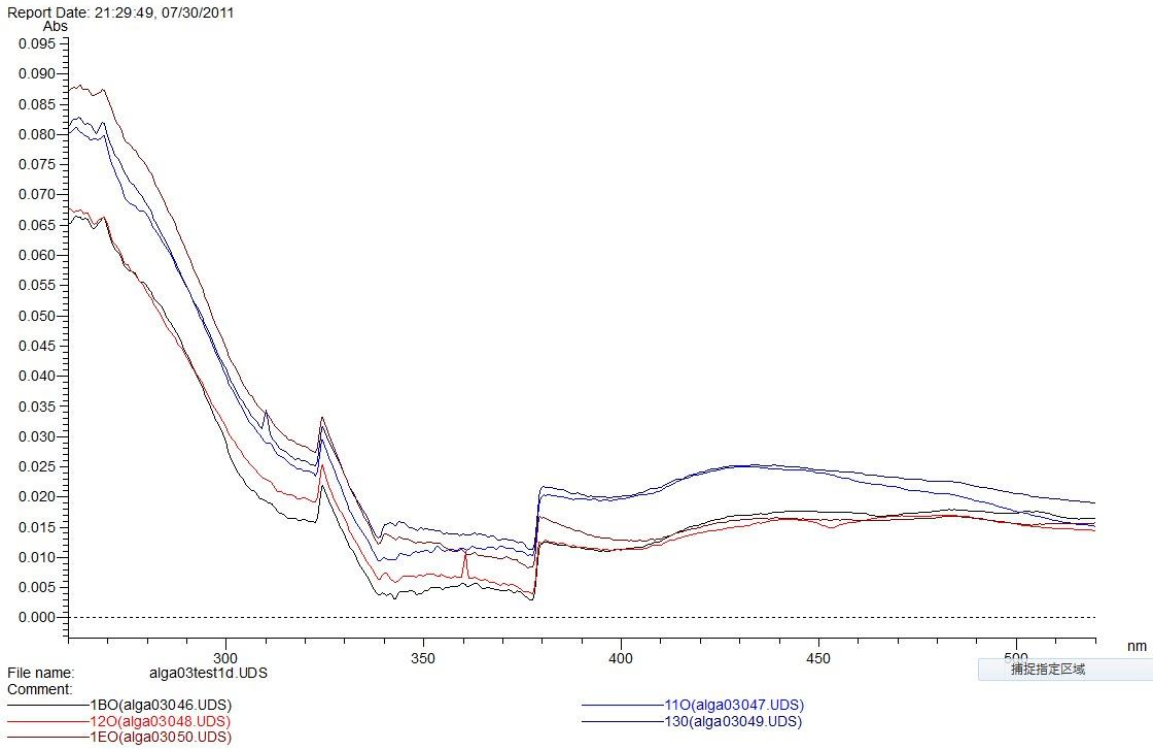

Figure 5-19: Wave length scan for test run No.1 Outlet samples

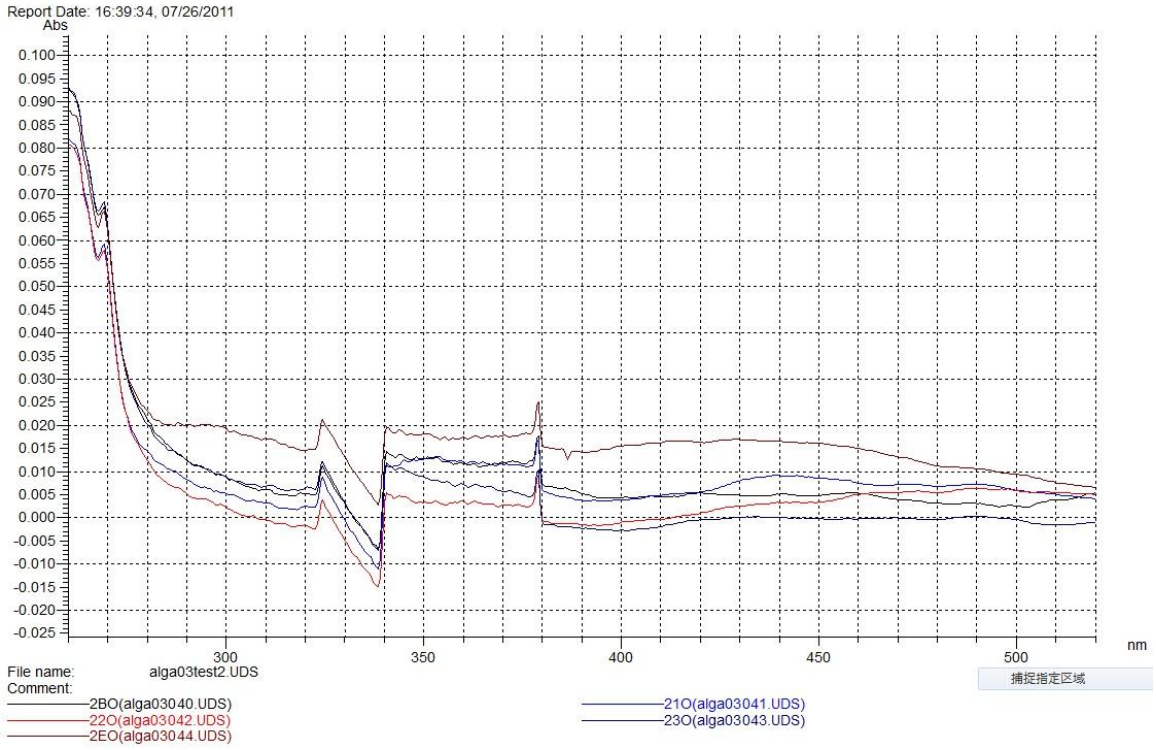

Figure 5-20: Wave length scan for test run No.2 Outlet samples

From below Figure 5-21 and Figure 5-22 a comparison of estimated concentration (%, weight) of inlet samples and Abs values of outlet concentration has been presented. It concludes that with the change on inlet concentration of 30 times the performance of the Evodos SPT centrifuge does not very that much for starch separation.

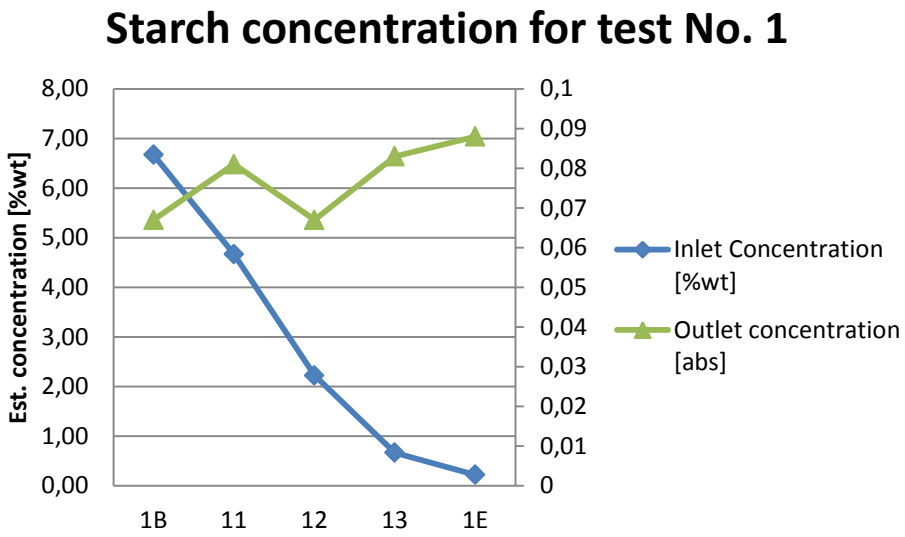

Figure 5-21: Starch concentration and Abs value for test run No. 1 inlet and outlet

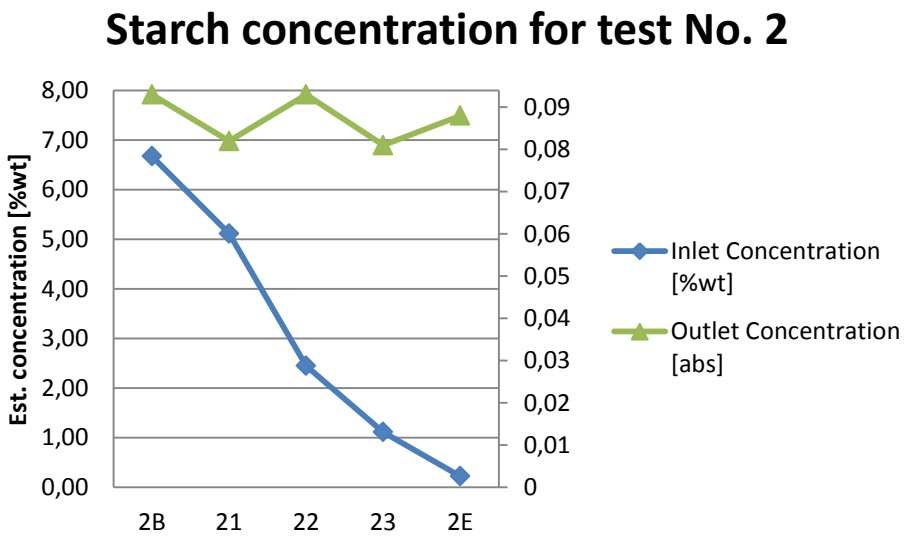

Figure 5-22: Starch concentration and Abs value for test run No. 2 inlet and outlet

The description and report of sampling of feed and effluent stream from starch test run at Evodos site is presented in this chapter. The introduction and experiment setup, measurement of particle distribution with laser particle size analyzer and measurement of starch granule concentration in suspension by spectrophotometry is given in section 5.1, 5.2 and 5.3 respectively.

Chapter 6 will conclude the thesis with key findings from CFD and test measurement results together with giving recommendations for future studies.

(this page is intentionally left blank)

CHAPTER 6:CONCLUSIONS AND RECOMMENDATIONS

In the thesis work, a Fluent model and a three-dimensional 1/8 of the complete geometry consisting of feed inlet, impeller chamber, 1st stage plate stack, middle disk, 2nd stage plate stack and the outer outlet chamber of the Evodos SPT centrifuge has been developed. The project has the challenge in both modeling the flow in a complex 3D geometry and modeling of the multiphase separation of micron sized particles.

In order to get a better understanding flow field and sedimentation inside the Evodos SPT centrifuge fluent simulation has been conducted on the model. For separation performance for particle of different sizes a series of DPM calculation has been done on the pre-calculated continuous phase simulation results. A starch test measurement has been conducted to measure the particle size distribution and granule concentration.

There are several conclusions could be drawn from the 3D CFD modeling of the Evodos SPT centrifuge and starch test run measurements:

CFD Model results:
- A 3D CFD Fluent model of the Evodos SPT centrifuge has been successfully developed and the simulation results provide deep insight into the flow field inside the centrifuge which is difficult if not possible for experimental researches.
- From the flow pattern analysis, the model predict a strong unsteady whirl in the inlet chamber caused by the impeller blade.
- From the pressure profile analysis, the model gives indication of a reverse pressure gradient at the inner side of a flow channel between parallel plates.
- The separation performance based on DPM predicts a cut-off sized of 1.5 μm for starch particles and 3μm for microalgae particles.

Starch test run measurement results:
- Both test runs particle size distribution results for inlet samples confirm with each other and corresponds well with the theoretical particle size distribution for starch.
- The cut-off size of 1 μm correspond well with the 2-3 μm claimed by Evodos by 2 starch test run results from particle size distribution result of outlet samples.
- For smaller inlet flow the concentration of starch granule does not show a significant improvement.
- A concentration factor of over 2000 for starch separation has been estimated by the concentration measurement. Converted concentration factor of approx. 100 for microalgae separation could be concluded compare to the concentration factor of 200 claimed by Evodos.

Validation of the model
- The shape and trend of the path line of the Fluent model has been partially validated by the visual impression from previous Evodos SPT centrifuge test runs for algae separation.
- The flow patter and pressure profile of the Fluent model has been partially validated by the theoretical formulas for tangential velocity and static pressure in the centrifuge.
- The separation performance comparison based on different particle sizes together with the Evodos expected value and starch test measurements results validates the CFD model.

This thesis work is a first attempt to model microalgae sedimentation in Evodos SPT centrifuge. Future CFD study may lead to improvement of the model and better prediction of the flow field and separation performance. The following recommendations could be drawn from the report:

- Study the geometry of the impeller blades effect on unsteady whirl behavior in the impeller chamber.
- Separation efficiency could be optimized by changing the shape and radius of internal parallel plate curvature for different particles and sized need for separation.
- Further develop and use more accurate physical properties on microalgae culture and other material for separation.
- Theoretically derive formula according to Sigma theory.
- Instead of liquid-solid two phase flow model used in the current model, use VOF method in Fluent to further study the air-liquid-solid three phase flow and the effect of the air core near the axis of the centrifuge. This will impose great demands on computing power and complexity of the model.
- Further study the effects and influence of the operation parameter e.g. flow rate, rotational speed, etc. over the separation performance.

REFERENCES

1. EPEA GmbH. *Cradle to Cradle Principles*. 2011; Available from: http://epea-hamburg.org/index.php?id=155.
2. Veringa, H.J. *Advanced techniques for generation of energy from biomass and waste*. 2004 [cited 2010 12-12]; Available from: http://www.ecn.nl/fileadmin/ecn/units/bio/Overig/pdf/Biomassa_voordelen.pdf.
3. Wikipedia. *Microalgae*. 2011; Available from: http://en.wikipedia.org/wiki/Microalgae.
4. Wijffels, R.H. and M.J. Barbosa, *An Outlook on Microalgal Biofuels.* Science, 2010. **329**(5993): p. 796-799.
5. Benemann, J.R., *Microalgae Biofuels: A Brief Introduction.* 2009.
6. Borowitzka, M.A., *Micro-algal biotechnology*. 1988: Cambridge University Press.
7. Agrawal, R. and N.R. Singh, *Solar Energy to Biofuels.* Annual Review of Chemical and Biomolecular Engineering, 2010. **1**(1): p. 343-364.
8. Wijffels, R.H., M.J. Barbosa, and M.H.M. Eppink, *Microalgae for the production of bulk chemicals and biofuels.* Biofuels Bioproducts & Biorefining-Biofpr, 2010. **4**(3): p. 287-295.
9. Schmid-Staiger, U., *Algae Biorefinery - Concepts*, in *National German Workshop on Biorefineries*. 2009: Worms, Germany.
10. Nyomi Uduman, Y.Q., Michael K. Danquaha, Gareth M. Forde, and Andrew Hoadley, *Dewatering of microalgal cultures: A major bottleneck to algae-based fuels.* Journal of Renewable and Sustainable Energy, 2009.
11. Mata, T.M., A.A. Martins, and N.S. Caetano, *Microalgae for biodiesel production and other applications: A review.* Renewable and Sustainable Energy Reviews, 2010. **14**(1): p. 217-232.
12. Bilanovic, D., G. Shelef, and A. Sukenik, *Flocculation of mictroalgae with cationic polymers - effects of medium salinity.* Biomass, 1988. **17**(1): p. 65-76.
13. Uduman, N., et al., *Dewatering of microalgal cultures: A major bottleneck to algae-based fuels.* Journal of Renewable and Sustainable Energy, 2010. **2**(1): p. -.
14. Grima, E.M., et al., *Recovery of microalgal biomass and metabolites: process options and economics.* Biotechnology Advances, 2003. **20**(7-8): p. 491-515.
15. Shelef, G.A.A.S., and M. Green, *Microalgae harvesting and processing: A literature review*.
16. Borowitzka, M.A., *Algal biotechnology products and processes - matching science and economics.* Journal of Applied Phycology, 1992. **4**(3): p. 267-279.
17. Heasman, M., et al., *Development of extended shelf-life microalgae concentrate diets harvested by centrifugation for bivalve molluscs - a summary.* Aquaculture Research, 2000. **31**(8-9): p. 637-659.
18. Danquah, M.K., et al., *Dewatering of microalgal culture for biodiesel production: exploring polymer flocculation and tangential flow filtration.* Journal of Chemical Technology and Biotechnology, 2009. **84**(7): p. 1078-1083.
19. Evodos B.V. *Evodos SPT home page*. 2010; Available from: http://www.evodos.eu/?id=4101; http://www.evodos.eu/?id=4505.
20. Semerjian, L. and G.M. Ayoub, *High-pH magnesium coagulation-flocculation in wastewater treatment.* Advances in Environmental Research, 2003. **7**(2): p. 389-403.
21. Bernhardt, H., Water Supply, 1994. **43**(222).
22. Sukenik, A. and G. Shelef, *Algal autoflocculation - verification and proposed mechanism.* Biotechnology and Bioengineering, 1984. **26**(2): p. 142-147.

23. Feris, L.A., et al., *Optimizing dissolved air flotation design system.* Brazilian Journal of Chemical Engineering, 2000. **17**(4-7): p. 549-555.
24. Bektas, N., et al., *Removal of phosphate from aqueous solutions by electro-coagulation.* Journal of Hazardous Materials, 2004. **106**(2-3): p. 101-105.
25. Rubio, J., M.L. Souza, and R.W. Smith, *Overview of flotation as a wastewater treatment technique.* Minerals Engineering, 2002. **15**(3): p. 139-155.
26. Edzwald, J.K., *Principles and applications of dissolved air flotation.* Water Science and Technology, 1995. **31**(3-4): p. 1-23.
27. Rushton, A., A.S. Ward, and R.G. Holdich, *Solid-liquid filtration and separation technology*. 2nd, completely rev. ed. 2000, Weinheim: Wiley-VCH. 587 S.
28. Evodos B.V. *Evodos SPT, a breakthrough in separator technology*. 2011; Available from: http://www.loviehoeve.be/evodos/EVODOS.htm.
29. Wikipedia. *Computational fluid dynamics*. 2011; Available from: http://en.wikipedia.org/wiki/Computational_fluid_dynamics.
30. X. Romaní Fernández, H.N., *Flow And Sedimentation In Industrial Solid Bowl Centrifuges: A Numerical And Experimental Study*, in *AFS 2010 Annual Conference & Exposition*. 2010: Grand Hyatt Hotel, San Antonio, TX.
31. Herman, P., *Simulation cuts time needed to develop lube centrifuge by 70%.* Journal Fluent software users, 2003.
32. Xia, J.-Y., et al., *Computational investigation of fluid dynamics in a recently developed centrifugal impeller bioreactor.* Biochemical Engineering Journal, 2008. **38**(3): p. 406-413.
33. Nowakowski, A.F., et al., *Application of CFD to modelling of the flow in hydrocyclones. Is this a realizable option or still a research challenge?* Minerals Engineering, 2004. **17**(5): p. 661-669.
34. Cullivan, J.C., et al., *New understanding of a hydrocyclone flow field and separation mechanism from computational fluid dynamics.* Minerals Engineering, 2004. **17**(5): p. 651-660.
35. Azadi, M., M. Azadi, and A. Mohebbi, *A CFD study of the effect of cyclone size on its performance parameters.* Journal of Hazardous Materials, 2010. **182**(1-3): p. 835-841.
36. Cortés, C. and A. Gil, *Modeling the gas and particle flow inside cyclone separators.* Progress in Energy and Combustion Science, 2007. **33**(5): p. 409-452.
37. Wardle, K.E., T.R. Allen, and R. Swaney, *Computational Fluid Dynamics (CFD) Study of the Flow in an Annular Centrifugal Contactor.* Separation Science and Technology, 2006. **41**(10): p. 2225-2244.
38. Jain, M., et al., *Using CFD To Understand How Flow Patterns Affect Retention of Cell-Sized Particles in a Tubular Bowl Centrifuge.* Industrial & Engineering Chemistry Research, 2005. **44**(20): p. 7876-7884.
39. ANSYS Inc., ed. *ANSYS FLUENT 12.0 Theory Guide*. 2009.
40. ANSYS Inc., ed. *ANSYS FLUENT 12.0 User's Guide*. 2009.
41. Ullmann, F., *Ullmann's encyclopedia of industrial chemistry Elektronische Daten*. 7th ed. 2010: Wiley-Blackwell. Online-Datei.
42. Wikipedia. *Reynolds number*. 2011; Available from: http://en.wikipedia.org/wiki/Reynolds_number.
43. Lun, I., R.K. Calay, and A.E. Holdo, *Modelling two-phase flows using CFD.* Applied Energy, 1996. **53**(3): p. 299-314.
44. Plat, R., *Gravitational and centrifugal oil-water separators with plate pack internals*. 1994, Delft University of Technology.
45. Isleib, D., *Density of potato starch.* American Journal of Potato Research, 1958. **35**(3): p. 428-429.

46. Holdich, R.G., *Fundamentals of Particle Technology*. 2002: Midland Information Technology and Publishing. 173.
47. Wikipedia. *Starch*. 2011; Available from: http://en.wikipedia.org/wiki/Starch.
48. Moura, R.A., *The effect of physical aging, starch particles size, and starch oxidationi on thermal-mechanical properties of poly(lactic acid)/starch composites*, in *Department of Grain Science and Industry College of Agriculture*. 2006, Kansas State University.
49. Park, S.-H., J.D. Wilson, and B.W. Seabourn, *Starch granule size distribution of hard red winter and hard red spring wheat: Its effects on mixing and breadmaking quality*. Journal of Cereal Science, 2009. **49**(1): p. 98-105.
50. Coulter, B., *Particle size analysis - Evaluating laser diffraction systems in the light of ISO 13320-1*. 2010.
51. Microtrac. *Microtrac S3500 Technology*. 2011; Available from: http://www.microtrac.com/ProductsTechnology/MicrotracS3500ParticleSizeAnalyzer/MicrotracS3500Technology.aspx.
52. Wikipedia. *Turbidity*. 2011; Available from: http://en.wikipedia.org/wiki/Turbidity.
53. Anderson, C.W., *National Field Manual for the Collection of Water-Quality Data (TWRI Book 9) Chapter 6.7 Turbidity*, USGS, Editor. 2005.

(this page is intentionally left blank)

APPENDIX A: Innowater project minutes of meeting

Appendix A1. Internal progress report 07-10-2010

Activities:

1. Meeting with Hen Boele in Delft, to know the basics of the Evodos' centrifuges (Aug.);
2. In Breda to see the machine on site (Aug.);
3. Literature research on centrifuges (July~);
4. Define modeling strategies:
    - Separately model different parts: Impeller; Plate stack (two stages);
    - Working fluid: firstly with pure water liquid
        i. to see if the model methods works,
        ii. and to study flow patterns and flow behaviors, velocity profile, turbulence intensity, pressure distribution etc..
    - then, with the mixture between water and microalgae.
5. Making CFD models:
    - Based on estimation before getting the geometry from Evodos, ¼ geometry was built. Results prove modeling approach and results reasonable and explainable (Sep.);
    - Impeller model based on the design data from Evodos, the results evaluation is attached in file1 (ongoing);
    - Make model between two plates to study flow pattern, flow path (check if it is laminar, or the turbulence density), so far, with simplified boundary profile at inlet;

Plan:

1. Finish 3D model between two plates (Oct. mid);
2. 15 plates model (1/8 whole geometry) of plate stack (Oct. end);
3. Connect the impeller model to 15-plate model together to one model (Nov. mid);
4. Implement the microalgae component into the liguid to form the fluid mixture by using certain method (Nov. end);
5. Measure the viscosity of microalgae liquid (Nov. end).

(Estimated) Difficulties:

1. Geometry limitation: 1/8 impeller only match 120 plates options among the 45, 60, 90, 120 options;
2. For the mesh creation of the thin geometry of 15 plates, this could cause problems because of the narrow long geometries, or could take too much time;
3. By certain methods to implement the microalgae fluid, the certain method could be Discrete phase? Multiphase? Or as liquid mixture?
4. For the whole model computation, more computation facilities could be required for further computation.

Optimization suggestion for the design (so far):

To avoid backflows or swirl flows (decrease energy consumption, and then improve efficiency) shows in the modeling results:

1. Add a skirt edge at the top of the impeller;
2. Change the 2D straight-up impeller design into leaning 3D.

Appendix A2. Minutes of meeting 25-11-2010

INNOWATER MEETING

Place of meeting
Evodos, Raton site, Raton B.V.
Takkebijsters 53, 4817BL Breda

Date of meeting
25-11-2010

Report by
Nieves Gonzalez-Ramon

Present
TU Delft, Bowen Yu
TU Delft, Zuopeng Qu
Evodos, Marco Brocken
Feyecon, Nieves Gonzalez-Ramon
Feyecon, Martijn van der Kraan

Absent

Copy to
TU Delft, Geert-Jan Witkamp
Evodos, Hen Boele
Feyecon, Adreas Weber

Page

Project
Innowater

Subject
Project progress meeting

Top	Time	Who	Content
1	14:00	NG	Introduction, additional points.
2	14:05		Overall situation of the project. One year status report was submitted October 2010, next report has to be produced March 2011. Delays on machine construction have occurred, but a formal request of prolongation of the project is still premature.
3	14:15		Visit to the workshop and to an existing centrifuge example similar to the one that will be built within the project.
4	15:00		Activities of TU Delft. The FD model of the centrifuge is developed in two parts with 1/8 of the circular section: A) the lower propeller part including separation disk B) the upper separation part. Bottlenecks: Convergence of the two parts is still not matching, parameters as density of particles need more accurate approximations.

5	15:45	Activities Evodos The machine design details for FD modeling were provided to Zuopeng. With a demo machine EVODOS ran tests at Schiphol Airport harvesting the algae at ~ 3 m3/hr at 3000 x G. Energy demand was < 1,6 kWh / m3 feedflow. Evodos found out that the corrosion problem with saline water will not occur for normal operation T (below 40C) so no need for vane coating neither catodic protection is envisaged. Mechanical improvements as having one stage centrifuge with double length veins and a separation plate at the bottom is considered.
6	16:15	Activities Feyecon Particle density determination methods have been researched in the literature and its application is ongoing. Preconcentration processes with superabsorber materials have been tested with fresh Nannochloropsis algae cultures. Preparation of open pond culture (30m2 raceway) in NL has been made that will allow harvesting tests upon availability of the centrifuge.
7	17:15	Future actions all partners (TU DELFT, Evodos, Feyecon). - A bulk material centrifuge test with starch particles will be done on week 29 NOV-3 DEC among TU Delft and Evodos. - Evodos finalises machine construction by 1 Feb 2011. - Zuopeng and Bowen finalise convergence of the two parts centrifuge model. Mechanical improvement as the tilting of the impeller plates will be studied on the obtained FD model. - Determination of the viscosity of algae cultures will be done by Zuopeng and Bowen with Feyecon assistance. -Measurements of algae particle densities will be done by Feyecon -Feyecon further explores pre concentration techniques -Tests on algae cultures will be planned between Feyecon and Evodos upon availability of the machine. -Next meeting at EVODOS location (Breda) on 9 FEBRUARY 2011 AT 11am

Appendix A3. Minutes of meeting 10-01-2011

INNOWATER MEETING

Place of meeting
Evodos, Raton site, Raton B.V.
Takkebijsters 53, 4817BL Breda

Date of meeting
10-01-2011

Report by
Bowen Yu

Present
TU Delft, Bowen Yu
Evodos, Jan-Kees Boele
Evodos, Hen Boele
Evodos, Remko van Dam

Absent

Copy to
TU Delft, Zuopeng Qu
TU Delft, Geert-Jan Witkamp
Evodos, Marco Brocken
Feyecon, Nieves Gonzalez-Ramon
Feyecon, Martijn van der Kraan
Feyecon, Adreas Weber

Page

Project
Innowater

Subject
Starch test sample taking and progress report meeting

Topic	Time	Who	Content
1	9:30	BY	Introduction
		JB	Preparation for starch test sample taking
		RD	Trouble shooting for motor problem of SPT centrifuge
2	12:30	BY	Progress report of the CFD work.
		JB	Presentation of the power point slides of 25-11-10
		RD	Point of interest/discussion:
		HB	- The path-line pattern shown in CFD transient model is confirmed by previous test photo provide by Evodos showing a curved solid deposition line between blades. A good indication of validation of the CFD model. Please refer to photos below - Contradict to the model, the SPT centrifuge is not completely filled with liquid. There are clear vertical interface (free surface) of water and air parallel to the shaft. The feed will leave the inlet as a jet of water and enter the rotating liquid pool. A new CFD multiphase modelling approach of VOF (volume of fluid) is proposed. - Due to the boundary condition of the model (open or restricted) the vertical pressure drop seems too big. - A validation of the model and test sample measurements will be done. - Raw data of the particle size measurement will be forwarded to RD of

			Evodos - A meeting of HB, BY, ZQ and GW to discuss the model is proposed
3	14:00	BY RD	2 test runs on 3000 l/hr and 1500 l/hr, 21 samples are taken. Please refer to Table 5-1: Sample ID, information and timing for test run No. 1 and Table 5-2: Sample ID, information and timing for test run No. 2
4	15:30		End of the meeting and test

Appendix A4. Minutes of meeting 10-03-2011

INNOWATER MEETING

Place of meeting
Evodos, Raton site, Raton B.V.
Takkebijsters 53, 4817BL Breda

Date of meeting
10-03-2011

Report by
Bowen Yu

Present
TU Delft, Bowen Yu
TU Delft, Zuopeng Qu
Evodos, Jan-Kees Boele
Evodos, Hen Boele
Feyecon, Nieves Gonzalez-Ramon
Feyecon, Martijn van der Kraan

Absent

Copy to
TU Delft, Geert-Jan Witkamp
Evodos, Marco Brocken
Feyecon, Adreas Weber

Page

Project
Innowater

Subject
Project progress meeting

Topic	Time	Who	Content
1	9:30	BY	Introduction
		JB	Preparation for starch test sample taking
		RD	Trouble shooting for motor problem of SPT centrifuge
2	12:30	BY	Progress report of the CFD work.
		JB	Presentation of the power point slides of 25-11-10
		RD	Point of interest/discussion:
		HB	- The path-line pattern shown in CFD transient model is confirmed by previous test photo provide by Evodos showing a curved solid deposition line between blades. A good indication of validation of the CFD model. Please refer to photos below - Contradict to the model, the SPT centrifuge is not completely filled with liquid. There are clear vertical interface (free surface) of water and air parallel to the shaft. The feed will leave the inlet as a jet of water and enter the rotating liquid pool. A new CFD multiphase modelling approach of VOF (volume of fluid) is proposed. - Due to the boundary condition of the model (open or restricted) the vertical pressure drop seems too big. - A validation of the model and test sample measurements will be done. - Raw data of the particle size measurement will be forwarded to RD of Evodos - A meeting of HB, BY, ZQ and GW to discuss the model is proposed

Appendix A5. Internal progress report 13-03-2011

Activities:

1. CFD models:
    a. the whole proposed centrifuge design was separated into five parts (Oct.);
    b. CFD models for the separated parts: methods working with water as working fluid (Oct.);
    c. Try to connect the different part together for the entire modeling domain (Nov.);
    d. CFD models for the entire centrifuge (Dec. Jan. Feb);
        i. Firstly does not converge;
        ii. Finally converged with optimized mesh of the full model;
        iii. Good and reasonable results (pressure, velocity, flow and particle tracks);
    e. CFD models for the flow in the channels between two blades (Nov.)
    f. Good particle tracks in the channel
2. Experimental comparison with modeling results (Jan. Feb.)
    a. Starch test instead of microalgae solution test because the microalgae is not available yet;
    b. Indirectly making comparison with modeling results;
    c. So far, good agreement of the particle tracks in the channels between modeling and experimental test;
3. Theoretical analysis for comparison with CFD modeling (ongoing work);
4. VOF model for the multiphase flow simulation (Jan. ongoing work)
    a. to study the interface between the gas and liquid in the centrifuge
    b. not for the project, but for publication;
    c. 2D model, because too time consuming

Meeting with Evodos:

- 2010-11-25: the 2nd progress meeting for the innowater project
- 2011-01-10: sample taking of starch test for the innowater project
- 2011-03-11: the 3rd progress meeting for the innowater project

Plan:

- Finish the CFD modeling part of centrifuge for innowater project;
- Continue the second part of the modeling work for algae cultivation;
- Come up with 1~3 journal publications;
    - CFD modeling with experimental comparison and theoretical analysis;
    - VOF modeling for the multiphase simulation;
    - CFD modeling of centrifuge together with cultivation modeling.

(Estimated) Difficulties:

- Limited time for cultivation modeling (three month left);
- Real experimental test with microalgae solution on field;
- Computational power for VOF model.

Optimization suggestion for the design (so far):

To avoid backflows or swirl flows (decrease energy consumption, and then improve efficiency) shows in the modeling results:

1. Add a skirt edge at the top of the impeller;
2. Change the 2D straight-up impeller design into leaning 3D.

APPENDIX B: Fluent computing environment

The simulation with a grid number below 1 million is performed on a desk top in Fluent 6.3.26 with Microsoft Windows 7 and Intel core 2 duo E8400 @3.00GHz with 4GB memory. The setup for the approach in Fluent is presented in Table B-1 as follows

Table B-1: Fluent computing environment desk top PC

	Approach used	Remarks
Solver	Pressure Based	
Time	Steady State/Transient	
Differencing Scheme	First Order Upwind	
Pressure-Velocity Coupling	PISO	
Properties		
Density		
Viscosity		

The simulation with a grid number above 1 million and up to 5 million (complete 3D centrifuage model) is performed on a work station in Fluent 12.0.7 with open SUSE 10.3 and 8 core Intel Xeon E5430 processor @2.66GHz with 16GB memory. The setup for the approach in Fluent is presented in Table B-2 as follows:

Table B-2: Fluent computing environment multi-core server

	Approach used	Remarks
Solver	Pressure Based	
Time	Transient	
Differencing Scheme	First Order Upwind	
Pressure-Velocity Coupling	PISO	
Properties		
Density		
Viscosity		

APPENDIX C: Original Project Proposal

Title: Modeling and optimization of microalgae dewatering with novel centrifuge
Keywords: CFD, microalgae, dewater, spiral plate centrifuge, stacked disk separator

Introduction

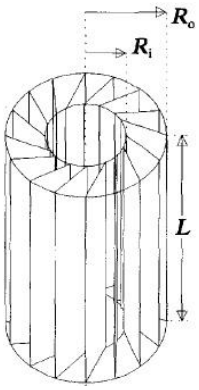

Microalgae can serve as a superior alternative and sustainable source of energy in the forms of biodiesel, bioethanol and biogas as they are oil-rich and grow many times faster than plants. Algae can be cultivated where land is not suitable for conventional crops, and production is largely dependent of the seasons. Furthermore, valuable components for pharmaceutical and nutritional use can be extracted from algae providing economic viability of the process. Finally, the growing of algae improves the overall atmospheric CO2 balance due to their activity as CO2 sink potentially replacing replacing intensive use of fossil fuels.

In algae processing, the first step is to harvest and dewater the algae. Currently available separation technologies are simply too expensive, economically and energy balance-wise to pursue low value products, such as liquid fuel. A novel separation technology developed by Evodos could make this process economically viable and relatively easy to scale up. The new type of centrifuge which uses, instead of a conventional conical disk stack, spiralized vertical plates. The plates (vanes) inside the centrifuge, which are almost perpendicular to the gravitational force, are able to separate very small particles (1.9-4 μm with a density almost equal to water). This creates a 'Y-flow', heavier material moves outwards and the lighter fraction moves inwards (in the shape of a 'Y'). There is no cross flow, which not only reduces the energy consumption, but more importantly, makes the use of chemicals such as flocculants and polymers obsolete.

This project is part of an ongoing effort between FeyeCon, Evodos, CleanAlgae and TU Delft under the EU INNOWATER program within water technologies. By CFD modeling of the centrifuge plates (vanes), inlet guide vanes, outlet guide vanes and 3D flow fields the centrifuge prototype designs could be optimized.

Objective
The objective of this final assignment is to develop CFD models to calculate the fluid flow distribution in a spiral vertical plate centrifuge and optimizing the centrifuge design. By optimise inlet and outlet guide vane design the high efficient energy transfer from the shaft to the system could be achieved. The model will also be validated using the currently available proto type centrifuge experiments data.

Activities
1. Literature research on the development and prospects of microalgae utilization;

2. Literature research on the development and modelling of algae harvesting (dewater) technologies;
3. Study CFD modelling and modelling methods and related modelling tools of centrifuge;
4. Development of CFD model of the inlet and outlet guide vanes in 3-D with 1 phase liquid flow;

5. Development of CFD models of the 1 phase liquid flow in a 3-D flow channel of centrifuge;
6. Evaluate inlet and outlet guide vane design to achieve maximum energy transfer;
7. Evaluate the flow behaviour (pattern) in the flow path between inlet guide vane and spiral plate stack;
8. Evaluate the flow behaviour between spiral plate vanes;
9. Evaluate (algae) feeding locations (size of disk) based on 3-D centrifuge model;
10. Based on results propose optimization in inlet and outlet guide vane design to achieve maximum energy transfer;
11. Based on results propose optimization in flow path design between inlet guide vane and spiral plate stack;
12. Final report writing.

Deliverables

1. Project execution plan (week 32)
2. Interim report containing first few chapters of the final report, including 3-D CFD model (week 42)
3. Draft final report (week 48)
4. Final report (week 50)

Literatures

1. Development of a system for the dewatering of microalgae. Bijlage A projectplan
2. Benemann J., Microalgae Biofuels: A Brief Introduction, ©John Benemann, February 1, 2009
3. Robert Plat, Gravitational and centrifugal oil-water separators with plate pack internals, PhD thesis 1994
4. Wijffels, R.H. and M.J. Barbosa, *An Outlook on Microalgal Biofuels.* Science, 2010. **329**(5993): p. 796-799.
5. Chisti, Y., *Biodiesel from microalgae.* Biotechnology Advances, 2007. **25**(3): p. 294-306.

More information

Zuopeng Qu: Z.Qu@TUDelft.NL

Professor: Prof. Dr. Geert-Jan Witkamp
Supervisors: Zuopeng Qu Msc.